

Criteria and guidance for the design of integral bridges in New Zealand

November 2015

John Wood, John Wood Consulting
Alexei Murashev, Opus International Consultants Ltd
Alessandro Palermo, University of Canterbury
Moustafa Al-Ani, Opus International Consultants Ltd
Kaveh Andisheh, University of Canterbury
Darren Goodall, Opus International Consultants Ltd

ISBN 978-0-478-44530-5 (electronic)
ISSN 1173-3764 (electronic)

NZ Transport Agency
Private Bag 6995, Wellington 6141, New Zealand
Telephone 64 4 894 5400; facsimile 64 4 894 6100
research@nzta.govt.nz
www.nzta.govt.nz

Wood, J, A Murashev, A Palermo, M Al-Ani, K Andisheh and D Goodall (2015) Criteria and guidance for the design of integral bridges in New Zealand. *NZ Transport Agency research report 577*. 108pp.

Opus International Consultants was contracted by the NZ Transport Agency in 2014 to carry out this research.

This publication is copyright © NZ Transport Agency 2015. Material in it may be reproduced for personal or in-house use without formal permission or charge, provided suitable acknowledgement is made to this publication and the NZ Transport Agency as the source. Requests and enquiries about the reproduction of material in this publication for any other purpose should be made to the Manager National Programmes, Investment Team, NZ Transport Agency, at research@nzta.govt.nz.

Keywords: bridges, construction, creep and shrinkage, design, earth pressures, integral seismic, soil-structure interaction, thermal effects

An important note for the reader

The NZ Transport Agency is a Crown entity established under the Land Transport Management Act 2003. The objective of the Agency is to undertake its functions in a way that contributes to an efficient, effective and safe land transport system in the public interest. Each year, the NZ Transport Agency funds innovative and relevant research that contributes to this objective.

The views expressed in research reports are the outcomes of the independent research, and should not be regarded as being the opinion or responsibility of the NZ Transport Agency. The material contained in the reports should not be construed in any way as policy adopted by the NZ Transport Agency or indeed any agency of the NZ Government. The reports may, however, be used by NZ Government agencies as a reference in the development of policy.

While research reports are believed to be correct at the time of their preparation, the NZ Transport Agency and agents involved in their preparation and publication do not accept any liability for use of the research. People using the research, whether directly or indirectly, should apply and rely on their own skill and judgement. They should not rely on the contents of the research reports in isolation from other sources of advice and information. If necessary, they should seek appropriate legal or other expert advice.

Acknowledgements

The authors would like to thank the New Zealand Transport Agency for the funding and support provided, without which this project would not have been possible. The authors are also grateful for the technical support and review provided by Professor Ian Buckle and Dr Phillip Yen.

Abbreviations and acronyms

AASHTO	American Association of State Highway and Transportation Officials
<i>Bridge manual</i>	NZ Transport Agency (2013) <i>Bridge manual</i> . 3rd edition.
Caltrans	California Department of Transportation
CBDG	Concrete Bridge Development Group
CEB	Comité Européen du Béton (European Committee for Concrete)
DBD	displacement-based design
DL	dead load
FBD	force-based design
fib	fédération internationale du béton (International Federation for Structural Concrete)
HFD	hyperbolic force displacement
MCE	maximum considered event
MSE	mechanically stabilised earth
NIWA	National Institute of Water and Atmospheric Research
PGA	peak ground acceleration
SDL	superimposed dead load
SDOF	single degree of freedom

Contents

- Executive summary.....7**
- Abstract.....8**
- 1 Introduction.....9**
 - 1.1 Definition of an integral bridge 9
 - 1.1.1 Concrete Bridge Development Group Technical Guide 1 – Integral Bridges (CBDG 1997) 9
 - 1.1.2 Highways Agency Advice Note BA 42/96 Amendment No.1 – The Design of Integral Bridges 11
 - 1.1.3 Transportation Research and Development Bureau Report 152 11
 - 1.1.4 Institution of Civil Engineers Proceedings – Integral Bridges 11
 - 1.1.5 1st Workshop on Integral Abutment/Jointless Bridges – Fuzhou, China, March 2014 11
 - 1.1.6 Seamless bridges 11
- 2 Performance of integral bridges13**
 - 2.1 General performance of integral bridges 13
 - 2.2 Seismic performance of integral bridges 13
 - 2.2.1 Performance of New Zealand integral bridges 13
 - 2.2.2 Performance of integral bridges in California 21
- 3 Design considerations27**
 - 3.1 Design implications and considerations for integral bridges 27
 - 3.1.1 Learnings from existing integral bridges 28
 - 3.1.2 Findings from the 1st International Workshop on Integral Abutment/Jointless Bridges 29
 - 3.1.3 Recommendations from USA practice 30
 - 3.2 Guidelines for static design of integral bridges 31
 - 3.2.1 General 31
 - 3.2.2 Structural form..... 31
 - 3.2.3 Bridge loading 32
 - 3.2.4 Creep and shrinkage 32
 - 3.2.5 Temperature loading of integral bridges 35
 - 3.3 Guidelines for seismic design of integral bridges 39
 - 3.3.1 General considerations 39
 - 3.3.2 Structural form..... 40
 - 3.3.3 Analysis method 40
 - 3.3.4 Abutment stiffness 43
 - 3.3.5 Abutment damping 44
 - 3.3.6 Backfill soil and strength parameters 45
 - 3.3.7 Soil gapping effects 45
 - 3.3.8 Modelling recommendations 46
 - 3.3.9 Piles in sloping ground 46
 - 3.4 Guidelines for geotechnical design of integral bridges 47
 - 3.4.1 General 47
 - 3.4.2 Types of abutment for integral bridge construction..... 47

3.4.3	Approach system.....	49
3.4.4	Mitigation of approach system settlements.....	51
3.4.5	Abutments supported on shallow footings	51
3.4.6	Abutments with MSE walls	52
3.4.7	Soil pressures	52
3.4.8	Earth pressures behind integral abutments and end screen walls	53
3.4.9	Strain ratcheting.....	54
3.4.10	Horizontal pressures on abutments accommodating thermal movements by rotation and/or flexure	55
3.4.11	Horizontal earth pressures on end screen and abutments that accommodate thermal movements by translation without rotation	56
3.4.12	Horizontal earth pressures on full height frame abutments on piles and embedded wall abutments (soil–structure interaction analysis).....	56
3.4.13	Horizontal earth pressures on bank pad abutments founded on a single row of embedded piles	57
3.4.14	ψ factors and partial factors for earth pressures behind integral abutments.....	57
3.4.15	Pressure envelope	57
3.4.16	Pile foundations.....	58
3.5	Maintenance.....	59
4	Conclusions and recommendations	60
4.1	Conclusions.....	60
4.2	Recommendations	60
5	References, codes and standards	61
5.1	References.....	61
5.2	Codes and standards.....	63
Appendix A: Concrete creep and shrinkage models		65
Appendix B: Creep and shrinkage of standard New Zealand precast concrete bridge decks		75
Appendix C: Simplified methods for creep of concrete superstructures		81
Appendix D: Design example.....		83

Executive summary

Integral and semi-integral bridges are a common form of construction in New Zealand, providing some marked advantages over other construction forms. Integral and semi-integral bridges minimise the use of bearings and expansion joints by providing a direct connection between superstructure and substructure. This form of construction is often preferred as it provides a number of advantages over conventional simply supported bridges, including lower construction and maintenance costs, improved constructability and durability, and improved vehicle ride quality.

However, there are a number of issues related to the design and construction of integral bridges which require either further investigation or clearer guidance within a New Zealand-specific context. The purpose of this report is, by using a combination of professional experience and international research, to identify these issues and provide guidance where currently available. They include performance and case studies, non-seismic effects such as concrete creep, shrinkage and temperature, seismic effects and geotechnical issues including soil-structure interaction.

In traditional simply supported bridges, structural/non-structural elements such as expansion joints, roller supports and abutment bearings accommodate rotations and displacements induced by creep and shrinkage and therefore reduce or minimise secondary stresses through the additional degrees of freedom. Due to the absence of aforementioned mechanisms to release structural stresses, secondary effects such as creep, shrinkage and thermal gradient have a significant influence on the behaviour of integral bridges. Several models for creep, shrinkage and thermal effects are presented and discussed in the report.

There are no well-established earthquake design procedures for bridges with integral abutments. Detailing of the abutment and the associated soil-structure interaction at the abutment and in the foundations needs careful consideration but the methods of analysis used for bridges with separated abutment structures are generally applicable. Displacement-based design principles are discussed and applied to integral bridges throughout this report.

Integral abutments should be designed to resist creep, shrinkage and thermal deformations of the superstructure. Assessment of movement should consider secondary effects in determining potential movements of abutments. Integral bridge abutments are subjected to significant cyclic movements due to the influence of secondary effects, and understanding the interaction between superstructure, substructure and soil during this cyclic loading is important for effective design and satisfactory performance of integral bridges. This report presents additional design requirements and considerations which are recommended for the geotechnical design of integral bridges to support the guidance found in the NZ Transport Agency's *Bridge manual*.

Overall, it is anticipated that while the purpose of this report is not to provide step-by-step guidance for the design of integral bridges, it will provide New Zealand bridge designers with the necessary information and highlight the necessary issues for consideration to ensure excellent performance of future integral bridges. This is aided by the parametric studies and worked example found in the appendices to the report.

Abstract

The use of integral and semi-integral bridges in New Zealand is fairly common practice due to advantages in ease of construction and savings in maintenance and whole-of-life costs. The aim of this report is to provide a summary of current best practice relating to the design and construction of integral and semi-integral bridges in New Zealand.

The issues considered throughout the report included the definition and performance of integral bridges, non-seismic effects such as concrete creep and shrinkage and thermal effects, seismic effects, geotechnical issues, and considerations pertaining to design and detailing. The aims of the report were achieved through a combination of review of existing literature, consideration of case studies of integral and semi-integral bridges, and consultation with bridge designers experienced in the design of integral bridge construction. The overall performance of integral bridges in New Zealand was found to be very good, while several issues relating to seismic effects, soil-structure interaction, concrete creep and shrinkage, and detailing were investigated.

1 Introduction

Integral and semi-integral bridges are a common form of construction, both in New Zealand and internationally, and have some marked advantages over other construction forms, such as reduced maintenance.

However, there are a number of issues related to the design and construction of integral bridges which require either further investigation or clearer guidance within a New Zealand-specific context, and these issues have been identified and expanded upon in this report. The issues of concern were categorised into three topics:

- 1 static design
- 2 seismic design
- 3 geotechnical considerations.

The methodology used throughout the report is a combination of review of existing literature, consultation with experienced bridge designers and consideration of a number of case studies. The main purpose of the report is to provide guidance to New Zealand bridge designers for the design of integral and semi-integral bridges, and where guidance is limited identify areas for future research.

1.1 Definition of an integral bridge

While the term 'integral bridge' is often used in design practice in New Zealand, there can be some ambiguity as to the strict definition of the term and how to differentiate between 'integral' and 'semi-integral' bridges. In this study, the following definitions are used for fully integral and semi-integral bridges:

*An **integral bridge** is a structure where there are no expansion joints in the superstructure between spans and between spans and abutments (but these joints may exist beyond the bridge).*

*An integral bridge where the superstructure and substructure are also designed to move together to accommodate the required translations and rotations (a monolithic structure) is termed **fully integral**.*

*An integral bridge which has bearings at the abutment and/or piers and as a result, the superstructure and substructure do not necessarily have to move together to accommodate the required translations and rotations, is termed **semi-integral**.*

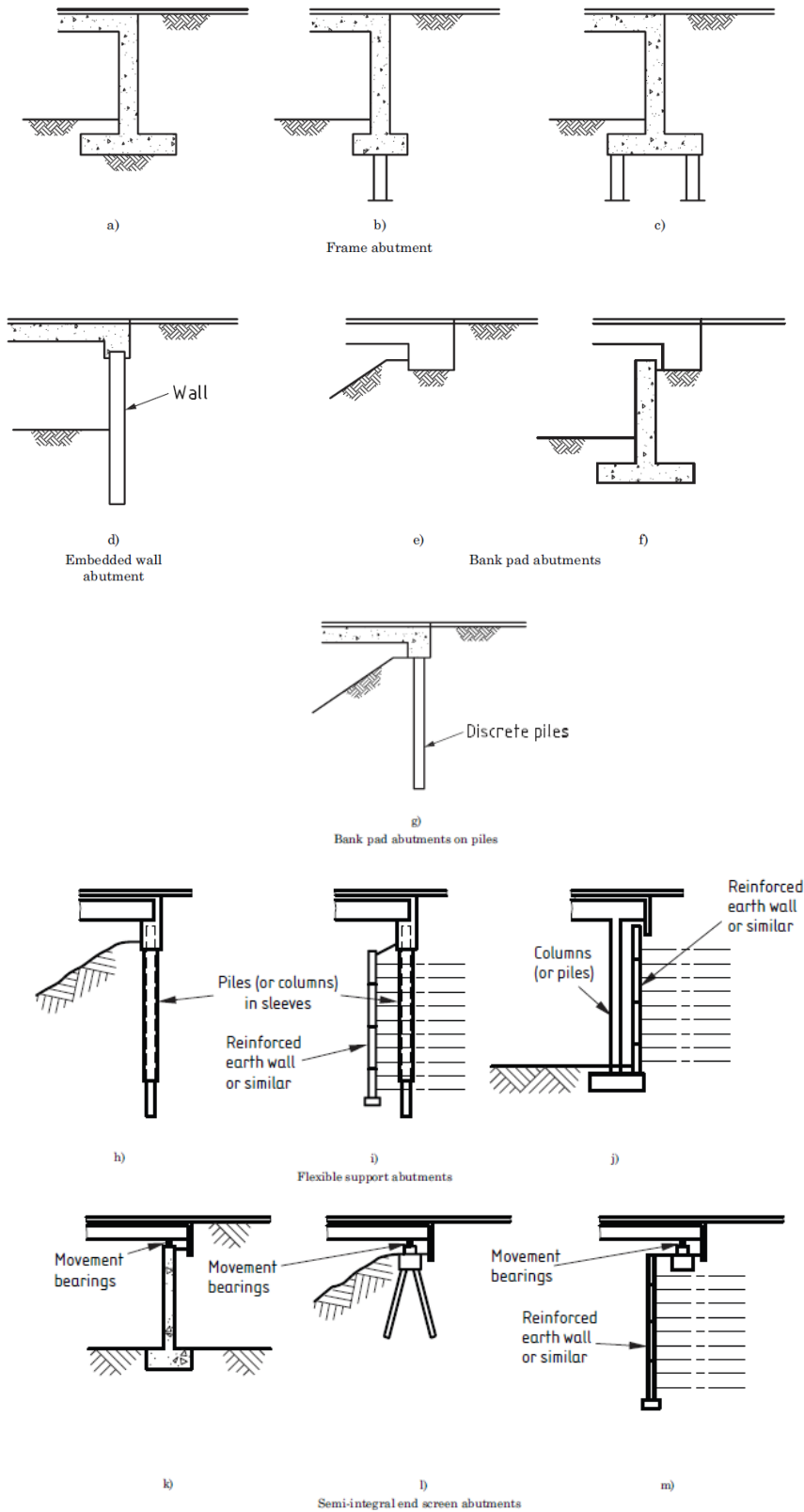
Therefore, an integral bridge can be fully or semi-integral at the abutments and/or at the piers. Typical integral bridge abutments are shown in figure 1.1. This definition has been arrived at based on definitions of integral bridges found in other literature, including:

1.1.1 Concrete Bridge Development Group Technical Guide 1 – Integral Bridges (CBDG 1997)

An integral bridge is defined as a bridge without joints for expansion between spans or between spans and abutments. In many cases there is no articulation, or only very limited articulation, at the abutments and piers.

The term 'semi-integral' is used to describe a bridge which has no expansion joints but does have bearings at the abutments, and the term 'fully integral' is used to describe a bridge which has neither expansion joints nor abutment bearings.

Figure 1.1 Types of abutment for integral bridge construction



Source: CBDG (1997)

1.1.2 Highways Agency Advice Note BA 42/96 Amendment No.1 – The Design of Integral Bridges

Integral bridges are designed without any expansion joints between spans or between spans and abutments. Resistance to longitudinal thermal movements and braking loads is provided by the stiffness of the soil abutting the end supports and, in some cases by the stiffness of the intermediate supports.

Expansion joints in bridge decks are prone to leak and allow the ingress of de-icing salts into the bridge deck and substructure, thereby resulting in severe durability problems. To overcome these problems, bridge decks up to 60 metres in length and with skews not exceeding 30° are generally required to be continuous over intermediate supports and integral with their abutments. (Highways Agency 2003)

1.1.3 Transportation Research and Development Bureau Report 152

Integral Abutment Bridges are structures where the superstructure and substructure move together to accommodate the required translation and rotation. There are no bridge expansion joints and in the case of fully integral abutment bridges, no bearings. In the United States of America (USA), there are more than 9,000 Fully Integral Abutment Bridges and 4,000 Semi-Integral Abutment Bridges. Integral Abutment Bridges have proven themselves to be less expensive to construct, easier to maintain, and more economical to own over their life span. (White 2007)

1.1.4 Institution of Civil Engineers Proceedings – Integral Bridges

Integral bridges are bridges which have no movement joints between the deck and the abutments, or between spans. Integral bridges are becoming increasingly popular around the world as engineers seek ways to avoid the very expensive maintenance problems that are being encountered on bridges with movement joints due to penetration of water and de-icing salts. (Hambly 1997)

1.1.5 1st Workshop on Integral Abutment/Jointless Bridges – Fuzhou, China, March 2014

A member of the research team for this study (Dr Alessandro Palermo, University of Canterbury) attended the 1st Workshop on Integral Abutment/Jointless Bridges in Fuzhou, China. With regard to the definition of integral bridges, he made the following observation:

Although this matter looks simple, it turned out to be quite complex and each attendant at the workshop had a different view. The word ‘Integral’ is usually limited to the abutments and doesn’t give a proper understanding about stiffness and strength of the connection. All attendants agreed we should start from the definition of the bridge system, identify the connections and based on that come out with a proper classification. China counts only 20 integral bridges so far constructed.

1.1.6 Seamless bridges

Seamless bridges are not commonly used in New Zealand but are being investigated and implemented overseas. Seamless bridges eliminate all expansion joints, even at the ends of the approach slabs, by limiting the longitudinal expansion and contraction of the bridge superstructure. The design of seamless

bridges is outside the scope of this report, but reference should be made to other research reports, such as Azizinamini et al (2013) if required.

2 Performance of integral bridges

2.1 General performance of integral bridges

One of the main drivers for the implementation of integral bridge construction over conventional bridges is the reduced maintenance requirements at the joints. As noted by Hambly (1997):

An increasingly analytical approach to bridge design in recent years has led to many modern highway bridges being designed with complicated movement joints and sliding bearings to accommodate calculated thermal effects. Unfortunately the maintenance problems that have developed at these movement joints and bearings have often been far worse than the problems they were intended to avoid. It is a case of the cure being worse than the disease, or 'Where ignorance is bliss, 'tis folly to be wise' Thomas Gray (1742).

Regional bridge consultants, who are responsible for the structural management of New Zealand state highway structures, have been consulted to provide their first-hand experiences of dealing with integral bridges. The vast majority of the consultants queried have found no major issues with these bridges, and many of the older bridges continue to provide very good levels of service.

Graeme Jamieson (BBO Consultants, Hamilton) stated:

During our Regional Bridge Consultancy inspection work we have seen many integral bridges over a sustained period which fall within the Bridge Manual length and skew defaults within which no specific measures need be taken. These have typically performed very well. This tends to suggest that longer integral bridges may well be viable, and international experience suggests that this is the case. However we agree with Bridge Manual requirements that careful analysis of all such is warranted.

Richard Kolkman (Opus Consultants, Whangarei) stated:

In Northland, we have many older monolithic T beam single span structures designed for Traction Engine loading that are effectively integral structures. These have generally performed well and the majority of structural issues are a function of factors other than design (ie materials and foundation issues).

2.2 Seismic performance of integral bridges

2.2.1 Performance of New Zealand integral bridges

A summary of the design details and performance of New Zealand integral abutment bridges which have been subjected to strong ground shaking is presented in table 2.1.

2.2.1.1 Flaxbourne River Bridge

Constructed in 1955, the Flaxbourne River Bridge on State Highway 1 is approximately 64m in overall length with two approach spans of 10.7m and three internal spans of 14.3m. The bridge has a continuous reinforced concrete T-beam superstructure with four longitudinal beams simply supported on the piers. There are no deck joints at the piers or abutments.

The four piers are reinforced concrete wall type, with the northern three supported on piles and the southern pier on a strip footing founded on papa rock. The beams are tied to the piers with two 32mm diameter dowel bars.

The southern abutment is a reinforced concrete column structure with its strip footing also founded on hard papa rock. A transverse diaphragm beam between the main beams is dowelled to the abutment column cap so at this end the superstructure is effectively pinned to the sub-structure and therefore the abutment is not strictly an integral type. The northern abutment is on concrete piles with the drawings showing a 1.1m deep combined cap and transverse diaphragm between the main beams providing integral action between the piles and superstructure. However, it appears that the bridge was constructed with a pile cap cast prior to forming the superstructure diaphragm on top of it giving an overall abutment wall depth of 1.6m. There may be a dowelled connection between the two making the abutment action similar to the southern abutment. Details of the bridge are shown in figure 2.1.

Figure 2.1 Flaxbourne River Bridge



The Flaxbourne River Bridge is located approximately 10km and 29km from the epicentres of the 2013 Lake Grassmere and Cook Strait earthquakes respectively. Peak ground accelerations (PGAs) of 0.59g and 0.22g were recorded in the respective events at the Ward Fire Station, which is located about 800m south of the bridge.

The earthquakes caused minor damage. There was spalling on both sides of the four main beams where they are seated on the southern-most pier. There was some spalling on the superstructure diaphragm beam where it was in contact with the abutment column capping beam at the south abutment of the bridge. This indicated a small amount of relative longitudinal movement between the superstructure and abutment. Cracks in the pavement and in the infill concrete cast against the south abutment indicated there had been longitudinal movement of the bridge but this appeared to be less than 30mm.

2.2.1.2 Wairau River Bridge

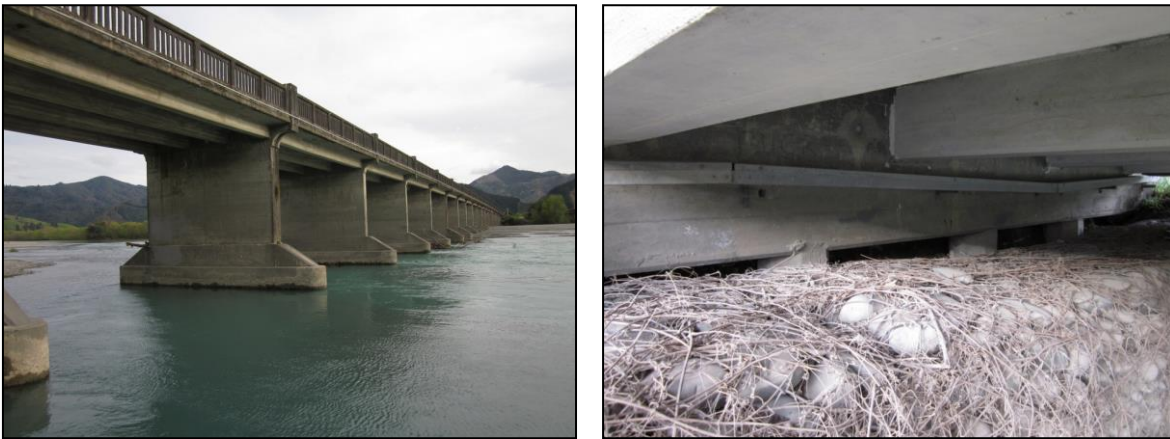
Constructed in 1939, the Wairau River Bridge on State Highway 1 is 293m in overall length with 24 equal spans of 12.2m. The bridge has a semi-continuous reinforced concrete T-beam superstructure with four longitudinal beams monolithic with the piers. The piers are reinforced concrete walls, with every fourth pier having two separate but contiguous walls with the joint between the walls allowing longitudinal movement. At the intermediate piers the deck reinforcement is discontinuous to form a deck joint but there are 'bonding' bars through the bottom of the beams. There are no deck joints at the abutments.

The abutments and piers are supported on octagonal reinforced concrete piles. Both abutments have a combined pile cap and transverse monolithic diaphragm beam which forms an abutment wall integral with the superstructure. The walls are approximately 1.3m and 1.8m deep at the south and north ends respectively. Details of the bridge are shown in figure 2.2.

The Wairau River Bridge is located approximately 35km from the epicentre of the Cook Strait earthquake and about 1km further from the epicentre of the Lake Grassmere earthquake. PGAs at the bridge site in both events were estimated to be approximately 0.13g.

The earthquakes caused minor cracking damage to the south abutment wall. There were fine vertical cracks near the base of the wall towards the centre of the bridge which may have been caused by flexure under transverse loading. Cracks with a maximum width of ~3mm were evident on the soil side at the ends of both abutment walls but these were deemed to be old cracks related to shrinkage shortening. Cracks in the pavement and soil surrounding the abutment piles indicated longitudinal movements of less than 20mm.

Figure 2.2 Wairau River Bridge



2.2.1.3 Spring Creek Bridge

Constructed in 1939, the Spring Creek Bridge on State Highway 1 is 43m in length with two end spans of 13.7m and a central span of 15.2m. The bridge has a continuous reinforced concrete T-beam superstructure with four longitudinal beams monolithic with the piers and abutments, which are aligned on a 45° skew. The piers consist of reinforced concrete walls.

The abutments and piers are supported on octagonal reinforced concrete piles. Both abutments have a 2.0m deep combined pile cap and transverse monolithic diaphragm beam integral with the superstructure. Details of the bridge are shown in figure 2.3.

The Spring Creek Bridge is located approximately 35km from the epicentres of both the Lake Grassmere and Cook Strait earthquakes. PGAs at the bridge site in both events were estimated to be approximately 0.15g.

The earthquakes caused minor cracking damage to the abutment piles and walls at both abutments. There were fine horizontal cracks near the tops of most of the abutment piles and fine vertical cracks in the walls mainly located above the piles. Settlement occurred in the backfill behind the abutments and minor pounding damage occurred between the ends of the bridge and separate wing walls on the approaches. There was no evidence of significant longitudinal movements.

Figure 2.3 Spring Creek Bridge



2.2.1.4 Halswell River Bridge

Constructed in 1937, the Halswell River Bridge on State Highway 1 is a single-span bridge with an overall length of 6.7m. The bridge has a reinforced concrete T-beam superstructure. The abutments are supported on octagonal reinforced concrete piles and have a 2.1m deep combined pile cap and transverse monolithic diaphragm beam integral with the superstructure. Details of the bridge are shown in figure 2.4.

Figure 2.4 Halswell River Bridge



The Halswell River Bridge is located approximately 32km and 12km from the epicentres of the 2010 Darfield and 2011 Christchurch earthquakes respectively. PGAs at the bridge site in both events were estimated to be approximately 0.3g. Flexural failures occurred in the abutment walls as a result of high pressures from liquefaction-induced lateral spreading.

2.2.1.5 Hawkins River Bridge

Constructed in 1939, the Hawkins River Bridge on State Highway 1 has six spans of equal length with an overall length of 82m. The superstructure consists of a reinforced concrete T-beam framed into the abutments and the central pier. At the intermediate piers the spans are connected by bars in the bottom of the beams with a joint gap constructed above the bottom section of the beams.

The piers consist of reinforced concrete walls, with both the piers and abutments founded on vertical reinforced concrete piles. The abutments have a 1.4m deep combined pile cap and transverse monolithic diaphragm beam integral with the superstructure. Details of the bridge are shown in figure 2.5.

The bridge is located 12km from the epicentre of the Darfield earthquake and about 12km from the closest point on the fault surface trace. The PGA at the site was estimated to be 0.45g.

The strong earthquake shaking caused minor structural damage, with concrete spalling and cracking observed in the tops of the piles at the underside of four of the five pier walls. The pile tops were not visible at the central pier. The damage was more pronounced at the second pier from each abutment than at the piers closest to the abutments and was most likely caused by the transverse response of the bridge.

At both abutments infill concrete had been placed below the underside of the abutment structural wall and around the piles to prevent scour of the abutment backfill. The maximum height of the infill was about 1m and it appeared to completely surround the piles. At the west abutment this infill concrete had wide vertical cracks near the interface with the piles. There was also cracking and spalling at the interface of the infill with the structural abutment wall at the east abutment but this was mainly in plaster that had been placed in the gaps in the horizontal construction joint. The cracking damage to the west abutment infill concrete suggested there had been significant longitudinal movement of the abutments, estimated to be in the order of 20mm.

Figure 2.5 Hawkins River Bridge



2.2.1.6 Selwyn River Bridge

The Selwyn River Bridge is a single-lane bridge constructed in 1931 across the Selwyn River, approximately 15km west of Darfield along State Highway 75. The 10-span bridge superstructure consists of simply supported 9.1m long monolithic reinforced concrete T beams. The piers and abutment walls are of reinforced concrete slab type construction founded on vertical reinforced concrete piles. Sliding and fixed span joints are provided at alternate piers except at the piers adjacent to the abutments which have one sliding and one fixed span end. At the fixed joints, bars extend from the pier into the ends of the beams and the adjacent spans are linked by bars in the bottom of the beams. At the sliding joints, the beams are seated on steel plates with holding down bolts in slotted holes. Linkage bars have been retrofitted to the sliding joints to anchor the beams to the tops of the piers. The end spans are anchored to the pile caps at the abutments with inclined bars anchoring into the beams. There is a joint between the beams and the pile cap but it appears to be a rigid joint with the deck cast monolithically with the back wall which

extends up from the pile cap. The combined height of the pile cap and back wall is approximately 2.1 m. Details of the bridge are shown in figure 2.6.

Figure 2.6 Selwyn River Bridge



The bridge is located approximately 22km west of the epicentre and about 16km north-west of the closest point on the fault surface trace of the Darfield earthquake. The PGA at the site was estimated to be about 0.45g.

Apart from minor concrete spalling on the top of one of the piles at the west abutment no earthquake related structural damage to the bridge was observed. There was no evidence of significant displacements of the bridge at the soil interface with the visible piles or at the abutments. At the west abutment, steps in the concrete kerb lines, repaired pavement, and settlement marks on the front face of the abutment wall and at guardrail posts indicated the approach fill had settled by about 50mm at the soil interface with the abutment backwalls. Settlement of about the same order was evident at the east abutment but it was not clear how much of this had existed prior to the earthquake.

2.2.1.7 Needles Creek Bridge

The 43m Needles Creek Bridge on State Highway 77, consisting of five spans, was constructed in 1939. The bridge superstructure is a continuous concrete slab monolithic with reinforced concrete wall type piers.

The abutments and piers are supported on octagonal reinforced concrete piles, with 1.2m deep monolithic pile caps at both abutments. Details of the bridge are shown in figure 2.7.

The Needles Creek Bridge is located 10km from the epicentre of the Lake Grassmere earthquake, with an estimated PGA at the bridge site of approximately 0.35g. There was no evidence of any structural damage or significant longitudinal movement resulting from the earthquake motions.

Figure 2.7 Needles Creek Bridge



2.2.1.8 Tirohanga Stream Bridge

The Tirohanga Stream Bridge is a two-span, 21 m long bridge constructed in 1953 on State Highway 77. The superstructure consists of two monolithic reinforced concrete T-beam spans of equal length, supported on reinforced concrete wall piers and abutments founded on vertical reinforced concrete piles. A joint in the deck at the pier extends over part of the beam depth with bottom bars in the beams providing linkage across the joint. The superstructure is monolithic with the 2.3 m high abutment walls. Details of the bridge are shown in figure 2.8.

The Tirohanga Stream Bridge is located approximately 27 km from the epicentre of the Lake Grassmere earthquake. The PGA at the bridge site in this event was estimated to be approximately 0.17g, with no evidence of any resulting structural damage or significant longitudinal movement.

Figure 2.8 Tirohanga Stream Bridge



Table 2.1 New Zealand integral bridges subjected to strong seismic motions

State high-way	Bridge name	Constr date	Length (m)	No. of spans	Foundation	Super-structure and piers	Abutment wall height, m	PGA est. g	Dist to EQ epicentre km	Main EQ event	EQ related damage
1	Wairau River Bridge	1939	293	24	Piles driven 410mm octagonal RC	RC T beams Wall type	1.3	0.13	35 36	Cook Strait Lake Grassmere	Fine cracking in abutment walls probably from transverse load. Wide cracks in wall ends probably from shrinkage effects.
1	Spring Creek Bridge	1939	43	3	Piles driven 360mm octagonal RC	RC T beams Wall type	1.8	0.15	35 35	Cook Strait Lake Grassmere	Fine cracking in most abutment piles. 3mm wide in one outer pile. Fine cracking in walls above piles.
1	Flaxbourne River Bridge	1955	64	5	Piles driven 410mm octagonal RC	RC T beams Wall type	1.1	0.4	9	Lake Grassmere	Spalling on beam faces at beam bearings on piers.
1	Needles Creek	1953	43	5	Piles driven 410mm octagonal RC	Concrete slab Wall type	1.2	0.35	10	Lake Grassmere	No visible structural damage.
1	Tirohanga Stream Bridge	1939	21	2	Piles driven 410mm octagonal RC	RC T beams Wall type	2.3	0.17	27	Lake Grassmere	No visible structural damage.
75	Halswell River Bridge	1937	6.7	1	Piles driven 360mm octagonal RC	RC T beams	2.1	0.3	32 12	Darfield Christchurch	Flexural failures in abutment walls caused by high pressures from lateral spreading.
77	Selwyn River Bridge	1931	92	10	Piles driven 410mm octagonal RC	RC T beams Wall type	2.1	0.45	22	Darfield	No visible significant damage.
77	Hawkins River Bridge	1939	82	6	Piles driven 360mm square RC	RC T beams Wall type	1.4	0.45	12	Darfield	Cracking and spalling in the tops of the pier piles. Abutment piles undamaged.

Note: EQ = earthquake; RC = reinforced concrete

2.2.2 Performance of integral bridges in California

The design of modern bridges in California, USA, has been heavily influenced by three major earthquakes: the San Fernando, Loma Prieta and Northridge earthquakes. The findings and learnings from each of these three major earthquakes were used to improve the design guidelines set out by both the California Department of Transportation (Caltrans) and the American Association of State Highway and Transportation Officials (AASHTO).

2.2.2.1 San Fernando earthquake

The magnitude 6.6 main shock of the San Fernando earthquake on 9 February 1971 resulted from displacements on a thrust type fault. The fault displacements originated at a point approximately 13km beneath the epicentre, which was located in an uninhabited region of the San Gabriel Mountains, and propagated southward along a fault plane inclined at 45° breaking the surface in the built-up area of Sylmar. A maximum PGA of approximately 1.2g was recorded by an accelerometer located on a steep rock ridge near one of the abutments of the Pacoima Dam. The PGAs recorded on the alluvial valleys of the Los Angeles basin ranged from 0.17 to 0.35g.

Approximately 70 freeway bridges (counting twin bridges as a single structure) were located within a 17km radius of the centre of maximum energy release located near the Pacoima Dam. Approximately 40 of these 70 bridges experienced significant damage, including five bridges that collapsed. These bridges were subjected to very intense ground motions with PGAs in the range of 0.25 to 0.5g (Jennings 1971).

The extensive freeway system of the Los Angeles basin utilises a very large number of bridge structures to distribute traffic at freeway interchanges and to carry the freeways over and under the city street systems. Most of the bridges are of prestressed concrete or reinforced concrete design, with box girder construction commonly used as well as some arch and girder type bridges. In general, bridges are the major structures on the freeway system and high earth retaining structures and tunnels are uncommon.

The most severe damage occurred to overpass structures at three major interchanges:

- 1 The Golden State (Interstate 5) and the Antelope Valley (California 14) freeways
- 2 The Golden State and the Foothill (Interstate 210) freeways
- 3 The Golden State and the San Diego (Interstate 405) freeways.

These three interchanges are all located within 10km of the Pacoima Dam. Most of the other damaged bridges are located on the Antelope Valley, Foothill and Golden State freeways.

Significant abutment damage was widespread and although mainly confined to bridges within a 17km radius of the Pacoima Dam, minor abutment damage occurred at more distant bridges. In particular abutment damage was severe on skewed bridges and was related to the tendency of skew bridges to rotate in a horizontal plane. Abutment damage was characterised by basic shear type failure in the components that either restrained or provided a connection to the superstructure. Abutments located on firm ground were relatively more rigid than the pier structure and consequently these initially carried a large proportion of the horizontal inertia loads.

Settlement of the backfill at abutment approaches was common and generally the settlement was most severe at bridges that showed evidence of significant horizontal movements. The unreinforced concrete freeway pavement is typically continuous through to the backface of the abutment where it is seated on a 100mm wide recess. In a number of cases, movement of both the bridge and the pavement was sufficient for the pavement to slip from the abutment recess and settle with the backfill. This type of failure should

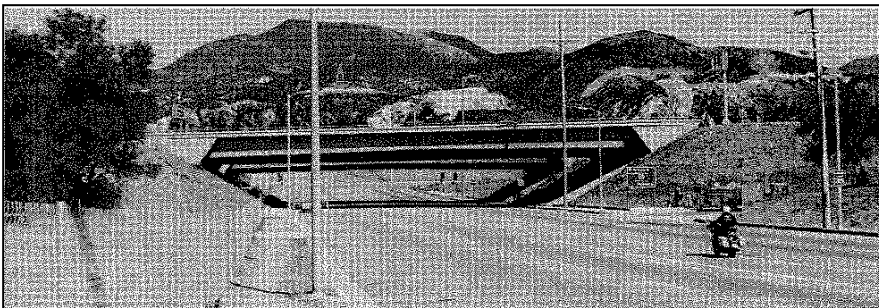
be avoided to ensure that highways are immediately available for the operation of emergency vehicles following an earthquake (Wood and Jennings 1971).

There is insufficient publically available information to allow for a comparative analysis between the performance of integral and non-integral bridges. However, the performance of three integral bridges during the San Fernando earthquake is described below.

Roxford Street Undercrossing

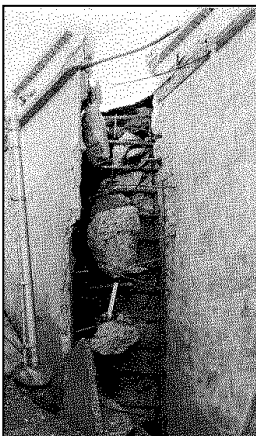
The Roxford Street Undercrossing bridges on the Foothill Freeway are twin single-span prestressed concrete box structures. The integral abutments of the 46m long bridges are located on filled embankments with 380mm diameter concrete pile foundations. Both bridges suffered lateral pile failures and the large bridge displacements caused extensive damage to the abutment wingwalls and approach pavement. Details of the damage and failures can be seen in figures 2.9 and 2.10.

Figure 2.9 Roxford Street Undercrossing



Some of the piles were exposed for inspection and it appeared that they had hinged at the underside of the pile cap and sheared through the soil. The eastern and western abutments of the southern bridge exhibited residual transverse displacements of 750mm and 70mm, respectively (Wood and Jennings 1971).

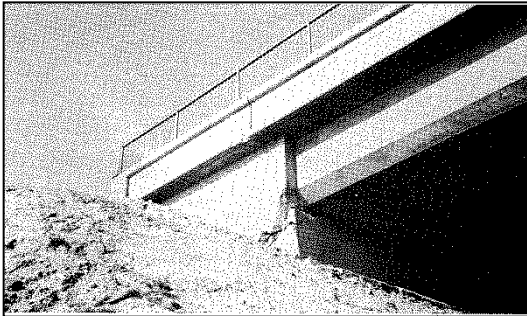
Figure 2.10 Roxford Street Undercrossing – damage to eastern abutment



Balboa Street Overcrossing

The 205m long, seven-span Balboa Street Overcrossing on the Golden Gate Freeway suffered severe concrete spalling and cracking damage in the main walls of its integral abutments as shown in figure 2.11. The reinforced concrete box superstructure is cast monolithically with the spread footing abutment structures (Wood and Jennings 1971).

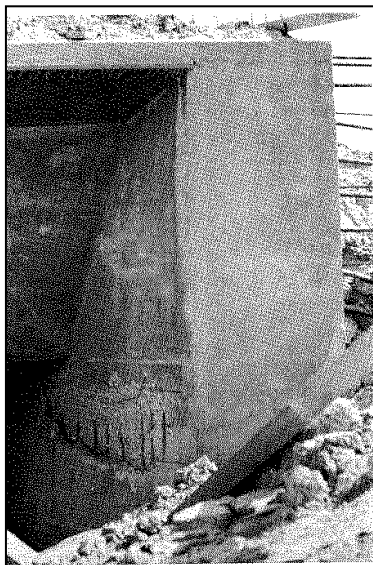
Figure 2.11 Balboa Street Overcrossing – damage to western abutment



Via Princessa Undercrossing

The twin 48m long single-span Via Princessa Undercrossing bridges on the Antelope Valley Freeway are prestressed concrete box-girder bridges constructed with integral abutments. The bridges were structurally complete at the time of the earthquake but backfilling behind the abutments was not finished. The main walls of the abutments were damaged by longitudinal movements as shown in figure 2.12. Failures were thought to be from combined effects of shear and bending in the abutment walls (Jennings 1971).

Figure 2.12 Via Princessa Undercrossing – damage to eastern abutment



2.2.2.2 Loma Prieta earthquake

The magnitude 7.1 Loma Prieta earthquake in 1989 was the largest earthquake to occur in the San Francisco Bay area following the 1906 San Francisco earthquake. The epicentre of the earthquake was located in the southern Santa Cruz Mountains. An outer zone of modified Mercalli intensity of VII extended more than 100km northwest to San Francisco and Oakland, and 50km southeast to Salinas and Hollister. Within these regions PGAs exceeded 0.6g close to the source and were as high as 0.26g at a distance of 100km. Strong shaking lasted less than 15 seconds, and local soil conditions significantly influenced the spatial distribution of damage (Basoz and Kiremidjian 1998).

Approximately 5% of all bridges within the earthquake-affected region sustained measurable damage, with the majority of bridge damage in the San Francisco Bay area 100km away from the epicentre. Thirteen of the state-owned bridges in the Bay area sustained major damage and were closed to traffic following the

earthquake. Soft soil at bridge sites contributed to the extensive damage observed this far away from the epicentre. Sections of three major bridge structures collapsed (Oakland Bay Bridge, Cypress Street Viaduct and Struve Slough).

Bridge data gathered by Caltrans identified a total of 76 damaged bridges. Forty-three of the damaged bridges had both concrete super and sub-structures and were subjected to PGAs greater than 0.1g. Basoz and Kiremidjian (1998) carried out correlation studies to identify the structural characteristics that contributed most to the damage observed on the concrete bridges that were subjected to ground accelerations greater than 0.1g. The bridges were categorised using three abutment types, three superstructure types and three pier types. Abutment types were; monolithic, non-monolithic and partially monolithic. Superstructure types were single-span, continuous multi-span and discontinuous multi-span. Pier types were; single column, multi-column and pier wall. Bridges that had a mixture of different types of components were omitted from their correlation data set. This resulted in a total of 28 damaged bridges of which six were recorded as having suffered major damage. The total number of bridges in the data set (both undamaged and damaged) was 709.

None of the single-span bridges with monolithic abutments were damaged. In comparison six single-span bridges with non-monolithic abutments were damaged. A total of 2.4% of the continuous multi-span bridges (six bridges) with monolithic abutments were damaged. In comparison 6.1% of the continuous multi-span bridges (nine bridges) with non-monolithic abutments and 13.1% of the continuous multi-span bridges (eight bridges) with partial monolithic abutments were damaged. Overall, the statistics from the Basoz and Kiremidjian (1998) correlation study showed that bridges with monolithic abutments were less likely to be damaged than bridges with other abutment types.

2.2.2.3 Northridge earthquake

The magnitude 6.7 Northridge earthquake on 17 January 1994 resulted in strong ground shaking in the Greater Los Angeles area with PGAs exceeding 1.0g in the region immediately surrounding the epicentre and generally exceeding 0.25g within 30km of the epicentre. Caltrans (1994) estimated that 1,600 state and county bridges (state bridges accounting for approximately 60% of that total) were subjected to PGAs of 0.25g or greater.

Seven highway bridges suffered partial collapse and another 170 bridges suffered damage ranging from minor cracking to the slumping of abutment fills. Many of the damaged structures were closed only temporarily for inspection and/or shoring but some were closed permanently and demolished. All of the bridges with collapsed spans were designed and constructed between the mid-1960s to the mid-1970s. Most had been retrofitted with cable restrainers, where appropriate. Some columns of bridges in the region of the epicentre had also been strengthened with steel-jackets which performed satisfactorily (Buckle 1994).

Basoz and Kiremidjian (1998) carried out correlation analyses for the Northridge earthquake in a similar manner to the Loma Prieta earthquake study described above to identify the structural characteristics that most contributed to the observed damage in concrete bridges subjected to strong ground accelerations. For the Northridge earthquake only bridges subjected to PGAs greater than 0.15g, rather than the 0.1g used for the Loma Prieta earthquake, were included in the study. The bridges were categorised using the same abutment, superstructure and pier types as used in the Loma Prieta earthquake study, and bridges with mixed structural forms were again excluded. This resulted in a total of 160 damaged bridges which included four collapsed bridges and 35 categorised as sustaining major damage. The total number of bridges in the data set (both damaged and undamaged) was 1,181.

Damage was observed in 7.9% of the single-span bridges with monolithic abutments (17 bridges). In comparison, 9.7% of the single-span bridges with non-monolithic abutments (10 bridges) were damaged. A total of 12.9 % of the continuous multi-span bridges (45 bridges) with monolithic abutments exhibited significant damaged, while 14.5 % of the continuous multi-span bridges (37 bridges) with non-monolithic abutments and 6.7 % of the continuous multi-span bridges (eight bridges) with partial monolithic abutments were damaged. Overall the statistics from the Basoz and Kiremidjian (1998) correlation study indicated that bridges with monolithic abutments were less likely to be damaged than bridges with non-monolithic abutments but the difference in performance was less marked than was case for the Loma Prieta earthquake. Factors such as the degree of damage are not considered in this simple comparison and might affect the performance comparison.

In the Caltrans (1994) Northridge post-earthquake investigation report (PEQIT report) it was stated that end-diaphragm abutments protected structures, or parts of structures, in which they were present to a greater degree than seat type abutments. In some cases this was observed to the point of success or failure. A design recommendation in the report stated: 'End-diaphragm abutments, or seat-type abutments that provide restraint to the superstructure, should be considered for use in high seismic regions'.

2.2.2.4 Other earthquakes

Meloland Road Overcrossing

The Meloland Road Overcrossing, designed in 1968, is located near El Centro in southern California. It is a 63m long reinforced concrete continuous box-girder bridge with two equal spans and integral abutments. The single-column pier at the centre of the bridge is approximately 6.1m high and is supported on a pile group consisting of 25 (5x5) driven concrete friction piles. The abutments are founded on seven concrete piles driven into stiff clay embankments overlaying native alluvium.

The superstructure, abutments, embankments and free field were instrumented with 26 strong-motion accelerometers (Werner et al 1987; Zhang and Makris 2001). The bridge was strongly shaken by the magnitude 6.4 Imperial Valley earthquake on 15 October 1979. The free-field PGAs near the pier were 0.32g in the longitudinal direction (north) and 0.30g in the transverse direction. The peak response accelerations recorded on the superstructure were 0.48g and 0.51g in the longitudinal and transverse directions respectively. The bridge was not damaged by the Imperial Valley earthquake.

Painter Street Overcrossing

The Painter Street Overcrossing, located near Rio Dell in northern California is a continuous, two-span, cast-in-place, prestressed post-tensioned concrete box-girder bridge. This 81m long bridge consists of two unequal spans (45m and 36m) supported on integral abutments and a reinforced concrete two-column bent. Both abutments and bent are skewed at an angle of 39. This bridge on Interstate Freeway 101 is typical of short bridges in California that span two- or four-lane divided highways.

The east abutment is monolithic with the superstructure and is supported on 14 concrete friction piles, while the west abutment contains a thermal expansion joint between the abutment diaphragm and the pile cap. The joint consists of a grease-coated metal strip resting on a neoprene strip designed to permit 25mm displacement in both the longitudinal and the transverse directions. The foundation of this abutment consists of 16 concrete friction piles.

The bridge was instrumented in 1977 with 20 accelerometers (Zhang and Makris 2001). Several earthquakes from 1980 to 1987, ranging in magnitude from 4.4 to 6.9, resulted in significant acceleration readings. On 25 April 1992, the bridge was strongly shaken by the magnitude 7.1 Petrolia earthquake with the bridge estimated to be approximately 18km from the fault. The free-field PGAs near the pier were

0.39g in the longitudinal direction and 0.30g in the transverse (north) direction. The peak response accelerations recorded on the superstructure were 0.48g and 1.23g in the longitudinal and transverse directions respectively. Amplified accelerations were recorded on the approach embankments with peaks in the longitudinal and transverse directions of 0.70g and 1.07g respectively. No damage to the bridge was observed following any of these earthquakes.

3 Design considerations

Integral and semi-integral bridges are a common form of construction, both in New Zealand and internationally, and have some marked advantages over other construction forms. Integral and semi-integral bridges aim to minimise the use of bearings and expansion joints by providing a direct connection between superstructure and substructure. This form of construction is often preferred where feasible as it provides a number of advantages over conventional simply supported bridges, including:

- lower maintenance cost
- improved durability
- lower construction cost
- easy to construct
- improved vehicle ride quality.

However, there are a number of issues related to the design and construction of integral bridges which require either further investigation or clearer guidance within a New Zealand-specific context, and these issues are identified and expanded upon throughout this report. They include performance and case studies, non-seismic effects such as concrete creep, shrinkage and temperature, seismic effects and geotechnical issues including soil-structure interaction.

The *Bridge manual* (3rd edition) (NZ Transport Agency 2013) (referred to henceforth as the *Bridge manual*) refers to a variety of design standards, both New Zealand and international, for various topics relating to the design of bridges in New Zealand. These include NZS standards (NZS 3101:2006, NZS 3109:1997, etc), AS standards (AS 3600–2009, AS 5100–2012, etc), AS/NZS standards (AS/NZS 1170:2002, AS/NZS 4671:2001, etc), UK Highway Agency standards (BD 57/01, BD 30/87, BA 42/96), ISO standards, and the AASHTO LRFD bridge design specifications 6th edition, among others. Similarly, a variety of technical reports are referenced, including NZ Transport Agency research reports, fib bulletins, MCEER/ATC guidelines and NZSEE bulletins among others.

The wide range of standards and other technical documents referenced in the *Bridge manual* can lead to ambiguity and confusion over which standard or document to refer to for issues that are not directly addressed in the manual. The purpose of this chapter is to provide a summary of guidelines for New Zealand bridge engineers for the design of integral bridges, including reference to relevant documents where possible.

3.1 Design implications and considerations for integral bridges

The *Bridge manual* specifies the following criteria for the design of bridges with integral and semi-integral abutments:

- Length between rear faces of abutments should not exceed 70m for concrete superstructures and 55m for steel superstructures.
- Abutment piles and surrounding soil should possess adequate flexibility to enable superstructure length changes to occur without structural distress.
- An approach settlement slab should be attached to the back face of the abutment.
- Measures should be taken to ensure the bridge approach remains serviceable.

- Design to avoid collapse under the maximum considered event (MCE), including potential design to withstand the maximum passive pressure capacity, should be able to be mobilised by the soil to act on the abutments.
- Creep, shrinkage and differential temperature effects for integral bridges should be accounted for as per *Bridge manual* provisions for all bridges. (New Zealand mean temperatures can be found from NIWA's New Zealand mean annual temperature (°C), 1971–2000).
- Allowance should be made for both forces and movements resulting from variations in the mean temperature of the structure, as below:
 - for steel structures $\pm 25^{\circ}\text{C}$
 - for concrete structures $\pm 20^{\circ}\text{C}$
- Allowance should be made for stresses and movements, both longitudinal and transverse, resulting from the temperature variation through the depth of the structure. The effects of vertical temperature gradients should be derived for both positive differential temperature conditions (where the top surface is hotter than the average temperature of the superstructure) and negative temperature differential conditions (where the top surface is colder than the average temperature of the superstructure).

For analysis of reinforced concrete members under differential temperature, the properties of the cracked section shall be used

3.1.1 Learnings from existing integral bridges

A review of the earthquake performance of integral abutments on state highway bridges in California, some of which is detailed in section 2.2.2, highlighted the following design considerations:

- Integral abutments are much stiffer than adjacent piers and therefore attract a large part of both the longitudinal and transverse inertia loads from the superstructure. They cannot be designed using a tributary mass approach.
- Earthquake forces on the abutments of long and wide freeway bridges can be large and special consideration is required in the detailing of the diaphragm wall and their foundations to resist these forces.
- Approach slabs, including concrete approach pavement, should be anchored or seated on a wide sill to avoid separation of the slab or pavement from the abutment wall.
- Backfilling behind the abutment with densely compacted cohesionless soils is important and can reduce the longitudinal displacements of straight bridges and the horizontal rotation of skewed bridges.
- Damping in the first longitudinal mode of vibration in shorter bridges is much higher than the 5% typically assumed in design. Damping in the first transverse mode can also be high but is dependent on the amount of relative displacement between the abutment and piers.

A review of the performance of New Zealand bridges with integral abutments also highlighted similar design considerations to those identified in the review of the California bridges. Considerations relevant to New Zealand bridges, which were mainly two lanes wide in comparison to the four or more traffic lanes of the California bridges, were identified as follows:

- On bridges less than 50m in length a large part of the longitudinal earthquake load can be resisted by the abutment walls. This applies to abutments where the backwalls are typically 1.5m or greater in height.
- On bridges longer than approximately 90m, the performance of the abutments and their foundations was much better than predicted by simple static analyses. High damping and travelling wave effects appeared to be significant on these longer bridges, and these effects need to be considered in design.

- While some cracking was observed following earthquake motions, concrete piles cast into abutment backwalls generally performed well.
- None of the abutments on older bridges subjected to strong shaking had settlement or approach slabs. In several cases the settlement of the backfill against the backwalls was significant and sufficient to affect vehicle passage. Better performance would be achieved by using settlement slabs.
- There was no evidence of large longitudinal displacements or significant gapping behind the abutments. Minor cracking developed in flexible pavements, which are common on New Zealand highways, but this was not of any concern and can be easily repaired. Reshaping the pavement to eliminate the settlement step would also eliminate pavement surface cracking. (If significant movement was detected, re-compacting the backfill close to the abutment should be carried out as part of the pavement repair).

3.1.2 Findings from the 1st International Workshop on Integral Abutment/Jointless Bridges

The 1st International Workshop on Integral Abutment/Jointless Bridges was held in Fuzhou, China in March 2014. A summary of the findings presented by international experts throughout the workshop is presented below.

- Integral bridges are often seen as more desirable than non-integral structures because their maintenance costs are reduced significantly due to the absence of movement joints in the superstructure. Additionally, one of the main issues noted with bridge performance is the durability of expansion joints and bearings. As a consequence, integral bridges have been strongly recommended for short-to-medium length bridges where expansion and contraction in the superstructure may be accommodated by flexure in the substructure.
- The most common type of bridge failure during an earthquake is unseating of the superstructure from piers and abutment seats. This is particularly true in bridges with simply supported spans and short seat widths at the supports. Continuous bridges with integral abutments are not susceptible to this mode of failure, which can lead to a marked improvement in their seismic performance over non-integral bridges.
- The positive engagement of the strength and stiffness of the backfill behind the abutment can also be used to attract seismic loads away from the piers, with the added damping in the soil used to reduce superstructure displacements in the longitudinal direction. However, the backfill must be carefully designed to ensure soil yielding occurs in compression in a quantifiable and reliable manner.
- Design of the abutment piles to avoid excessive yielding is critical to the satisfactory performance of integral bridges subjected to seismic actions. There is currently little guidance available for quantifying soil-pile interaction for piles in sloping ground, and further research is required on this issue to determine the capacity and stiffness of such piles. Recent research indicates that the lateral stiffness of piles in slopes up to 45° is up to 50% lower, when pushed away from the slope, than for piles in flat ground.
- Abutment height has a significant influence on pile displacement, with increased abutment heights recommended to increase the length limits of integral bridges to sustain thermal displacements.
- Bridges with skew angle greater than 20° experience significant pile transverse movement, while skewed bridges with skew angles less than 20° exhibited negligible pile transverse movement under seasonal temperature variations.

- A concrete bridge has a longer allowable total length than a steel bridge as the former is less sensitive to seasonal temperature variations.
- All thermal movements of integral bridges occur at the abutments and this area requires special attention to avoid development of a severe 'bump' at the end of the bridge. Finite element analyses show that the zone of surface deformation extends from the back of the abutment a distance equal to approximately three-to-four times the height of the abutment.
- Movement of the abutment into the approach fill develops passive earth pressure that is displacement dependent. Using full passive pressure regardless of displacement is not conservative because it reduces the flexural effects of dead and live load in the bridge girders.
- The soil displacement around the piles is similar to the displacement of the abutment. The relative displacement between the piles and ground is therefore relatively low, resulting in similarly low shear forces at the top of the pile.
- The total lateral movement of the top of the pile relative to the end embedded in the ground is important because it reduces the axial load capacity of the pile. This lateral movement is one of the key variables in assessing the maximum design length of integral abutment bridges. The cyclic nature of these movements raises concern about the vulnerability of piles to cyclic loading.
- Settlement of the approach fill will occur with time. This can be mitigated through the use of well-compacted and well-drained backfill material but cannot be eliminated entirely.

3.1.3 Recommendations from USA practice

The following were the recommendations from the Workshop on Integral Abutments and Jointless Bridges held by the Federal Highway Association (FHWA) in 2005, and represent general practice by USA bridge designers. While not all of the below recommendations are directly applicable to New Zealand design practice, they provide guidance for important design considerations for integral bridges.

- Use embankment and stub-type abutments.
- Use a single row of flexible piles and orient piles for weak-axis bending.
- Use steel piles for maximum ductility.
- Embed piles at least two pile sizes (diameters) into the pile cap to achieve fixity to abutment.
- Provide an abutment stem wide enough to allow for some misalignment of piles.
- Make wingwalls as small as practicable to minimise the amount of structure and earth that displace with the abutment during thermal expansion of the deck.
- For shallow superstructures, use cantilevered turn-back wingwalls (parallel to the centre line of the road) instead of transverse wingwalls.
- Provide loose backfill behind cantilevered wingwalls.
- Provide well-drained granular backfill to accommodate the imposed expansion and contraction.
- Provide drains under and around abutments and wingwalls.
- Encase stringers completely in the end-diaphragm concrete.
- Provide holes in steel beam ends to thread through longitudinal abutment reinforcement.

- Provide temporary support bolts anchored into the pile cap to support beams in lieu of cast bridge seats.
- Tie approach slabs to abutments with hinge type reinforcing.
- Use generous shrinkage reinforcement in the deck slab above the abutment.
- Pile length should not be less than 3m to provide sufficient flexibility.
- Provide pre-bored holes to a depth of 3m for piles if necessary for dense and/or cohesive soils to allow for flexing as the superstructure translates.
- Provide pavement joints to allow bridge cyclic movements and pavement growth.
- Where possible, provide symmetry in integral bridges to minimise potential longitudinal forces on piers and to equalise longitudinal pressure on abutments.
- Provide two layers of polyethylene sheets or a fabric under the approach slab to minimise friction against horizontal movement.
- Limit use of integral abutment to bridges with skew less than 30° to minimise the magnitude and lateral eccentricity of potential longitudinal forces.

3.2 Guidelines for static design of integral bridges

3.2.1 General

Integral bridges should be designed according to the *Bridge manual* using the same limit state principles as any other bridge type.

3.2.2 Structural form

Integral bridges have been mainly constructed fully cast in place but in principle, all forms of integral abutments and joints can be used with any precast bridge girder (Beca and Opus 2008) if the spans are limited up to 30–35m. The selection between precast concrete and steel superstructure forms is governed by functional requirements and project economics in the same manner as for traditional simply supported bridges.

Integral abutment forms such as piled abutments, spread footings, full-height abutments and mechanically stabilised earth (MSE) walls are mainly dictated by geotechnical considerations. However, detailing of the abutment-to-deck joint requires special consideration for precast concrete superstructure, with particular attention required for:

- embedment of precast concrete beams into the abutment
- the reinforcement detail for the moment connection between the abutment and precast beams
- detailed construction staging consideration of beams and abutments for prediction of beam-end rotations due to creep and shrinkage.

The last item above is of particular concern for full monolithic integral bridges. End rotations and longitudinal displacements due to thermal variations are critical for both monolithic and partially precast solutions.

The height of abutment walls is generally governed by geometrics and roading requirements, while the wall thickness is either governed by passive pressure developed from thermal or seismic loads. The relative stiffness per unit metre of the abutment and the deck influences the moment restraint.

3.2.3 Bridge loading

The loads, associated load factors and combinations are specified in section 3 of the *Bridge manual*).

3.2.3.1 Dead and live loads

The magnitude of dead and superimposed dead loads varies according to the bridge geometry. When applying load combination particular consideration must be given to the following:

- maximum and minimum moments at the end bridge deck and abutment sections
- the end moments and section stresses at initial (elastic), infinite (creep, shrinkage and thermal effects included), and any other relevant points in time, accounting for the influence of construction type.

3.2.3.2 Longitudinal braking/traction forces

These forces can be relevant in bridges located in low-seismic areas, as they result in overall longitudinal movements that activate soil pressures at the abutments.

In traditional design, longitudinal forces are distributed to the substructure based on bearing fixity and relative substructure flexibility. For integral bridges, the backfill is in full contact with the end diaphragm and provides a significant amount of stiffness relative to the other substructure components. If the bearing condition is fixed, it is acceptable to assume for bridges with one to three spans that the longitudinal forces are absorbed by the passive pressure and stiffness provided by the backfill soil. However, this should be verified by a geotechnical engineer.

3.2.4 Creep and shrinkage

3.2.4.1 Introduction

Creep and shrinkage need to be considered together as they are dependent on similar parameters. They are time-dependent effects that cause axial shortening and rotation at the girder ends, inducing stresses in the continuous deck. Shrinkage is a form of drying phenomenon caused not only by the withdrawal of free water in the concrete stored in unsaturated air, but also by the volume change of gel particles due to removal of absorbed water. Approximately half of the total shrinkage normally occurs in the first three-to-four months after casting.

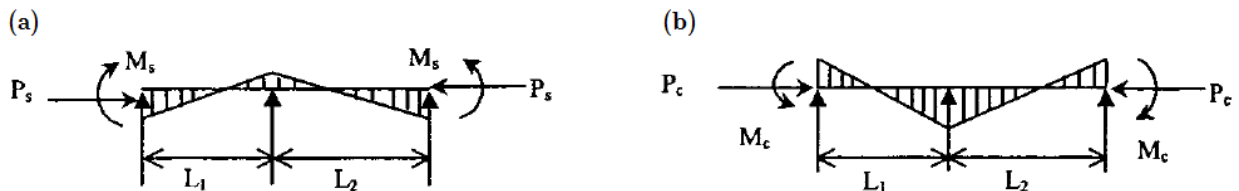
Creep represents the increase in strain over time due to a sustained load that can be represented with an apparent decrease in Young's modulus. Creep is related to moisture exchange between concrete and the surrounding air, and therefore the shape of the section and the perimeter exposed are critical parameters to consider in accounting for creep. Without moisture exchange, creep occurs due to a stress-induced redistribution of capillary water within the structure of hardened cement paste and displacement of gel particles. This kind of creep is called basic creep. Basic creep properties can be obtained by measuring the length change of submerged cylinders with sustained stress. When concrete members are exposed to air, moisture exchange will occur. In addition to basic creep, another type of creep, called drying creep will occur. Drying creep may be caused by many mechanisms such as the migration of solid particles when water is diffusing out of the loaded gel micro-pores, micro-pre-stress or micro-cracking produced by drying.

In traditional simply supported bridges, structural/non-structural elements such as expansion joints, roller supports and abutment bearings accommodate rotations and displacements induced by creep and shrinkage and therefore reduce or minimise secondary stresses through the additional degrees of freedom.

Due to the absence of aforementioned mechanisms to release structural stresses, secondary effects such as creep, shrinkage and thermal gradient have a significant influence on the behaviour of integral bridges.

Concrete creep and shrinkage can reduce the effective pre-stressing force in pre-stressed concrete bridge beams while also causing secondary loads at integral abutments. Figure 3.1 shows an example moment diagram of a two span integral bridge due to concrete creep and shrinkage, illustrating the significant influence of these secondary actions on integral bridges.

Figure 3.1 (a) Moment due to differential shrinkage effects of composite concrete bridges; (b) moment due to creep effects for composite pre-stressed concrete bridges (Arockiasamy et al 2004)



Shortening and rotations induced by the above-mentioned creep and shrinkage are thought to be problems primarily of interest for integral bridges. Calculating these effects for non-integral bridges lacking the associated support restraints is possible, and can be of interest, but requires the definition and quantification of numerous design parameters which are typically difficult to accurately predict.

3.2.4.2 Material and section parameters

Many factors influence the effect of creep and shrinkage on the response of concrete members in integral bridges. Factors influencing concrete shrinkage include water-cement ratio, water content, workability, type and content of aggregate, and relative humidity. Factors that affect concrete creep include sustained stress, concrete strength, type, size and content of aggregate, water-cement ratio, slump, air content, loading age, relative humidity, volume-surface ratio and temperature.

Table 3.1 shows the effect of some of these parameters on concrete creep and shrinkage. Up and down arrows indicate positive and negative correlation, respectively, between the parameter and the expected concrete creep or shrinkage.

Table 3.1 Factors affecting concrete creep and shrinkage

Factors influencing creep	Creep	Factors influencing shrinkage	Shrinkage
Concrete strength	↓	Water to cement ratio	↑
Aggregate content	↓	Aggregate content	↓
Relative humidity	↓	Relative humidity	↓
Slump	↑	Aggregate-cement ratio	↓
Temperature	↑		
Sustained stress up to $0.5f'_c$	↑		
Volume-surface ratio	↓		
Loading age	↓		

There are currently numerous models for predicting the creep and shrinkage of concrete beams, a variety of which have been incorporated into various international design standards including:

- ACI 209R-92
- ACI 209-2004
- CEB-FIP 90
- RILEM-B3 (1995)
- BS 8110-1 (1997)
- SABS0100 (1992)
- AASHTO LRFD (2007)
- fib Model Code 2010
- AS 5100.5 (2004)
- AS 3600 (2009).

The accuracy of the above design models has previously been analysed and compared in various literature, with results showing a variance of at least 25% can exist between the predicted and measured values for all of the models. The *Bridge manual* refers New Zealand bridge designers to AS 3600 for the prediction of creep and shrinkage in concrete structures. The creep and shrinkage models found in several international design standards are compared in appendix A, with a parametric analysis.

3.2.4.3 Unrestrained shortening and rotation

The unrestrained shrinkage strains of beams and decks can be estimated from section 4.2.1 of the *Bridge manual*. Shrinkage strains in slabs are usually larger than those in the beams. Long-term shrinkage strains in service (at time = ∞) are generally in the range of 30–50 $\mu\epsilon$.

Unrestrained creep strains of beams can be estimated by referring to the same section of the *Bridge manual*, considering dead loads and superimposed dead loads. A combination of these loads and pre-stressing force generates an almost uniform stress distribution in the order of ~8–10MPa. Assuming a creep factor of 1.8 (for a 100-day-old beam), the resulting strain is equal to ~60 $\mu\epsilon$.

The shortening due to the combined unrestrained shrinkage and creep effects is greater in precast concrete beams than in the deck, resulting in differing compressive forces acting in the beams and deck. The combined compressive forces generate a hogging moment which results in end rotations, which for a span-to-depth ratio of 1:15 to 1:20 can be estimated as 0.002–0.003 radians.

The maximum thermal strains are of the same order as creep and shrinkage; however, the effect of daily temperature changes is generally greater than the creep-shrinkage effects. Therefore it can be concluded that shortening of the deck will not cause any gap to the abutment

3.2.4.4 Restraint abutment moment

Beam end rotations have a significant effect on design of the bridge superstructure. The restraint moment can build up a factor of $(1-e^{-\phi})$ if simplified creep aging models are adopted (Mattock 1961; Clark 1985).

To maximise the benefit of integral bridges under dead load (DL), superimposed dead load (SDL) and pre-stressing precast concrete beams should be propped before casting the deck and/or casting the wet monolithic joint at the deck-to-abutment connection.

The effect of DL, SDL and pre-stressing can be approximated to a constant hogging moment which, for stiff abutment restraints, will develop a negative restraint moment which is factored by $(1-e^{-\phi})$. If the abutment is flexible with respect to the deck a compatibility relationship at infinite time should be developed at the time of the casting of the wet joint. Effective or age-adjusted modulus can be used to account for creep. For more details refer to appendix C and fib Model Code 2010 (fib 2010).

Regardless of geometry, time of casting and environmental factors the restraint moments at integral abutments can be in the range of 50% to 75% of the fully fixed moment.

3.2.4.5 Effect on integral abutments

Relaxation creep of pre-stressing strands causes sagging moments over the supports due to the restraint conditions of the superstructure at the abutments. The effect of residual creep should be considered starting from the time of casting of the joints. A similar effect occurs at the abutments, for which stiffer abutments will attract larger sagging moments.

Creep due to DL and SDL causes significant hogging moments over the supports.

The moment distribution given by creep, shrinkage and pre-stressing losses can be computed by using simplified algebraic methods without considering the soil-structure interaction (ie no soil springs). The effect of the soil assuming a triangular distribution can be added to if passive pressure is developed.

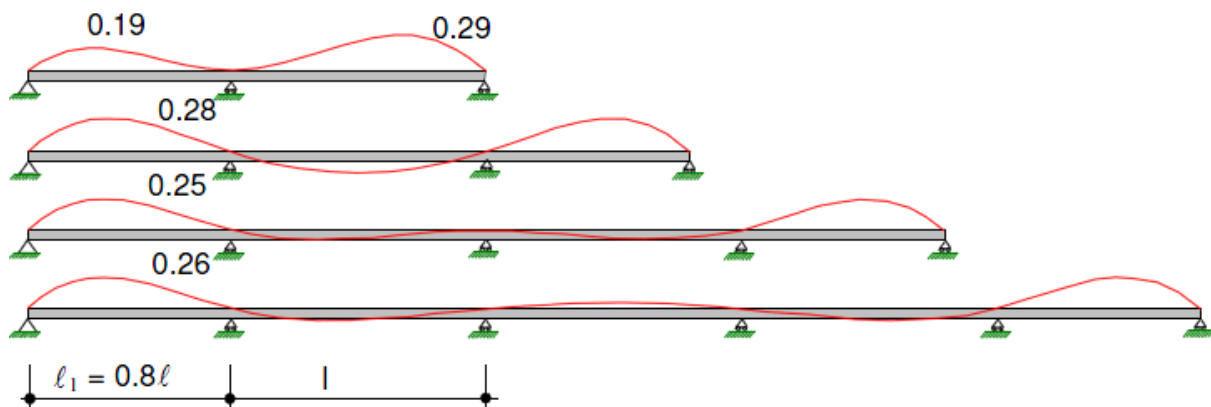
3.2.5 Temperature loading of integral bridges

Differential thermal gradients through the beam depth cause significant internal forces and associated stresses that are important for the deck design. Stresses resulting from temperature variations are one of the key differences between an integral bridge and a jointed one.

Depending on the structural form both longitudinal displacements and end rotations can be significant. Considering a thermal range of 40°C for concrete bridges the total strain will be $480\mu\epsilon$. For a bridge length of 60m this leads to a longitudinal unrestrained displacement of 28.8mm. If the foundations restrain this thermal displacement a considerable axial load will develop in the deck and will be transferred through the abutments.

Thermal variation along the depth of the bridge superstructure can also induce large rotations, which leads to the development of significant secondary moments along the deck and at the supports. Figure 3.2 presents an example of the deformations in two to five-span integral bridges due to differential thermal gradients in the superstructure (Burdet 2010).

Figure 3.2 Schematic deflection of superstructure of integral bridges due to change of temperature



The continuity from superstructure to substructure in integral bridges results in the transfer of thermal deformations induced in the bridge deck into the abutment walls, piles and surrounding soil. The complex nonlinear soil-structure interaction resulting from these deformations is compounded by secondary stresses resulting from creep, shrinkage and other effects. The magnitude and mode of deformation, the overall soil response and the overall structural response are heavily influenced by the level of compaction in the granular fill behind the abutment walls and adjacent to the piles along with the relative flexural stiffness of the bridge deck, abutment wall, foundation piles, lateral pressure of soil behind the wall and confining stress level in the soil (Shah et al 2008).

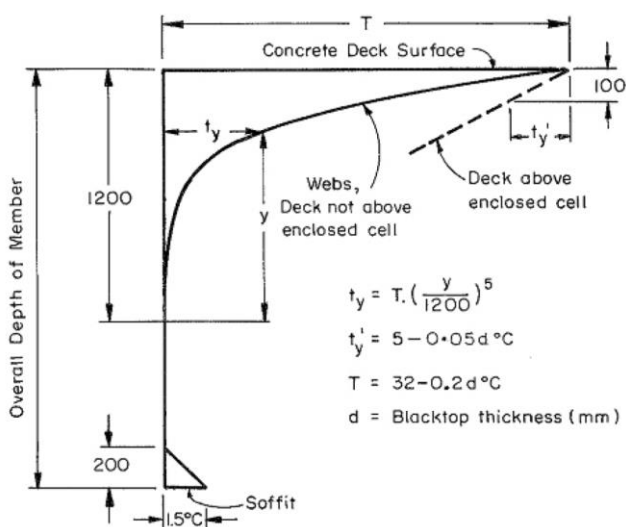
Previous research has determined that the parameters affecting thermal behaviour of integral bridges can include (Olson et al 2013):

- overall bridge length
- abutment skew
- span between intermediate supports
- pile type, size, and orientation
- live loading
- abutment-backfill type and compaction
- strength of the soil surrounding the piles
- girder size and type (pre-stressed concrete vs steel)
- time-dependent behaviour of concrete, including shrinkage
- abutment depth.

3.2.5.1 An analytical model to calculate stresses due to temperature gradients

A simple analytical method has been developed which can be utilised by designers to calculate thermally induced stresses in integral bridge superstructures. The *Bridge manual* guidance for temperature profile in a beam, as shown in figure 3.3, has been adopted in this method. According to the *Bridge manual*, the overall temperature changes are $\pm 25^\circ\text{C}$ for steel structures and $\pm 20^\circ\text{C}$ for concrete structures.

Figure 3.3 Temperature variation with depth



Source: NZ Transport Agency (2013)

The proposed analytical method comprises two main steps (Priestley and Buckle 1979):

- 1 Self-equilibrating stresses are calculated by considering the bridge as simply supported.
- 2 The stresses caused by support fixity at the abutments and piers (called continuity stresses) are calculated based on consideration of the implied boundary conditions and added to the self-equilibrating stresses.

Step one:

Since the temperature gradient is nonlinear, it produces a nonlinear free-strain distribution over the cross section. However, for the assumption of plane sections remaining plane to hold true, self-equilibrating stresses must be generated to balance the free strain distribution. Superposition of the two aforementioned stresses results in the 'real strain' with linear distribution for the statically-determinate simply-supported bridge case (Priestley and Buckle 1979).

The self-equilibrating stress can be calculated by equation 3.1, with reference to the appropriate literature (Priestley and Buckle 1979) and the design example in appendix D:

$$\begin{aligned} \begin{Bmatrix} \varepsilon_b \\ \varepsilon_t \end{Bmatrix} &= \begin{bmatrix} \sum_{n=1}^n \left[\left(1 - \frac{y_n}{h}\right) A_n \right] & \sum_{n=1}^n \left[\frac{y_n}{h} A_n \right] \\ \sum_{n=1}^n \left[\left(1 - \frac{y_n}{h}\right) A_n y_n \right] & \sum_{n=1}^n \left[\frac{y_n}{h} A_n y_n \right] \end{bmatrix}^{-1} \begin{Bmatrix} \sum_{n=1}^n A_n \varepsilon_{fn} \\ \sum_{n=1}^n A_n y_n \varepsilon_{fn} \end{Bmatrix} \\ \varepsilon_{Rn} &= \left(1 - \frac{y_n}{h}\right) \varepsilon_b + \frac{y_n}{h} \varepsilon_t \\ \varepsilon_{sen} &= \varepsilon_{Rn} - \varepsilon_{fn} \\ \sigma_{sen} &= \varepsilon_{sen} E \end{aligned} \tag{Equation 3.1}$$

where:

ε_b = real strain at the bottom of the cross section

ε_t = real strain at the top of the cross-section

y_n = distance from the bottom to the centroid of the nth layer

A_n = area of the nth layer

h = height of the cross section

ε_{fn} = free strain at an nth layer

ε_{Rn} = real strain at an nth layer

ε_{sen} = strain due to self-equilibrating stresses at an nth layer

σ_{sen} = self-equilibrating stress at an nth layer

Figure 3.4 shows the deflection and rotation of the simply supported model. The rotation and maximum deflection at the mid-span of the simply supported bridge can be determined as follows by equation 3.2:

$$\begin{aligned} \theta &= \frac{\varepsilon_t - \varepsilon_b}{h} \\ \Delta &= \frac{\theta L^2}{8} \end{aligned} \tag{Equation 3.2}$$

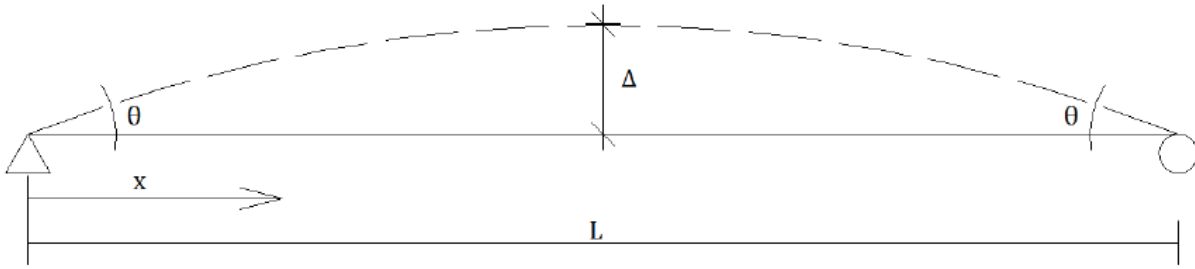
where:

θ = rotation

Δ = deflection at mid-span of simply supported bridge

L = length of the bridge

Figure 3.4 Deformation of a simply supported bridge due to temperature variations



Step two:

Since integral bridges are not simply supported, support conditions should be applied. The support conditions are dependent on the bridge arrangement. For a two-span bridge, shown in figure 3.5, the moments and forces required to change from the simply-supported condition to the integral condition is shown in figure 3.6, with the equations below defining this behaviour.

Figure 3.5 Structural model of a two-span integral bridge

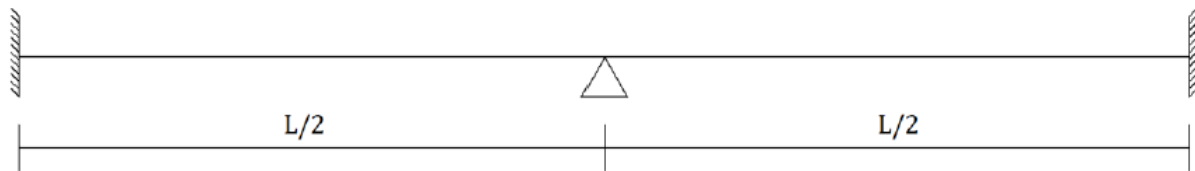
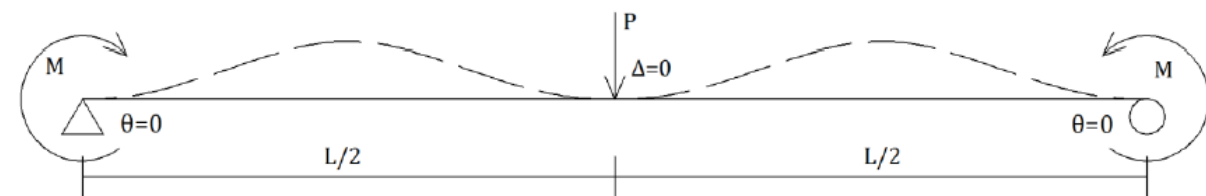


Figure 3.6 Actual boundary condition of a two-span integral bridge



$$\frac{ML}{2EI} + \frac{PL^2}{16EI} = \theta \tag{Equation 3.3}$$

$$\frac{ML^2}{16EI} + \frac{PL^3}{38EI} = \Delta$$

The total stresses can be calculated by combining continuity stresses and self-equilibrating stresses as in equation 3.4:

$$\sigma_{cn} = \frac{M(y_c - y_n)}{I} \tag{Equation 3.4}$$

$$\sigma_{Tn} = \sigma_{sen} + \sigma_{cn}$$

where:

M = internal moment at examined cross section

σ_{cn} = continuity stress at the nth layer of the examined cross section

y_n = distance from the bottom to the centroid of the cross section

I = moment of inertia of the cross section

y_c = distance from the bottom to the centroid of the nth layer

σ_{Tn} = total stress at the nth layer of the examined cross section

Appendix D provides a set of example calculations to thoroughly demonstrate this method.

3.2.5.2 Effect on integral abutments

Thermal contraction generates minimal earth pressures at the abutments, and the gap formed behind the abutments is negligible if the bridge is less than 100m in length.

Thermal expansion leads to significant earth pressures generated at the abutment wall, which can be critical. The actual earth pressure is generally lower than the full passive pressure, and should be calculated using a soil-spring model with realistic soil parameters. Lower and upper bound analyses, using the shallowest and deepest soil layers respectively, should be carried out to determine the sensitivity of the structure to the soil parameters used. Soil effects are more significant for full-height abutments than piled foundations/abutments.

3.3 Guidelines for seismic design of integral bridges

There are no well-established earthquake design procedures for bridges with integral abutments. Detailing of the abutment and the associated soil-structure interaction at the abutment and in the foundations needs careful consideration but the methods of analysis used for bridges with separated abutment structures are generally applicable.

3.3.1 General considerations

The following issues relating to the seismic performance of integral bridges should be taken into consideration during design:

- Approach slabs, including concrete approach pavement, should be anchored or seated on a wide sill to avoid separation of the slab or pavement from the abutment wall.
- Integral bridges should be designed to avoid collapse under the MCE, including allowance for potential mobilisation of full passive pressure at the abutments.
- Integral abutments should not be designed using a tributary mass approach as the stiffness of integral abutments is considerably higher than that of adjacent piers and therefore integral abutments attract a large proportion of both longitudinal and transverse superstructure inertia loads.
- Detailing of the diaphragm wall and foundations of the abutments of large and wide bridges requires special consideration due to the expected large seismic forces.
- Backfilling behind the abutment with densely compacted cohesionless soils should be adopted where possible as it can reduce the longitudinal displacements of straight bridges and the horizontal rotation of skewed bridges.
- Damping in the first longitudinal mode of vibration in shorter bridges is much higher than the 5% generally assumed in design. Damping in the first transverse mode can also be high but is dependent on the relative displacement between the abutment and piers.
- The influence of high damping and travelling wave effects on the performance of longer bridges (longer than 90m) is significant and needs to be considered through detailed analysis methods.

- The use of settlement slabs is highly recommended to reduce the effect of backfill settlement on post-earthquake performance.
- The most common type of bridge failure during an earthquake is unseating of the superstructure from piers and abutment seats. This is particularly true in bridges with simply supported spans and short seat widths at the supports. Continuous bridges with integral abutments are not susceptible to this mode of failure, which can lead to a marked improvement in their seismic performance over non-integral bridges.
- The positive engagement of the strength and stiffness of the backfill behind the abutment can also be used to attract seismic loads away from the piers, with the added damping in the soil used to reduce superstructure displacements in the longitudinal direction. However, the backfill must be carefully designed to ensure soil yielding occurs in compression in a quantifiable and reliable manner.
- The influence of sloping ground on the lateral stiffness of piles needs to be considered where applicable.
- For integral bridges with steel superstructure, holes should be provided in the steel beam ends to thread through longitudinal abutment reinforcement.
- Where possible, provide symmetry in integral bridges to minimise potential longitudinal forces on piers and to equalise longitudinal pressure on abutments.

3.3.2 Structural form

The shape of the abutment and height of the abutment walls will generally be determined by other design considerations rather than seismic performance.

The elastic response of the backwall, represented by the initial stiffness at small displacements, is almost independent of the wall height but the ultimate passive resistance is proportional to the square of the wall height so generally there are advantages in having the backwall as high as practicable.

The main advantage of using an integral abutment is the elimination of joints and as such most multi-span bridges with integral abutments are also continuous over the piers. Unless the bridge is founded on rock or very firm soil the abutments and piers of continuous bridges should be founded on piles. Single-span bridges will generally perform satisfactorily with spread footing foundations but soil improvement or the use of MSE walls beneath the footings will be required on soft soil sites.

Semi-integral abutment types where the bridge is supported on bearings at the abutments may provide satisfactory earthquake performance. For this type of abutment the superstructure end diaphragm wall needs to be relatively deep. Alternatively a friction slab can be used to provide both longitudinal and transverse resistance at the abutments.

3.3.3 Analysis method

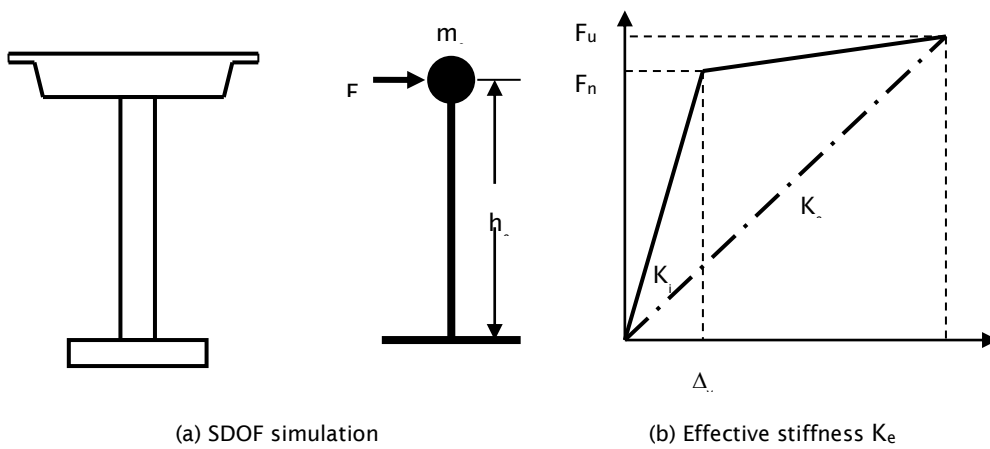
The displacement-based design (DBD) method is recommended for the analysis of bridges with integral abutments. This analysis method provides a more acceptable method of allowing for the relative stiffness of the piers and abutments, and the effects of soil-structure interaction damping from the sub-structure components than force-based design (FBD) procedures. FBD may still be appropriate for some bridges, such as those in low seismicity regions. However, the DBD method has been included as one of the recommended design methods in a recent draft amendment to section 5 of the *Bridge manual* and the DBD provisions in this draft document are recommended for integral abutment bridges. The use of DBD is particularly appropriate for integral bridges due to the significant influence of soil-structure interaction on

the longitudinal response and influence of geometric parameters (abutment width, abutment-deck connections, pier height profile) especially on the transverse response of bridges.

The procedure for displacement-based seismic design of bridges has been outlined in detail by Priestley et al (2007) and is only briefly described here. There are four stages in the process:

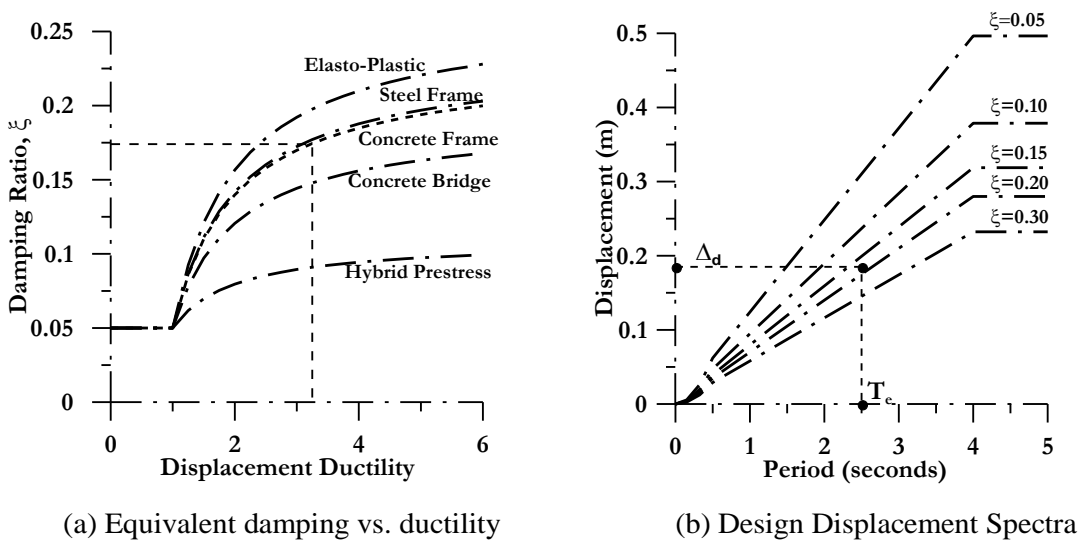
- 1 Representation of the bridge as an equivalent single degree of freedom (SDOF) structure (figure 3.7 (a)).
- 2 Representation of the seismic response by the effective stiffness at the design response displacement (figure 3.7 (b)).

Figure 3.7 Single degree of freedom bridge system



- 3 Determination of relationship between displacement ductility demand and equivalent viscous damping (figure 3.8 (a)).
- 4 Representation of seismicity by displacement spectra for different levels of equivalent viscous damping (figure 3.8 (b)).

Figure 3.8 Design damping and spectra



The design procedure is typically represented by the following sequence:

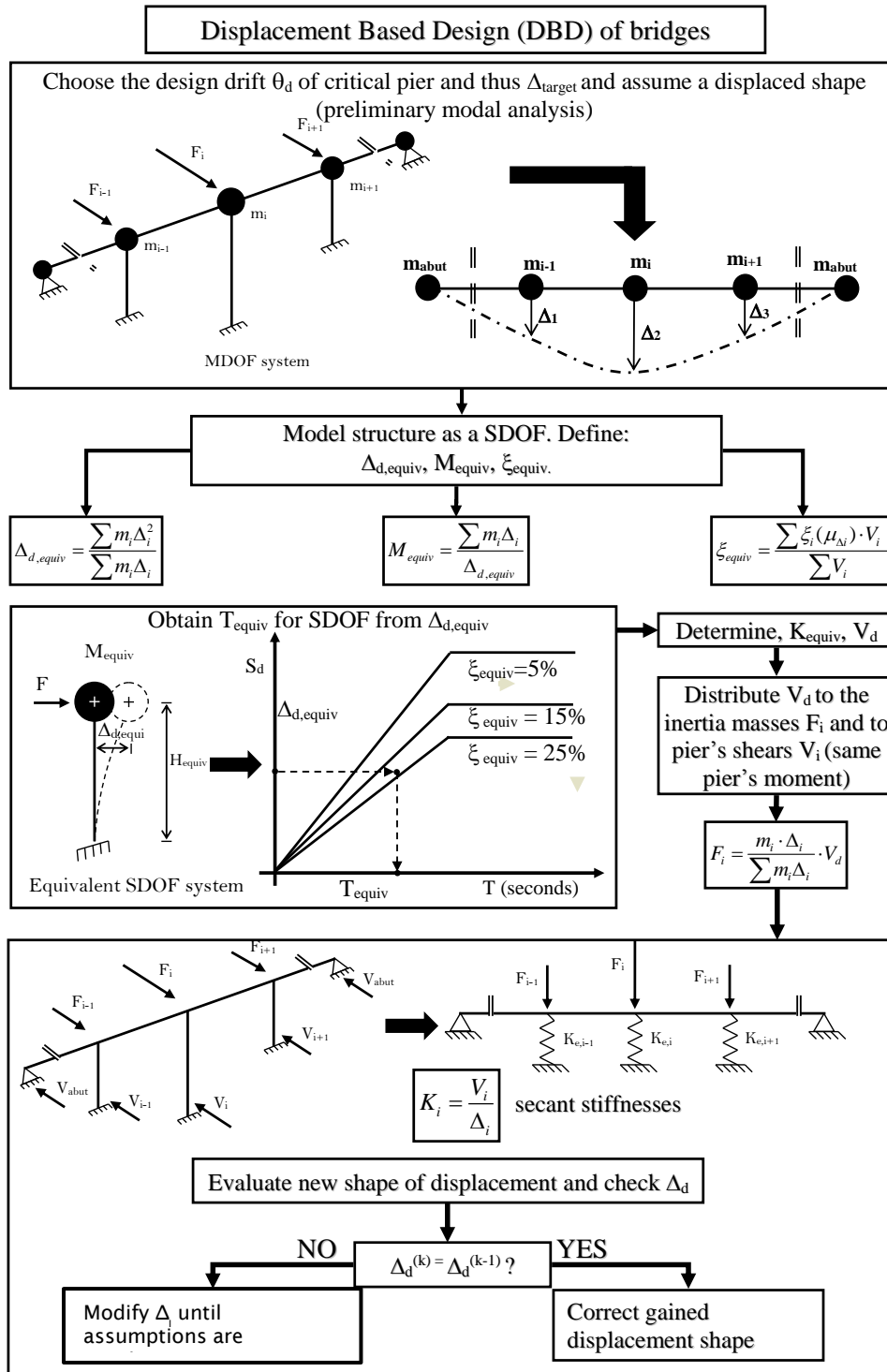
- 1 Determine the critical displacement capacities of the piers from code-specified strain or drift limits.
- 2 Estimate the inelastic mode shape and hence determine the critical pier.
- 3 Scale the inelastic mode shape so the critical pier just reaches its limit state.
- 4 Determine the characteristic equivalent SDOF displacement and mass for the bridge.
- 5 Determine the equivalent viscous damping for the bridge from the damping of the individual components (piers and abutments).
- 6 From the design displacement response spectra set with the characteristic displacement and equivalent viscous damping, determine the effective period at peak displacement response.
- 7 From the calculated period, determine the equivalent effective stiffness.
- 8 From the effective stiffness and the characteristic displacement, determine the frame design lateral earthquake force (total base shear).
- 9 Distribute the design force to the mass locations in proportion to mass and displacement.
- 10 Analyse the frame, using effective stiffness values for the piers, to determine moments in plastic hinges.
- 11 Use capacity design principles to determine required shear strength.

Under longitudinal seismic response the design displacements will be the same for all piers and the integral abutments. If the pier heights are different, yield displacements will differ, and hence the ductility demand and the damping will be different for the different piers and abutments. The effective damping for each pier and abutments should include contributions from structural deformation of the pier or abutment, and from foundation and bearing compliance, where appropriate.

Under transverse response, the design displacement at each pier and the abutments will generally be different, depending on the transverse mode shape. The analysis may require iteration when the seismic inertia forces are carried by two or more different load paths (eg superstructure flexure to abutments and pier inelastic bending to the pier foundations). An initial estimate of the proportion of the total seismic inertia forces carried by superstructure flexure can be made, enabling the system damping to be found. This can be checked by structural analysis after the design base shear is determined and the seismic forces are distributed to the different mass locations. A flow chart illustrating the DBD procedure for a bridge is shown in figure 3.9.

The final design of all bridges with significant irregularity of structural form resulting from high horizontal curvature and/or adjacent piers of significant difference in stiffness should be verified by modal response spectrum analysis using effective member stiffness at expected maximum displacement demand together with appropriate damping levels, or non-linear time-history analysis.

Figure 3.9 Flow diagram of displacement-based design procedure



Source: Palermo and Pampanin (2008)

3.3.4 Abutment stiffness

The stiffness of the soil against the abutment walls is best represented in the bridge model by Winkler springs, which can also be used to model the soil surrounding any abutment piles and under the footing

where appropriate. The backwall springs should be determined using the hyperbolic force-displacement (HFD) relationship presented by Khalili-Tehrani et al (2010). This relationship has been calibrated against earlier log-spiral hyperbolic force-displacement models (Shamsabadi et al 2004; 2005; 2006; 2007) which in turn were calibrated against several small-scale and full-scale tests of abutment walls and pile caps. The form of the HFD equation is:

$$F(y) = \left(\frac{a_r y}{H + b_r y} \right) H^n \quad (\text{Equation 3.5})$$

where:

F and y = lateral force per unit width of the backwall and the deflection respectively

parameters a_r and b_r = height-independent parameters that depend only on the backfill properties

H = backwall height.

A particular advantage of the above HFD equation is that the parameters are defined in terms of soil internal friction, cohesion, unit weight and soil strain at 50% of the ultimate stress. These parameters can be determined by soil testing and in many cases can be estimated without testing. The soil strain at 50% of ultimate stress can be estimated from typical values for different soils published by Shamsabadi et al (2007; 2009) and Khalili-Tehrani et al (2010).

The HFD equation is strictly only applicable for a wall that is uniformly translated against the backfill. In many applications the wall will rotate as well as translate against the backfill and for these cases it is best to represent the force against the backfill by a series of Winkler springs over the height of the wall. The force-displacement relationship for each spring should be based on assuming a linear increase of stiffness with depth and with the total stiffness of the springs adding to the stiffness represented by the HFD equation.

The Winkler springs for the piles should be based on nonlinear P-Y curves derived by the method of Lam and Martin (1986), as presented in Volume II of *Seismic Design Highway Bridge Foundations* (FHWA/RD-86/102, 1986).

The passive resistance and stiffness of abutment walls is reduced by skew angles. Passive force-deflection curves for skewed abutments based on laboratory testing of model walls have been presented by Jessee and Rollins (2013) and compared with numerical studies undertaken on skewed abutments by Shamsabadi et al (2006). Reference should be made to these papers to derive appropriate reduction factors and force-displacement curves for design.

3.3.5 Abutment damping

The damping associated with abutment dynamic cyclic loading can be estimated from the test results of Rollins et al (2010), which included full-scale tests on a pile cap to quantify the effects of cyclic and dynamic loading on the force-displacement relations for typical pile caps and abutment walls. A range of backfill conditions was investigated, including no backfill, loosely and densely compacted clean sand, loosely and densely compacted fine gravel and loosely and densely compacted coarse gravel. The research concluded that the response of pile caps and abutment structures on piles subject to variable frequency loadings can be quantified using an average damping of at least 15%. The precise damping depended on whether the inertial and total earth pressure forces acted in phase or out of phase. The values measured during slow cyclic loading appear to be appropriate for most bridge abutment applications. Median values for densely compacted sand, fine gravel and coarse gravel were all about 18% (slightly greater at 19% for fine gravel).

3.3.6 Backfill soil and strength parameters

A densely compacted coarse gravel should be used as backfill material when this type of material is available. Based on the results of their pile cap tests, Rollins et al (2010) made the following comments on backfill soils:

- Given the dramatically different load-displacement response of loosely and densely compacted soils, engineering professionals should take significant measures to assure that backfill compaction requirements are met and that those requirements result in a high relative density if significant passive earth force is required.
- For the design of concrete foundations and abutments backfilled with well-compacted granular materials, in the order of 95% modified Proctor density or 75% relative density, the log-spiral approach can be used with a soil friction angle of 40°C and a wall friction/soil friction ratio of 0.6 to 0.75 to determine the passive earth force. These parameters should give a lower-bound solution to the passive response of backfill subjected to static, cyclic and dynamic loadings. The designer who has performed field shear strength testing and is confident in the resulting parameters can use them in determining a larger passive earth force, noting that calculated passive earth coefficients increase 10% to 15% for each 1°C increase in the soil friction angle beyond 40°C.

Under longitudinal earthquake loading overestimating the stiffness of the soil will lead to a conservative estimate of the pressures on the wall, whereas underestimating the soil stiffness will lead to a conservative estimate of the proportion of the superstructure inertia load carried on the piers. For design it is important that the maximum likely forces on the abutment walls and piers be evaluated using upper and lower bound soil strength parameters.

The length of the compacted zone of backfill should extend for at least the height of the wall behind the backface of the abutment and vertically below the bottom of the wall about 25% of the height of the wall. Reference should be made to the test results in Rollins et al (2010) for appropriate soil strength parameters if densely compacted coarse gravels are not used as backfill.

3.3.7 Soil gapping effects

There is very little published material available for determining the magnitude of the gap between the backfill and the wall that may develop under cyclic loading at large displacements. In the Rollins et al (2010) experimental tests, gaps did not develop as the pile cap was jacked further against the backwall after completing each set of static cyclic and dynamic loading tests and did not cycle back to the initial displacement position or in the opposite direction.

Static cyclic load tests reported by Rollins and Cole (2006) on a full-scale pile cap indicate that gaps of 50% to 70% of the peak displacement may develop in a coarse gravel backfill. However, these tests do not simulate the inertia loads in the backfill that arise in strong shaking. Cyclic inertia loads in the backfill force the backfill material back against the backwall to potentially develop active pressures against the backwall.

For time-history analyses it is recommended that the sensitivity of gapping effects be investigated by assuming that in the worst case a gap of 30% of the peak passive displacement develops.

The impact of gapping on dynamic response can be reduced by using friction slabs. Settlement slabs should be anchored to the abutment and be located at a depth of approximately 1 m so that they effectively act as friction slabs and improve the bridge performance by reducing any gapping and increasing the damping. Sliding of settlement slabs and abutment footings is a very effective method of increasing damping.

3.3.8 Modelling recommendations

The appropriate procedure for modelling integral bridge abutments will depend on the level of design complexity required and the software package used by the designer. However, irrespective of either, designers should account for the following when modelling the behaviour of integral bridge abutments:

- The stiffness of the soil behind the abutment wall in the longitudinal direction should be modelled using soil springs.
- The interaction between piles and the soil should be modelled using Winkler springs applied in the longitudinal and transverse directions. The recommendations of section 3.3.9 should be referred to for piles in sloping ground.
- Connections between the piles, abutment, and bridge superstructure should be modelled to reflect the intended connection between the respective elements, including moment-rigidity.
- Where seismic inertial loads are expected to be significant, non-linear soil springs should be used to account for potential soil yielding and the associated influence on pile and abutment response.
- The influence of backfill on transverse abutment response is minimal, and therefore the transverse stiffness of abutments is primarily composed of pile stiffness and stiffness of the surrounding soil.

3.3.9 Piles in sloping ground

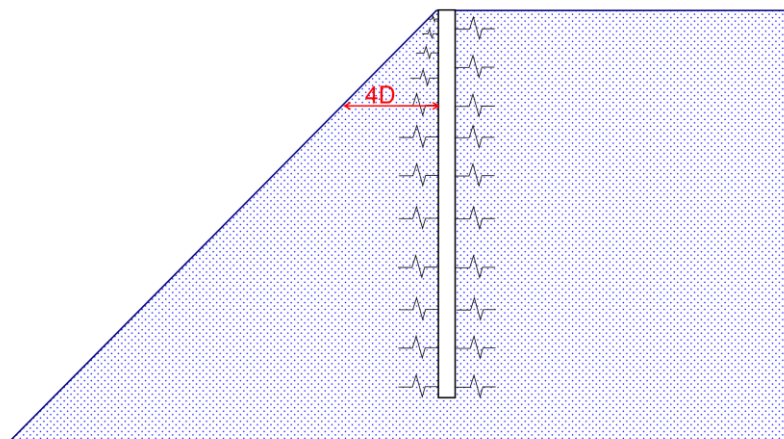
The stiffness of soils in sloping ground is of particular relevance for bridge abutments, with ground often sloping away from the abutments. Bridge abutment piles are often located at the crest of sloping ground, and therefore the influence of sloping ground on the lateral stiffness of soils should be considered.

The following approach is recommended to account for the influence of the sloping ground on pile response:

- For ground sloping up away from the pile, the same soil springs should be applied to the piles as for horizontal ground.
- For ground sloping down away from the pile, the soil springs applied to the piles should vary linearly from 0 at the top to the full soil springs (as for horizontal ground) at a depth at which the slope width is four times the pile diameter. This approach is shown schematically in figure 3.10.

Alternatively, the recommendations set out in Georgiadis and Georgiadis (2010) can be adopted where more detailed modelling and analysis is required.

Figure 3.10 Piles in sloping ground



3.4 Guidelines for geotechnical design of integral bridges

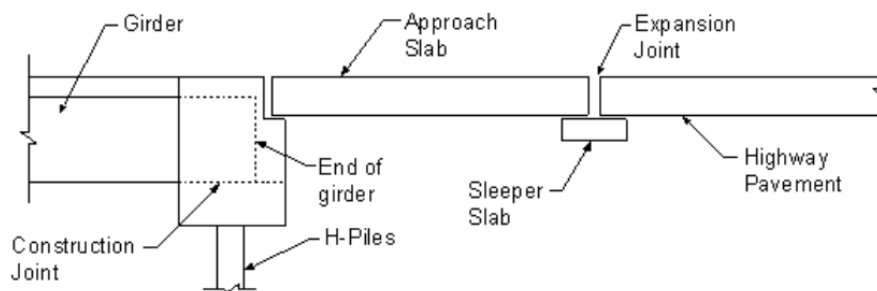
3.4.1 General

Integral abutments should be designed to resist creep, shrinkage and thermal deformations of the superstructure. Assessment of movement should consider temperature, creep and long-term pre-stress shortening in determining potential movements of abutments. As temperatures change daily and seasonally, the length of an integral bridge varies, pushing the abutment against the approach fill and pulling it away. As a result the bridge superstructure, the abutment, the approach fill, the foundation piles and the foundation soil are all subjected to cyclic loading. Understanding their interactions is important for effective design and satisfactory performance of integral bridges.

Geotechnical design of integral bridges and integral bridge abutments should be carried out generally in accordance with the *Bridge manual*, in which the geotechnical provisions are generally based on the provisions of BA 42/96. This section presents additional design requirements and considerations which are recommended for the geotechnical design of integral bridges.

Figure 3.11 schematically shows the main elements of an integral bridge system, which consist of bridge deck, girders, integral cast abutments and approach slabs. The bridge movement is accommodated at the ends of the approach slabs, with sleeper slabs often used to provide vertical support at this location.

Figure 3.11 Elements of an integral bridge system



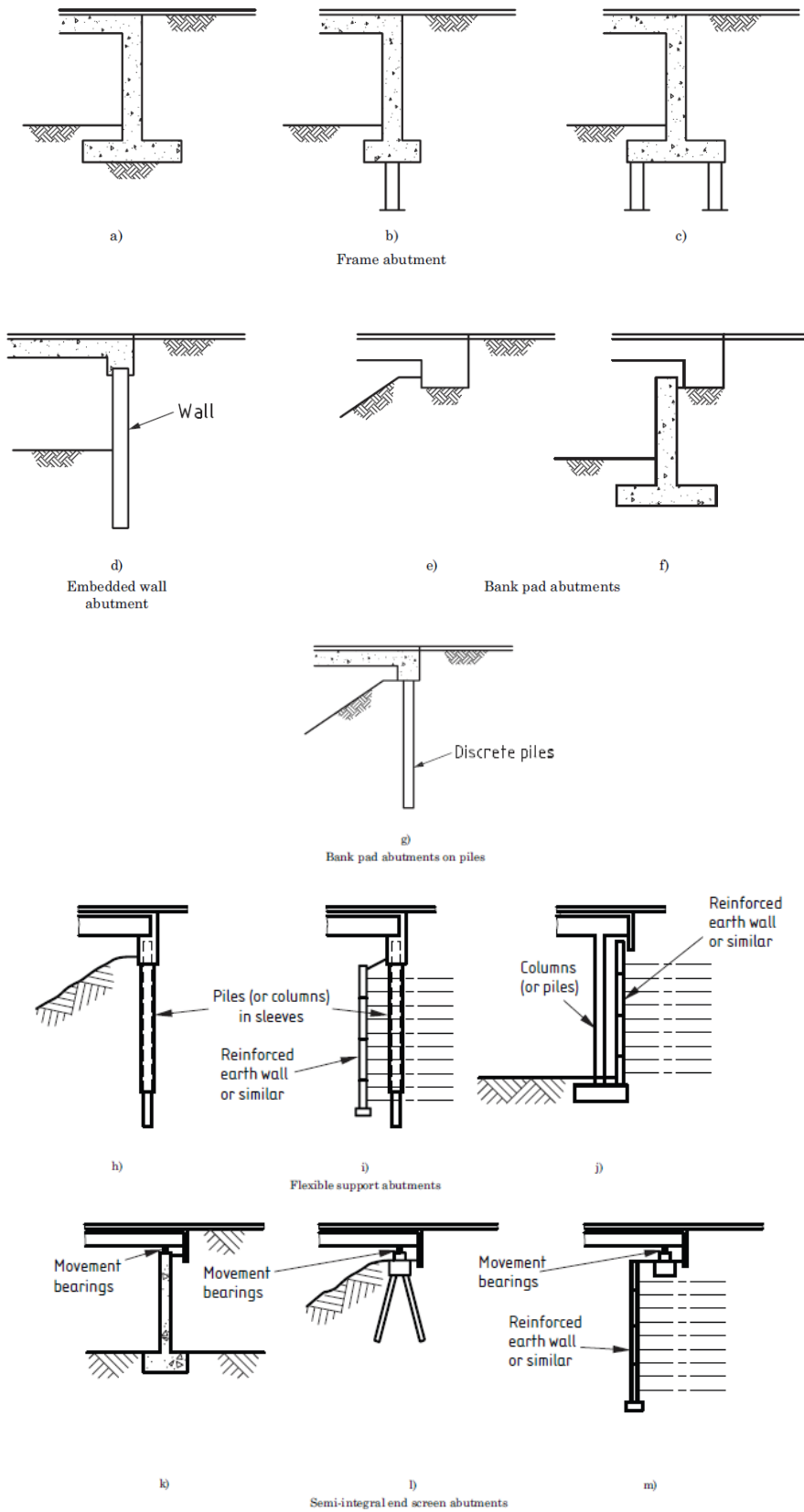
3.4.2 Types of abutment for integral bridge construction

There are three main categories of abutment used with integral bridges:

- 1 full height frame abutments shown in figures 3.12a, 3.12b and 3.12c)
- 2 embedded wall abutments shown in figure 3.12d
- 3 end screen abutments shown in figures 3.12e to 3.12m).

End screen abutments include bank pad abutments (supported on ground or on piles), flexible support abutments and semi-integral abutments, where the earth pressure resisting expansion is applied to the end screen at the end of the deck only.

Figure 3.12 Types of abutment for integral bridge construction



3.4.3 Approach system

The approach system of an integral bridge consists of the backfill, the approach fill, an approach (or settlement) slab and the foundation soil.

Integral bridges are vulnerable to differential settlement between the approach system and the bridge abutment, resulting in a noticeable 'bump' near abutments. These bumps may occur due to the following (Arsoy et al 1999):

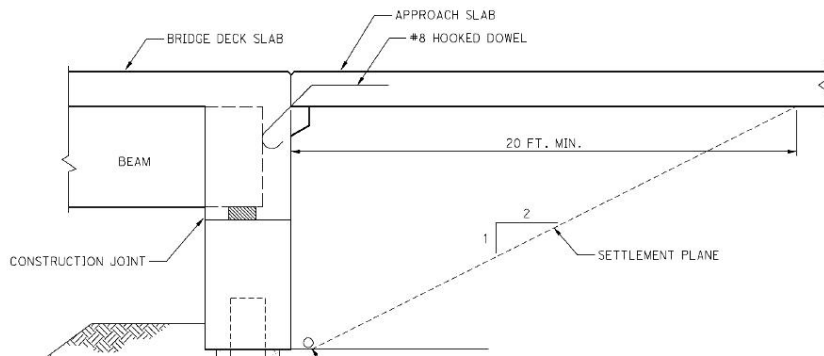
- significant earth pressure against the abutment wall due to cyclic bridge expansion (ie cyclic compression and decompression of the backfill due to temperature cycles)
- settlement of in-situ soil under the approach embankment (when in-situ soils are soft or compressible)
- settlement of abutment structural foundation
- consolidation of fill material (for poor fill materials and poorly compacted fills)
- high traffic loads
- poor drainage of fill
- loss of fill by erosion.

The intended function of an approach slab is to span the void that may develop beneath the slab, provide a ramp for the differential settlement between the abutment and the embankment, and to seal against water percolation and erosion of the backfill material. A void between the backfill and the abutment is likely to develop for integral bridges due to abutment movement. However when an approach slab is used, the 'bump' occurs at the end of the approach slab.

The length of the zone of surface deformation extends from the abutment at a distance equal to twice the height of the abutment, and therefore the length of the approach slabs should be two to three times the height of the abutment. This recommendation is based on the fact that a displacing abutment causes movement of a wedge of the backfill with a height equal to the height of the abutment and a length equal to $\tan(45+\phi/2)$ times the height of the abutment, which is roughly twice the abutment height.

The minimum recommended length of the approach slab for both integral and semi-integral abutments is 6m. The approach slab should be positively attached to the backwall by reinforcing bars anchored as shown in figure 3.13 (Arsoy et al 1999), but creating a moment connection between the approach slab and the deck slab is not recommended. The connection should be detailed to act as a pin with tension steel transferred across the approach span into the backwall of integral and semi-integral abutments. The detail should allow for some tolerance between the slab and the corbel such that no damage occurs due to settlement.

Figure 3.13 Positive connection of approach slab to backwall

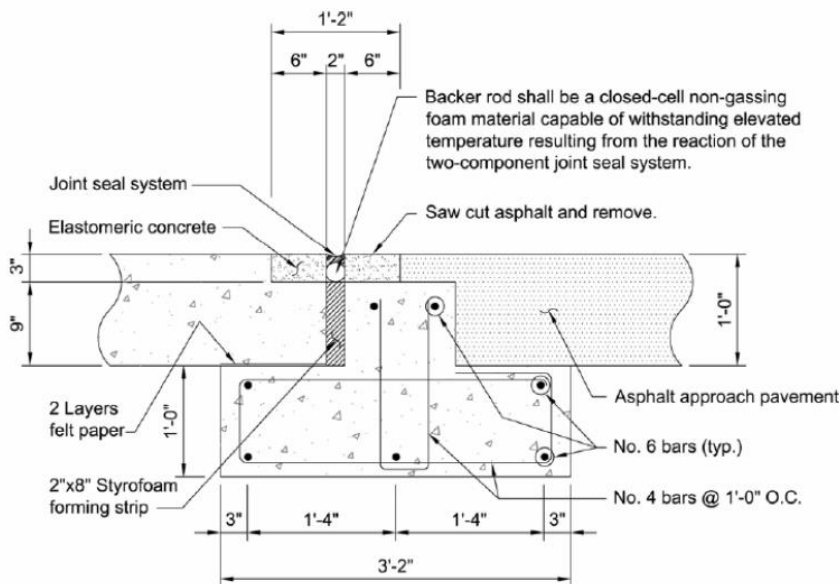


Source: Arsoy et al (1999)

A final consideration for the approach slab is the development of compression forces. Sufficient allowance for expansion of the superstructure must be accommodated in the sleeper slab. Otherwise compression can be introduced into the slab by closing the expansion gap and subsequently activating the passive pressure behind the sleeper slab, or from contact with the adjacent roadway pavement. The latter can often be a major issue for spalling and buckling of the adjacent pavement.

A sleeper slab is placed at the roadway end of the approach slab. The intent of this slab is to provide a relatively solid foundation for the far end of the approach slab and to provide a location for limited expansion and contraction. A typical detail, recommended by Wasserman and Walker (1996), is shown in figure 3.14. A disadvantage of this sleeper slab detail is the potential for pavement cracking in thin sections of pavement.

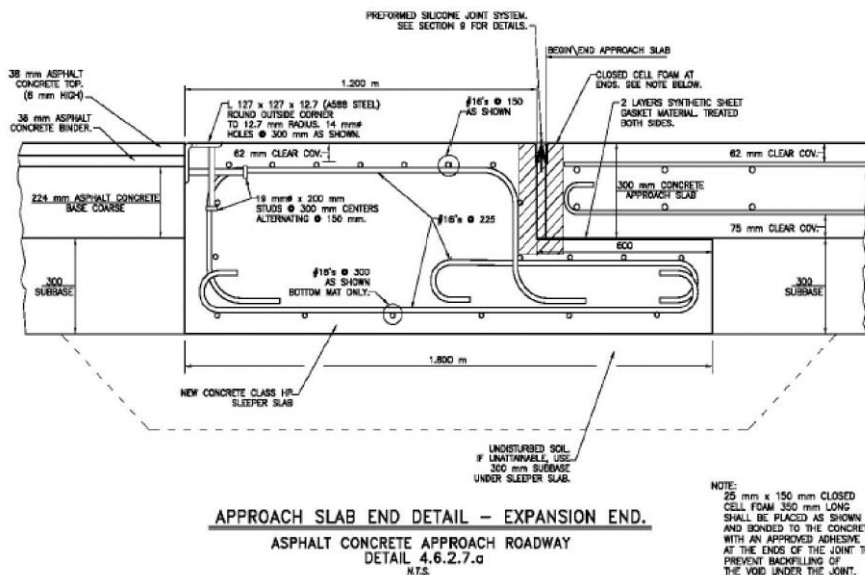
Figure 3.14 Suggested sleeper slab details - dimensions in imperial units



Source: Wasserman and Walker (1996)

In a modified sleeper slab detail developed by the New York State Department of Transportation, the stem of the sleeper slab extends to the pavement surface and therefore a sharp change in pavement thickness is avoided and potential for pavement cracking is substantially reduced (figure 3.15).

Figure 3.15 Detail of a sleeper slab with asphalt pavement approach developed by New York State Department of Transportation – dimensions in imperial units



Source: Azizinamini et al (2013)

3.4.4 Mitigation of approach system settlements

To ensure efficient performance of the approach system, the following issues should be carefully considered and addressed during the design and construction of integral bridges (Arsoy et al 1999):

- The cyclic nature of the abutment movement will loosen dense backfill and densify the loose backfill within the close proximity of the abutment. In other words, deformation induced by the abutment results in a density that is independent of the initial density of the backfill material. Therefore, the use of very dense backfill is not likely to reduce settlement associated with moving abutments. As such, approach slabs or continuous pavement patching are normally required to compensate for the anticipated approach fill settlement.
- An efficient drainage system should be incorporated in the design. To avoid water intrusion behind the abutment the approach slab should be connected directly to the abutment and appropriate provisions made to provide for drainage of any entrapped water.
- Detailed settlement analysis should be performed to estimate settlements of the bridge and its approaches.
- High-quality compaction specifications and procedures should be used.
- If large settlement due to soft or compressible in-situ soils is expected, soil improvement such as replacement, preloading, vertical drains, and other stabilisation techniques should be considered. Also, consideration should be given to construction of the embankment of lightweight materials.

3.4.5 Abutments supported on shallow footings

The following is recommended for abutments supported by shallow spread footings (Azizinamini et al 2013):

- The end movement of the bridge should be accommodated by sliding of the footing.

- There should be a safe distance from the footing to the face of the slope, and slope protection measures put in place to prevent instability or washing out of soil beneath the footing.
- Integral abutments should not be constructed on spread footings founded or keyed into rock unless one end of the span is free to displace longitudinally. An alternative is to use a semi-integral abutment. For footings founded on rock, a layer of granular fill should be placed on top of a levelling layer or site concrete (immediately beneath the footing) to facilitate sliding.
- The abutment wall should be designed for shear and moments resulting from both expansion and contraction movements.
- The resistance to contraction should include friction on the bottom of the footing and passive soil pressure from the soil in front of the abutment.
- For footings supported on a layer of granular soil for sliding on rock, geogrids and geotextiles can be used to contain the granular soil.
- For footings founded on soft or compressible soil, mechanical stabilisation of the soil below the footing may be required to avoid large total and differential settlements.
- Spread footings should be avoided for multi-span bridges if there is a risk of differential settlement.

3.4.6 Abutments with MSE walls

Full height abutments with MSE retaining walls may be considered in the design of integral bridges. Loads due to the movement of the backwall and piles should be considered in the design of the MSE walls.

If the piles are not isolated from the MSE wall (eg sleeved) and can apply load to the wall, shear forces, bending moments in the piles and lateral soil pressures applied to the MSE block should be considered in the design. The interaction between the MSE structure and the piles can be analysed using pile load/deflection methods, eg p-y relationships for soil springs (Lam and Martin 1986). The lateral pressures applied by the pile should be considered as additional loading on the MSE wall.

The following design details are recommended for MSE abutments (Azizinamini et al 2013):

- Provide a clear horizontal distance of at least 0.5m between the MSE facing panels and the piles.
- Sleeving of the piles should be considered to reduce loads applied to the MSE structure and to reduce negative skin friction where applicable. This can be achieved by providing a casing through the reinforced fill block. This needs to be balanced against earthquake design requirements as this approach can result in large gaps being required.

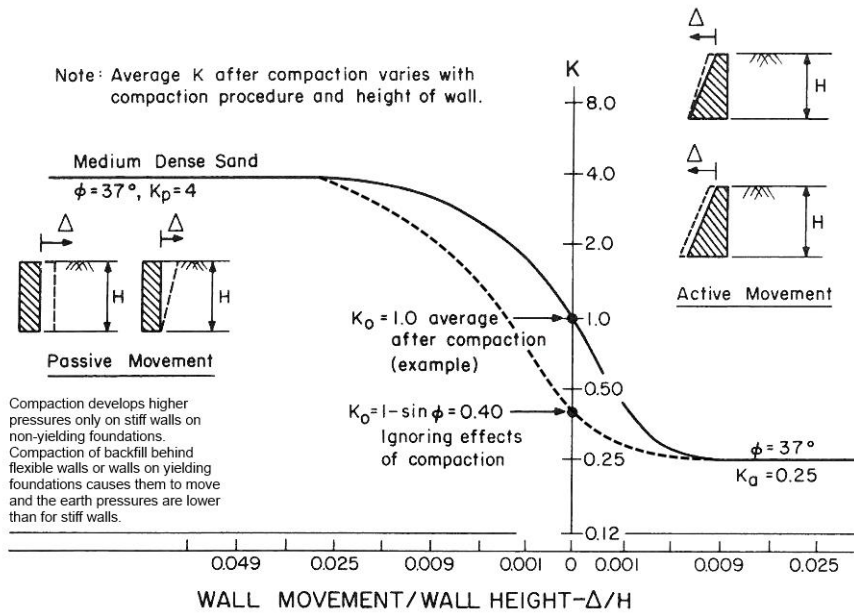
3.4.7 Soil pressures

The magnitude of soil pressure behind the abutment wall and the nonlinear distribution of this pressure depend on a number of factors, including:

- wall displacement
- soil type
- depth
- pile stiffness
- direction of the displacement.

As the abutment wall moves toward the backfill, passive pressure is engaged, and when it moves away from the backfill, active pressure and surcharge pressure may be generated. This relationship between wall movement and earth pressure is illustrated in figure 3.16.

Figure 3.16 Example of a relationship between wall movement and earth pressure



Source: Clough and Duncan (1991)

3.4.8 Earth pressures behind integral abutments and end screen walls

3.4.8.1 Earth pressure coefficient for integral bridge abutments subject to strain ratcheting

The coefficient of earth pressure that develops behind integral abutments and end screen walls during expansion (K^*) is proportional to the design value of $K_{p;t}$, determined using the design value of the triaxial angle of internal friction ϕ' . For unfavourable passive pressure, the value of $K_{p;t}$ may be interpolated from table 3.2. The values of ϕ' triax given in table 3.2 are the design values of the triaxial ϕ' .

Table 3.2 Maximum (unfavourable) values of $K_{p;t}$

$\phi'_{\text{triax;d}}$	Values of $K_{p;t}$				
	Inclination of abutment face				
	Vertical	Forwards		Backwards	
		+10°	+20°	-10°	-20°
30°	4,29	3,67	3,15	5,00	5,79
35°	5,88	4,86	4,02	7,09	8,49
40°	8,38	6,65	5,28	10,51	13,06
45°	12,57	9,51	7,20	16,52	21,45
50°	20,20	14,24	10,28	28,10	38,55

NOTE Values of $K_{p;t}$ are the horizontal component of K_p with $\delta_d/\phi' = 0,5$ calculated from the equations given in BS EN 1997-1:2004, Annex C using the design values of the triaxial ϕ' .

In the absence of test results for ϕ'_{triax} , its design value can be obtained from equation 3.6:

$$\phi'_{\text{max triaxial}} = 0.6\phi'_{\text{max plane strain}} + 0.4\phi'_{\text{cv}} \quad (\text{Equation 3.6})$$

where:

$\phi'_{\text{max triaxial}}$ = maximum angle of internal friction for plain strain conditions

ϕ'_{cv} = critical angle of shearing resistance.

Values of K_p for favourable passive pressure for vertical walls may be taken from BS EN 1997-1:2004, figure C.2.1, with $\delta d/\phi'd = 0$.

3.4.9 Strain ratcheting

For integral bridges which are subject to many thermal cycles, the repeated backward and forward movement of the abutment generates pressures when the bridge is expanding which are significantly higher than those that would occur with a single thermal cycle. After many cycles, this pressure tends to approach a maximum value with a pressure coefficient of K^* . K^* is dependent on the total movement of the end of the deck from its maximum contraction position to its maximum expansion position. The characteristic value of the movement (dk) is given by equation 3.7:

$$dk = \alpha L_x (T_{e;\text{max}} - T_{e;\text{min}}) \quad (\text{Equation 3.7})$$

where:

α = coefficient of thermal expansion of the deck

L_x = expansion length measured from the end of the bridge to the position on the deck that remains stationary when the bridge expands

$T_{e;\text{max}}$ and $T_{e;\text{min}}$ = characteristic maximum and minimum uniform bridge temperature components for a 50-year return period given in the UK National Annex to BS EN 1991-1-5.

It is notable that dk is not affected by the temperature at which the deck is attached to the abutments.

The design value of d may be found from equation 3.8:

$$dd = 0.5dk (1 + \psi\gamma_Q) \quad (\text{Equation 3.8})$$

where, for the combination of actions under consideration:

γ_Q = partial factor for thermal actions

$\psi = 1.00$, ψ_0 , ψ_1 or ψ_2 for thermal actions as appropriate (see BS EN 1990:2002).

Where the earth pressure due to a combination of long-term thermal cycling and longitudinal traffic action (braking and acceleration) is being assessed, the value of dd given above should be increased by the sway displacement caused by the design value of the longitudinal traffic action.

dd may be reduced for bridges with axially flexible decks. Where the elastic shortening under K^* pressure is significant, the reduction in dd may be taken as the elastic shortening of the expansion length of the deck when the deck expands.

3.4.10 Horizontal pressures on abutments accommodating thermal movements by rotation and/or flexure

For full height abutments on spread footings which accommodate thermal movements by rotation and/or flexure, the design value of the earth pressure coefficient for expansion K_d^* may be calculated from equation 3.9, but should not be taken as greater than $K_{p;t}$:

$$K_d^* = K_0 + ((Cd'_d)/H)^{0.6} K_{p;t} \tag{Equation 3.9}$$

where:

H = vertical distance from ground level to the level at which the abutment is assumed to rotate; that is, the underside of the base slab for rotationally flexible foundations and the top of the base slab for rotationally rigid foundations (see figure 3-17a). For an abutment wall that is pinned at or near its base, H is measured from ground level to the level of the pin.

d'_d = wall deflection at a depth $H/2$ below ground level when the end of the deck expands a distance dd as determined above. d'_d may conservatively be taken as $0.5d_d$ for abutments with rotationally rigid foundations and $0.7dd$ for abutments with pinned walls or rotationally flexible foundations.

C =:

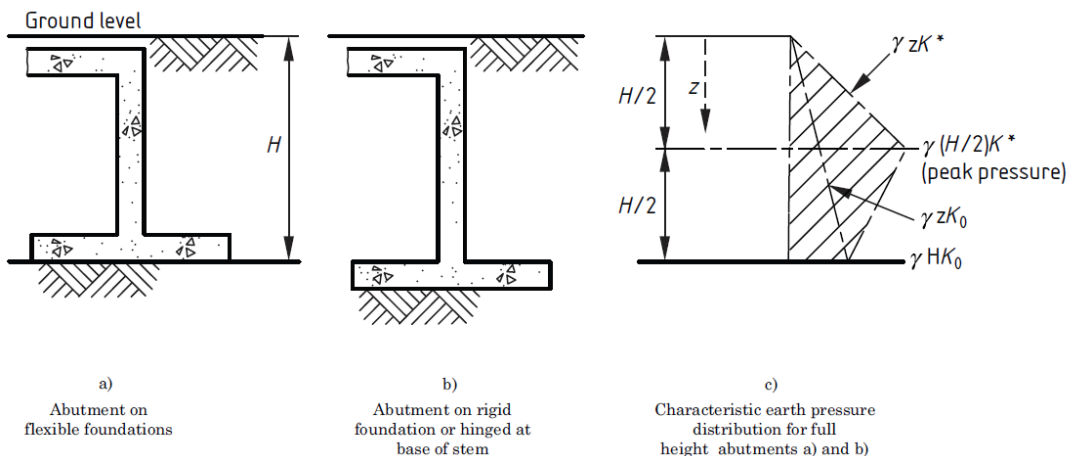
- 20 for foundations on flexible (unconfined) soils with $E \leq 100$ MPa
- 66 for foundations on rock or soils with $E \geq 1000$ MPa
- or found by linear interpolation for values of E between 100 MPa and 1,000 MPa
- $K_{p;t}$ is taken from table 3.2.

In determining C , the Young's modulus of the ground, E , maybe taken as the secant drained vertical Young's modulus established at 50% of the maximum stress at failure in a standard drained triaxial compression test.

The pressure distribution on the retained face can be simulated as shown in figure 3.17c, namely:

- a triangular pressure diagram from ground level to $H/2$ based on the pressure coefficient K_d^*
- a trapezoidal pressure diagram between $H/2$ to H with the pressure coefficient reducing linearly from K_d^* at mid-height to K_0 at depth H , where K_0 is the at-rest coefficient of earth pressure.

Figure 3.17 Earth pressure distributions for abutments which accommodate thermal expansion by rotation and/or flexure



3.4.11 Horizontal earth pressures on end screen and abutments that accommodate thermal movements by translation without rotation

For abutments that accommodate thermal movements by translation without rotation, such as bank pad and semi-integral end screen abutments, the earth pressure coefficient for expansion, K_d^* , may be calculated from equation 3.10, but should not be taken as greater than $K_{p;t}$:

$$K_d^* = K_0 + ((40d'_d)/H)^{0.4} K_{p;t} \quad \text{(Equation 3.10)}$$

where:

H = height of the end screen;

d'_d = movement of the end screen calculated at H/2 below ground level.

For this type of abutment, the pressure diagram may be assumed to be triangular with the design pressure at depth z equal to $\gamma z K_d^* \gamma_c$.

3.4.12 Horizontal earth pressures on full height frame abutments on piles and embedded wall abutments (soil–structure interaction analysis)

3.4.12.1 Abutments with granular soils

For full height integral abutments founded on a single row of vertical piles and integral embedded wall abutments, the horizontal earth pressure at various depths below ground level should be found using a soil-structure interaction analysis which takes account of:

- the non-linear response of the soil to deck expansion and contraction
- the effect of strain ratcheting on soil properties, which may be based on 120 cycles with an amplitude of dk
- variations of soil properties at different depths
- the degree of compaction of the soil
- the rotational and axial stiffness of the deck
- horizontal soil arching between the piles
- the staged application of the thermal effects
- the early and later life of the structure
- the envelope of possible combinations of minimum earth pressures with maximum expansion and maximum earth pressures with minimum expansion.

The accuracy of any soil–structure interaction software and numerical model used in the analysis should be demonstrated by calibration against comparable laboratory and/or field monitoring to demonstrate compatibility in deflection and soil pressures down the depth of the abutment after 120 thermal cycles between $T_{e;min}$ and $T_{e;max}$.

3.4.12.2 Abutments with cohesive soils

For a piled or embedded integral abutment with cohesive soils, the effects of strain ratcheting in the cohesive soils may be ignored and the pressure on the wall and piles when the end of the deck expands, can be calculated using a conventional soil–structure interaction analysis and an appropriate value of E for the soil.

3.4.13 Horizontal earth pressures on bank pad abutments founded on a single row of embedded piles

A bank pad abutment supported on a single row of piles may be designed as a piled abutment. Account should be taken in the design of any inclined slope in front of the piles. This may be done by using software that can accommodate a berm, and/or by taking the value of K_a and K_p on the front face of the piles as that applicable to the inclined slope (see also clause 7.2 in CIRIA report C580 (Gaba et al 2003)). The effect of horizontal soil arching between the piles should also be assessed. However, unless it can be shown by a rigorous analysis that the strains across the whole width of fill behind the piles are not significantly different from the strains that would occur with a continuous embedded wall, the horizontal pressure behind the end screen itself should be calculated as for a bank pad abutment supported on fill.

3.4.14 ψ factors and partial factors for earth pressures behind integral abutments

The vertical earth pressure behind an integral abutment due to the weight of soil is considered to be a permanent action and is therefore factored by γ_G (where γ_G is the partial factor for the weight of soil). Because it is a permanent action, no ψ factor is applied to it in accordance with BS EN 1990.

Horizontal earth pressures applied to integral abutments are dependent on the thermal expansion of the bridge deck, with this thermal expansion determined by applying relevant values of ψ and γ_Q . Account of this may be taken by using the values of d_d specified above when calculating the design value of the earth pressure coefficient, K_d .

From this, it follows that the design value of the horizontal earth pressure at depth z when K_d governs is $\gamma z K_d^* \gamma_G$. For γ_m , the National Annex to BS EN 1997-1 states that the value of γ_m should be taken as either the value given in the tables in the National Annex or the reciprocal of that value (denoted γ_m^*), whichever results in the more onerous effects. The upper value of $\tan \phi_K'$ should therefore be divided by γ_m^* for unfavourable passive pressures and favourable active and at rest pressures, and the lower value of $\tan \phi_K'$ divided by γ_m for favourable passive pressures and unfavourable active and at rest pressures.

The use of γ_m^* is required because BS EN 1997-1:2004 states that geotechnical parameters are always divided by γ_m^* . Dividing a geotechnical parameter by γ_m^* is numerically equivalent to multiplying it by γ_m . Therefore, the approach in the National Annex to BS EN 1997-1 effectively requires geotechnical parameters to be divided by or multiplied by γ_m^* , whichever results in the more onerous effects.

3.4.15 Pressure envelope

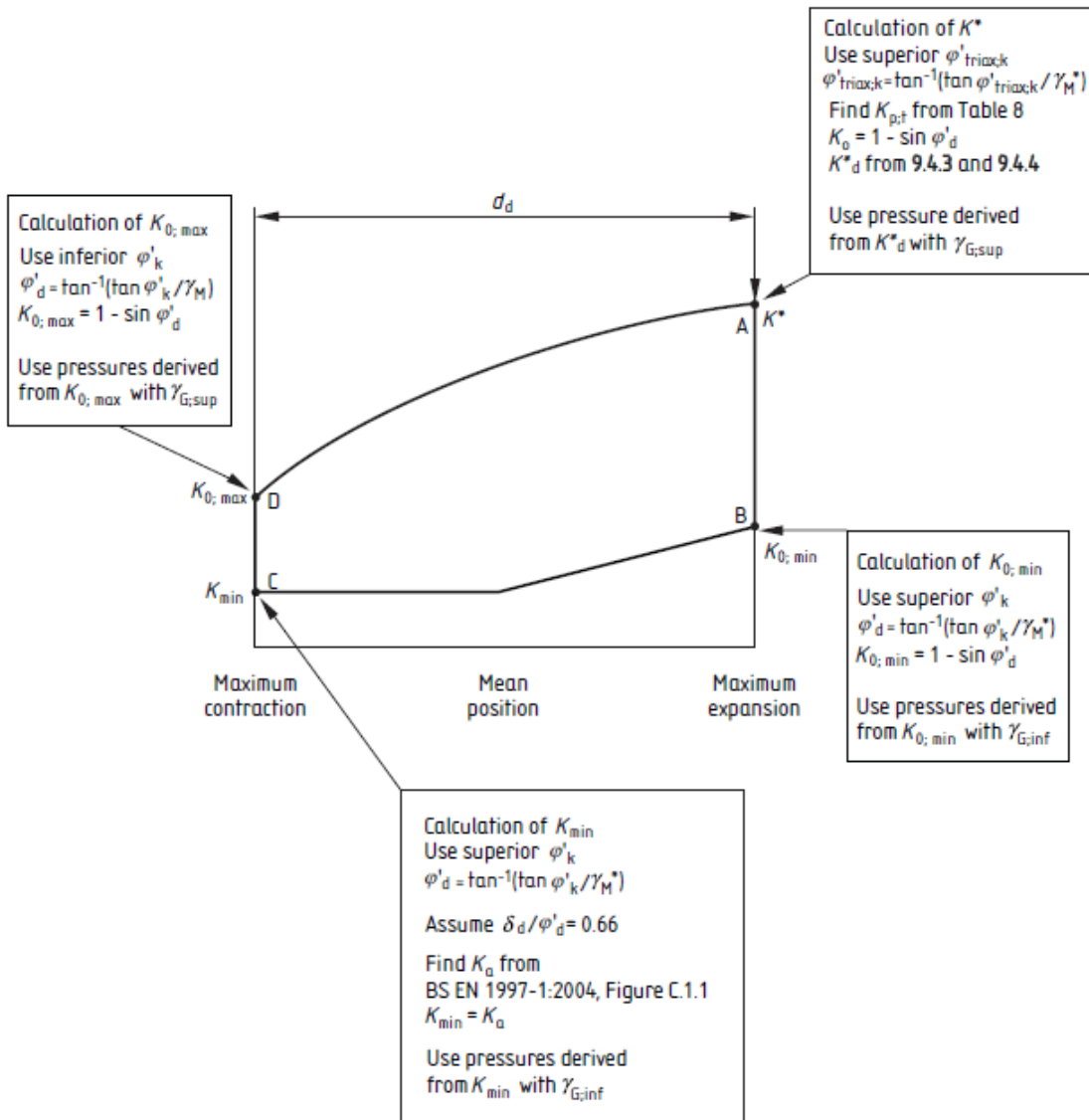
The earth pressure on the retained face of an integral abutment is dependent on the following:

- the thermal movement range based on a 50-year return period
- the direction of movement (expanding or contracting)
- the actual amount of expansion or contraction for the combination of actions or design situation under consideration.

The design values of the movements to be identified in the relevant design situation are given in section 3.4.9 of this report. In some circumstances, minimum earth pressures are more unfavourable than maximum earth pressures, so both expansion and contraction have to be assessed. Figure 3.18 gives an envelope of the pressure coefficients that should be used with expansion and contraction for limit equilibrium calculations.

It should be noted, however, that recent research (Huntley and Valsangkar 2013) has been unable to establish a relationship for earth pressures for integral bridges based on full-scale monitoring data and earth pressure measurements.

Figure 3.18 Pressure coefficient envelope



NOTE 1 Figure ABCD shows the maximum and minimum pressure coefficients to be considered with expansion and contraction when the design value of the thermal movement is d_d as described in 9.4.2 and 9.4.7.

NOTE 2 The superior characteristic and inferior characteristic values of ϕ' represent the limiting values between which the shear strength of the backfill have to lie (see 9.10).

NOTE 3 $\gamma_{G,inf}$ and $\gamma_{G,sup}$ are the favourable and unfavourable values of γ_G for the weight of soil.

NOTE 4 γ_M^* is the reciprocal value of γ_M given in the tables in the UK National Annex to BS EN 1997-1 (see 9.4.7).

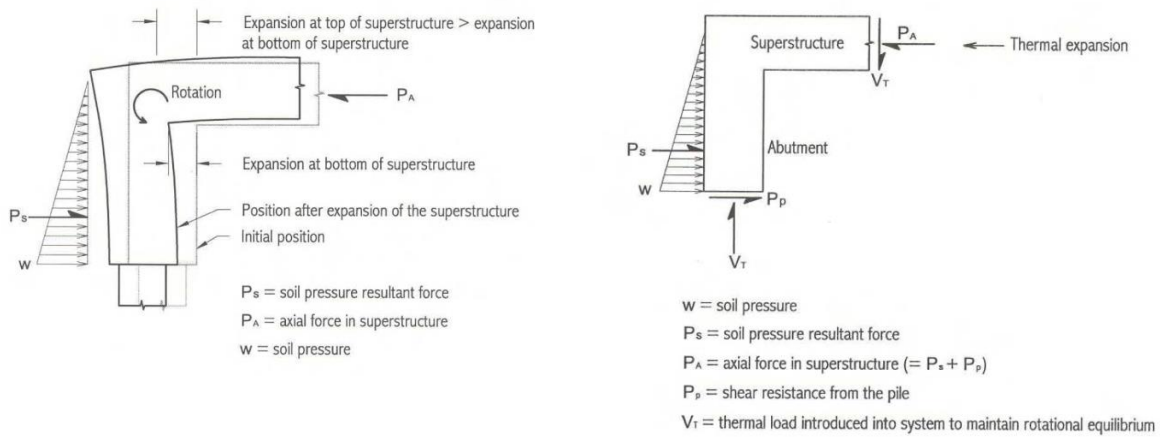
3.4.16 Pile foundations

Abutment piles of straight bridges should be oriented so the strong axis of the piles is perpendicular to the longitudinal direction of the bridge (Doust 2011). This orientation results in weak-axis bending of the

piles due to longitudinal movement of straight non-skew bridges. A procedure has been developed to determine the optimum abutment pile orientation for curved girder integral bridges (Doust 2011).

The ability of piles to accommodate lateral displacements from secondary loads is a significant factor in determining the maximum length of integral bridges. As piles deflect laterally due to abutment movement, the axial load capacity is reduced for a number of reasons. First, pile-bending stresses from lateral movement will be superimposed on axial stresses, thereby reducing the axial load capacity. Second, movement of the pile could affect the behaviour of the soil, including the ability of the soil to carry vertical load through frictional resistance. Last, an additional vertical force, or thermal load, will be introduced into the bridge-pile system in order to maintain static equilibrium as shown in figure 3.19. A moment M , and shear force V are generated due to the eccentricity between the soil pressure resultant force and the elevation of the superstructure.

Figure 3.19 Effect of thermal expansion on stress state of abutment and piles



Source: Wiss et al (2002)

3.5 Maintenance

It should be recognised that integral bridges require continuous, yet reduced, maintenance. Depending on the circumstances, the maintenance may comprise asphalt overlays and approach slab adjustment or replacement. If a joint is required at the sleeper slab it will also require maintenance. Maintenance issues have also been recently encountered relating to transverse and diagonal deck slab cracking, stage construction issues, lateral rotation of superstructure, erosion of embankments and marginal quality of structure movement systems.

4 Conclusions and recommendations

4.1 Conclusions

An integral bridge, as defined at the outset of this report, 'is a structure where there are no expansion joints in the superstructure between spans and between spans and abutments (but these joints may exist beyond the bridge)'. The purpose of this report was to provide commentary on the form and performance of integral bridges, and to provide guidance to New Zealand bridge designers for the design of integral bridges.

A review of the performance of integral bridges found that integral bridges generally performed well under normal service conditions. The performance of integral bridges subjected to significant seismic actions was found to be positive overall, although the increased significance of soil-structure interaction on the response of integral bridges was noted to require further consideration during design.

While some uncertainty remains regarding how to best address some issues relating to the design of integral and semi-integral bridges, the following issues were identified as of particular significance and were addressed in detail throughout the report:

- The structural form adopted at supports and in particular the connection details between superstructure and substructure.
- The considerable actions imposed through secondary static effects, including creep, shrinkage and temperature. Guidance was provided for formulations to be used during design, and a detailed example and parametric analyses provided in the appendices.
- Preferred structural forms for integral bridges in moderate-to-high seismicity regions.
- Analysis methods for seismic design, with an emphasis on DBD. The modelling of integral abutments and the soil-structure interface was of particular interest due to the considerable influence of soil response on overall integral bridge response during seismic motions.
- Geotechnical analysis and design for integral bridges, with guidance for approach system form and abutment form. The effect of abutment form selection on horizontal earth pressures and overall soil response was addressed with great detail.

Overall, it is anticipated that while the purpose of this report is not to provide step-by-step guidance for the design of integral bridges, it will provide New Zealand bridge designers with the necessary information and highlight the necessary issues for consideration to ensure excellent performance of future integral bridges.

4.2 Recommendations

Contained within this report are a number of recommendations for bridge designers to be considered during the design of integral bridges. These recommendations have been categorised into static design (section 3.2), seismic design (section 3.3) and geotechnical design (section 3.4). Furthermore, further research is recommended into several issues associated with the aforementioned topics, including:

- the effect of design parameters on abutment damping
- the influence of soil gapping effects on integral bridge seismic response
- the lateral response of piles in sloping ground
- the influence of integral connection details on horizontal earth pressures and strain ratcheting at integral bridge abutments.

5 References, codes and standards

5.1 References

- Arockiasamy, M., Butrieng, N., and Sivakumar, M. (2004). State-of-the-art of integral abutment bridges: design and practice. *Journal of Bridge Engineering* 9, no.5: 497–506.
- Arsoy, S., RM Baker and M Duncan (1999) *The behaviour of integral abutment bridges*. Blacksburg, Virginia: Virginia Polytechnic and State University.
- Azizinamini, A., Ozyildirim, H. C., Power, E. H., Kline, E. S., Mertz, D. R., Myers, G. F., & Whitmore, D. W. (2013). Design guide for bridges for service life (No. SHRP 2 Renewal Project R19A).
- Basöz, NI and AS Kiremidjian (1998) Evaluation of bridge damage data from the Loma Prieta and Northridge, California earthquakes. *Technical report MCEER 98-0004*. US Multidisciplinary Center for Earthquake Engineering Research (MCEER).
- Beca Carter Hollings & Ferner Ltd and Opus International Consultants Ltd (Beca and Opus) (2008) Standard precast concrete bridge beams. *NZ Transport Agency research report 364*. 56 pp.
- Buckle, IG (1994) The Northridge, California earthquake of January 17, 1994: performance of highway bridges. *Technical report NCEER 94-0008*. US National Center for Earthquake Engineering Research.
- Burdet, OL (2010) Thermal effects in the long-term monitoring of bridges. Report presented at *34th IABSE Symposium on Large Structures and Infrastructures for Environmentally Constrained and Urbanised Areas, vol A-755*. Venice, 2010. 7pp.
- Caltrans (1994) *The Northridge earthquake: post earthquake investigation*. (PEQIT) Sacramento: California Department of Transportation: Division of Structures.
- Clark, LA (1985) *Concrete bridge design to BS 5400*. London: Construction Press.
- Clough, GW and JM Duncan (1991) *Earth pressures*. Pp234–235 in H-Y Fang (Ed) *Foundation engineering handbook*. 2nd ed. New York: van Nostrand Reinhold.
- Concrete Bridge Development Group (CBDG) (1997) *Technical guide 1 – report of a study tour to North America*.
- Dicleli, M (2005) Integral abutment-backfill behavior on sand soil – pushover analysis approach. *Journal of Bridge Engineering* 10, no.3: 354–364.
- Doust, SE (2011) Extending integral concepts to curved bridge systems. *Civil Engineering Theses, Dissertations, and Student Research paper 41*.
- Gaba, AR, B Simpson and WBDR Powrie(2003) Embedded retaining walls guidance for economic design. *CIRIA report C580*.
- Georgiadis, K and M Georgiadis (2010) Undrained lateral pile response in sloping ground. *Journal of geotechnical and geoenvironmental engineering* 136, no.11: 1489–1500.
- Hambly, EC (1997) Integral bridges. *Proceedings of the ICE-Transport* 123, no.1: 30–38.
- Huntley, SA and AJ Valsangkar (2013) Field monitoring of earth pressures on integral bridge abutments. *Canadian Geotechnical Journal* 50, no.8: 841–857.

- Jennings, PC (1971) *Engineering features of the San Fernando earthquake of February 9, 1971*. California Institute of Technology.
- Jessee, S and KM Rollins (2013) Passive pressure on skewed bridge abutments. Pp2024–2027 in *Proceedings of the 18th International Conference on Soil Mechanics and Geotechnical Engineering*, ISSMGE.
- Khalili-Tehrani, P, E Taciroglu and A Shamsabadi (2010) Backbone curves for passive lateral response of walls with homogeneous backfills. *Soil-Foundation-Structure Interaction* 149.
- Kim, W and JA Laman (2010) Integral abutment bridge response under thermal loading. *Engineering Structures* 32, no.6: 1495–1508.
- Lam, IP and GR Martin (1986) Seismic design of highway bridge foundations. Vol II Design procedures and guidelines. *FHWA report RD-86/102*.
- Lee, J (2010) *Experimental and analytical investigations of the thermal behavior of prestressed concrete bridge girders including imperfections*. PhD dissertation. Georgia Institute of Technology.
- Lehane, B. M., Keogh, D. L., & O'Brien, E. J. (1999). Simplified elastic model for restraining effects of backfill soil on integral bridges. *Computers & structures*, 73(1), 303-313.
- Mattock, AH (1961) Precast-prestressed concrete bridges 5: creep and shrinkage studies. *Journal of the PCA Research and Development Laboratories* 3, no.2: 32–66.
- Moorty, S and CW Roeder (1992) Temperature-dependent bridge movements. *Journal of Structural Engineering* 118, no.4: 1090–1105.
- Olson, SM, KP Holloway, JM Buenker, JH Long and JM LaFave (2013) Thermal behavior of IDOT integral abutment bridges and proposed design modifications. *Research report FHWA-ICT-12-022*.
- Palermo, A and S Pampanin (2008) Enhanced seismic performance of hybrid bridge systems: comparison with traditional monolithic solutions. *Journal of Earthquake Engineering* 12, no.8: 1267–1295.
- Perry, VH and M Royce (2010) Innovative field-cast UHPC joints for precast bridge Decks (side-by-side deck bulb-tees) design: prototyping, testing and construction. *Third fib International Congress*, Washington DC, 2010.
- Priestley, MJN and IG Buckle (1979) Ambient thermal response of concrete bridges. *Road Research Unit bulletin* 42. Wellington, 83pp.
- Priestley, MJN, GM Calvi and MJ Kowalsky (2007) *Displacement-based seismic design of structures*. Pavia, Italy: IUSS Press.
- Rojas, E (2014) Uniform temperature predictions and temperature gradient effects on I-girder and box girder concrete bridges. *All Graduate Theses and Dissertations, paper 2193*.
- Rollins, KM and RT Cole (2006) Cyclic lateral load behavior of a pile cap and backfill. *Journal of geotechnical and geoenvironmental engineering* 132, no.9: 1143–1153.
- Rollins, KM, TM Gerber and KH Kwon (2010) Lateral pile cap load tests with gravel backfill of limited width. *Utah Department of Transportation research report UT-10.17*.
- Rollins, KM and SJ Jessee (2012) Passive force-deflection curves for skewed abutments. *Journal of Bridge Engineering* 18, no.10: 1086–1094.
- Shah, BR, D Peric and A Esmaily (2008) Effects of ambient temperature changes on integral bridges. *Kansas Department of Transportation technical report K-TRAN: KSU-06-2*.

- Shamsabadi, A, L Yan and G Martin (2004) *Three dimensional nonlinear seismic soil-foundation-structure interaction analysis of a skewed bridge considering near fault effects*. USC Digital Library.
- Shamsabadi, A, M Ashour and G Norris (2005) Bridge abutment nonlinear force-displacement-capacity prediction for seismic design. *Journal of Geotechnical and Geoenvironmental Engineering* 131, no.2: 151-161.
- Shamsabadi, A and S Nordal (2006) Modeling passive earth pressures on bridge abutments for nonlinear seismic soil-structure interaction using Plaxis. *Plaxis Bulletin* 20: 8-15.
- Shamsabadi, A and M Kapuskar (2006) Practical nonlinear abutment model for seismic soil-structure interaction analysis. *Fourth International Workshop on Seismic Design and Retrofit of Transportation Facilities*, San Francisco. 13-14 March 2006.
- Shamsabadi, A., Kapuskar, M., & Martin, G. R. (2006). Three-dimensional nonlinear finite-element soil-abutment structure interaction model for skewed bridges. In Fifth National Seismic Conference on Bridges & Highways (No. B15).
- Shamsabadi, A, KM Rollins and M Kapuskar (2007) Nonlinear soil-abutment-bridge structure interaction for seismic performance-based design. *Journal of Geotechnical and Geoenvironmental Engineering* 133, no.6: 707-720.
- Shamsabadi, A, P Khalili-Tehrani, JP Stewart and E Taciroglu (2009) Validated simulation models for lateral response of bridge abutments with typical backfills. *Journal of Bridge Engineering* 15, no.3: 302-311.
- Wassermann, EP and JH Walker (1996) Integral abutments for continuous steel bridges. *Workshop on Integral abutment bridges*. Pittsburgh PA, 13-15 November 1996. 31 pp.
- Werner, SD, JL Beck and MB Levine (1987) Seismic response evaluation of Meloland Road Overpass using 1979 Imperial Valley earthquake records. *Earthquake engineering & structural dynamics* 15, no.2: 249-274.
- White, H (2007) Integral abutment bridges: comparison of current practice between European countries and the United States of America. *Special report 152, Transportation Research and Development Bureau*.
- Wiss, Janney & Elstner Associates Inc (2002) *Synthesis of technical information for jointless bridge construction*. Vermont Agency of Transportation, phase 1 report.
- Wood, J and P Jennings (1971) Damage to freeway structures in the San Fernando earthquake. *Bulletin of the New Zealand Society for Earthquake Engineering* 4, no.3: 347-376.
- Zhang, J and N Makris (2001) *Seismic response analysis of highway overcrossings including soil-structure interaction*. Pacific Earthquake Engineering Research Center, College of Engineering, University of California.

5.2 Codes and standards

- AASHTO (2012) *AASHTO LRFD bridge design specifications*. 6th edition. Washington DC: AASHTO.
- American Concrete Industry (ACI) (2004) ACI 209-2004 Guide for modeling and calculating shrinkage and creep in hardened concrete.
- American Concrete Industry (ACI) (2008) ACI 209R-92 Prediction of creep, shrinkage and temperature effects in concrete structures

- British Standards Institution (1997) BS 8110-1:1997 Structural use of concrete. Code of practice for design and construction.
- British Standards Institution (2003) UK National Annex to Eurocode 1. Actions on structures. General actions. Thermal actions.
- Comité Européen du Béton (CEB) (1978) CEB-FIP model code for concrete structures (CEB-FIP 78).
- Comité Européen du Béton (CEB) (1993) CEB-FIP model code 90 (CEB-FIP 90).
- European Committee for Standardisation (2002) BS EN 1990:2002 Basis of structural design.
- European Committee for Standardisation (2004) BS EN 1997-1:2004. Eurocode 7: Geotechnical design – Part 1: General rules.
- fédération internationale du béton (fib) (2010) fib model code for concrete structures 2010 (fib 2010) – final draft. Lausanne, federation internationale du beton bulletin nos. 65/66.
- New Zealand Transport Agency (2013) *Bridge manual*. 3rd ed. SP/M/022.
- RILEM (1995) RILEM-B3 Creep and shrinkage prediction model for analysis and design of concrete structures – model B3.
- South African Bureau of Standards (1992) SABS0100 (1992) Code of practice for the structural use of concrete.
- Standards Australia (2009) AS 3600–2009 Concrete structures.
- Standards Australia (2012) AS 5100–2012 Australian bridge design code.
- Standards NZ (1997) NZS 3109:1997 Concrete construction.
- Standards NZ (2001) AS/NZS 4671:2001 Steel reinforcing materials.
- Standards NZ (2002) AS/NZS 1170:2002. Structural design actions.
- Standards NZ (2006) NZS 3101:2006 Concrete structures standard.
- The Highways Agency (UK) (2001) BD 57/01 Design for durability.
- The Highways Agency (UK) (1995) BD 30/87 Backfilled retaining walls and bridge abutments.
- The Highways Agency (UK) (1996) BA 42/96 The design of integral bridges.

Appendix A: Concrete creep and shrinkage models

Concrete creep and shrinkage were studied during the research using the model codes CEB-FIP 78, CEB-FIP 90 and fib 2010. This appendix presents the creep and shrinkage coefficients suggested by the codes. Parametric analyses were carried out to study the effects of humidity and notational thickness on creep and shrinkage coefficients and the results of these analyses are shown in 3D and 2D graphs.

A1 Creep

A1.1 Creep models

Model Code CEB-FIP 78

The creep coefficient, $\varphi(t, t')$, can be mathematically presented as in equation A.1 (CEB-FIP 78):

$$\varphi(t, t') = \beta_a(t') + \varphi_d \times \beta_d(t - t') + \varphi_f \times [\beta_f(t) - \beta_f(t')] \quad (\text{Equation A.1})$$

Where:

$\beta_a(t')$ = instantaneous creep deformation at time of loading

$\beta_d(t - t')$ = time-dependent non-ageing creep

$[\beta_f(t) - \beta_f(t')]$ = time-dependent aging creep.

$$\begin{aligned} \beta_a(t') &= 0.8 \times \left[1 - \frac{f_{cm}(t')}{f_{cm}(\infty)} \right] \\ \varphi_d &= 0.4 \\ \beta_d(t - t') &= \left[\frac{t - t'}{t - t' + 328} \right]^{1/4.2} \\ \varphi_f &= \varphi_{f1} \times \varphi_{f2} \\ \varphi_{f1} &= 4.45 - 0.035 \times RH \\ \varphi_{f2} &= e^{\left[4.4 \times 10^{-5} \times h_0 - \frac{0.357}{h_0} - \ln\left(\frac{h_0^{0.1667}}{2.6}\right) \right]} \\ \beta_f(t) &= \left[\frac{t}{t + K_1(h_0)} \right]^{K_2(h_0)} \\ K_1(h_0) &= e^{\left[\frac{5.02}{h_0} + \ln(6.95 \times h_0^{2.25}) \right]} \\ K_2(h_0) &= e^{\left[0.00144 \times h_0 - \frac{1.1}{h_0} - \ln(1.005 \times h_0^{0.2954}) \right]} \end{aligned} \quad (\text{Equation A.2})$$

Model Code CEB-FIP 90

The creep coefficient, $\varphi(t, t')$ predicted by CEB-FIP 90 can be mathematically presented as in equation A.3.

$$\begin{aligned} \varphi(t, t') &= \varphi_0(t') \times \beta_c(t - t') \\ \varphi_0(t') &= \varphi_{RH} \times \beta(f_{cm}) \times \beta(t') \\ \varphi_{RH} &= 1 + \frac{1 - RH/RH_0}{0.46 \times (h/h_0)^{1/3}} \\ \beta(f_{cm}) &= \frac{5.3}{(f_{cm}/f_{cm0})^{0.5}} \\ \beta(t') &= \frac{1}{0.1 + (t'/t_1)^{0.2}} \\ \beta_c(t - t') &= \left[\frac{(t - t')/t_1}{\beta_H + (t - t')/t_1} \right]^{0.3} \\ \beta_H &= 150 \times \left[1 + \left(1.2 \times \frac{RH}{RH_0} \right)^{18} \right] \times \frac{h}{h_0} + 250 \leq 1500 \end{aligned} \quad (\text{Equation A.3})$$

Model Code fib 2010

The creep coefficient, $\varphi(t, t')$, can be mathematically presented as in equation A.4 (fib 2010):

$$\begin{aligned}
 \varphi(t, t') &= \varphi_{bc}(t, t') \times \varphi_{dc}(t, t') && \text{(Equation A.4)} \\
 \varphi_{bc}(t, t') &= \beta_{bc}(f_{cm}) \times \beta_{bc}(t, t') \\
 \beta_{bc}(f_{cm}) &= \frac{1.8}{(f_{cm})^{0.7}} \\
 \beta_{bc}(t, t') &= \ln\left[\left(\frac{30}{t'_{adj}} + 0.035\right)^2 \times (t - t') + 1\right] \\
 \varphi_{dc}(t, t') &= \beta_{dc}(f_{cm}) \times \beta(RH) \times \beta_{dc}(t') \times \beta_{dc}(t, t') \\
 \beta_{dc}(f_{cm}) &= \frac{412}{(f_{cm})^{1.4}} \\
 \beta(RH) &= \frac{1 - RH/100}{\sqrt[3]{0.1 \times h/100}} \\
 \beta_{dc}(t') &= \frac{1}{0.1 + (t'_{adj})^{0.2}} \\
 \beta_{dc}(t, t') &= \left[\frac{(t - t')}{\beta_n + (t - t')}\right]^{\gamma(t')} \\
 \gamma(t') &= \frac{1}{2.3 + \frac{3.5}{\sqrt{t'_{adj}}}} \\
 \beta_n &= 1.5 \times h + 250 \times \alpha_{fcm} \leq 1500 \times \alpha_{fcm} \\
 \alpha_{fcm} &= \left(\frac{35}{f_{cm}}\right)^{0.5} \\
 \varphi_{\sigma}(t, t') &= \varphi(t, t') e^{[1.5 \times (k_{\sigma} - 0.4)]} \\
 0.4 < k_{\sigma} &\leq 0.6 \quad k_{\sigma} = \frac{|\sigma|}{f_{cm}(t_0)}
 \end{aligned}$$

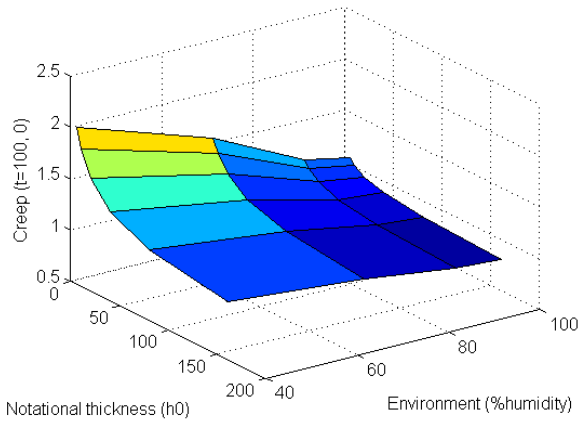
A1.2 Parametric analyses of creep

The aim of the parametric analyses was to study the effects of humidity percentage and notational thickness on the creep coefficient. To meet this aim, 3D graphs for $t=100, 1,000$ and $10,000$ days were prepared as follows:

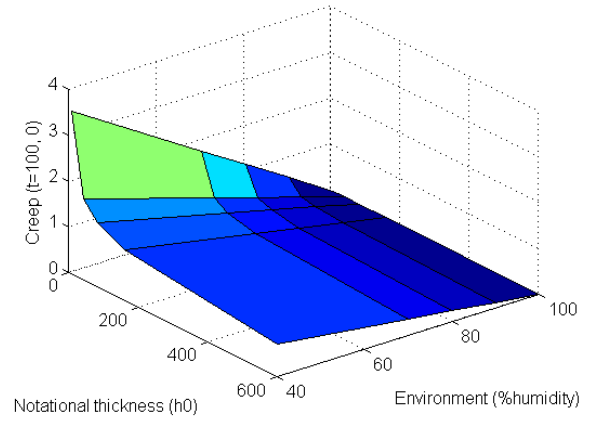
A1.2.1 3D graphs

The 3D graphs in figures A.1, A.2 and A.3 show the effects of both notational thickness and humidity on the creep coefficient predicted by CEB-FIP 78 and fib 2010, whereby the creep coefficient increases with the reduction in humidity and notational thickness.

Figure A.1 Creep for concrete with $t=100$ days age

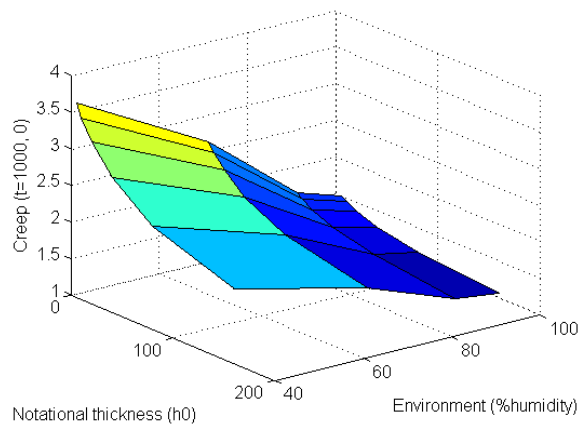


a) CEB-FIP 78

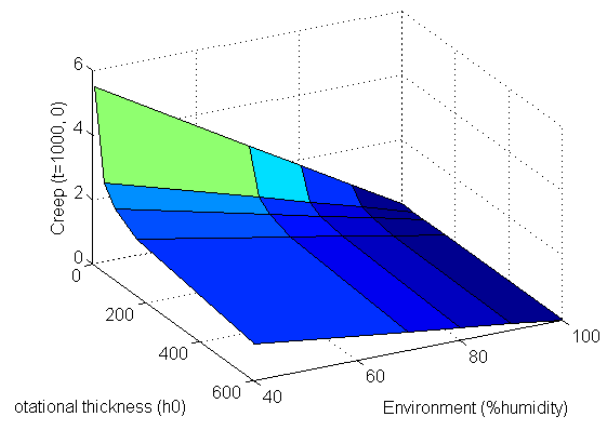


b) fib 2010

Figure A.2 Creep for concrete with $t=1,000$ days age

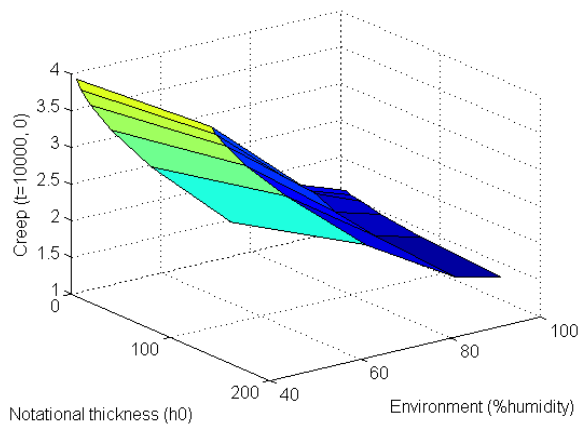


a) CEB-FIP 78

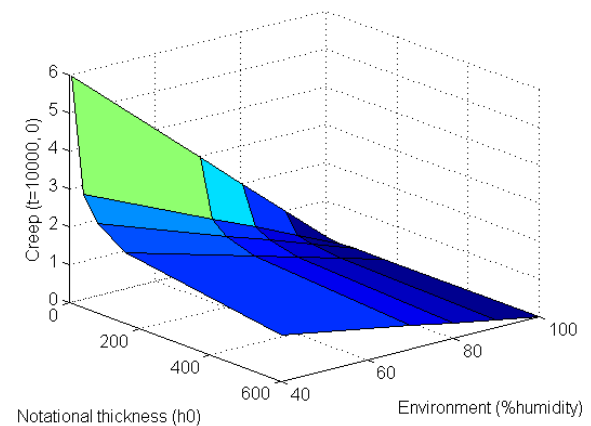


b) fib 2010

Figure A.3 Creep for concrete with $t=10,000$ days age



a) CEB-FIP 78

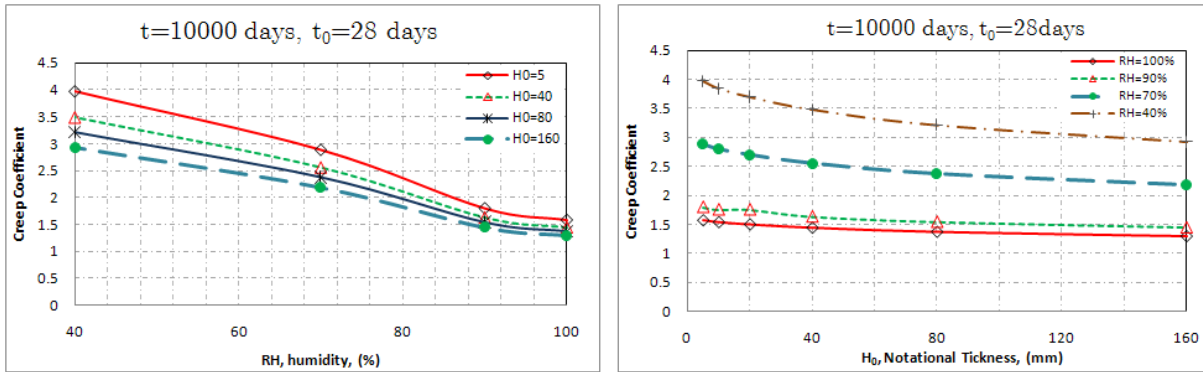


b) fib 2010

A1.2.2 2D graphs

To better understand the effect of notational thickness and humidity, 2D graphs were prepared as shown in figures A.4 and A.5:

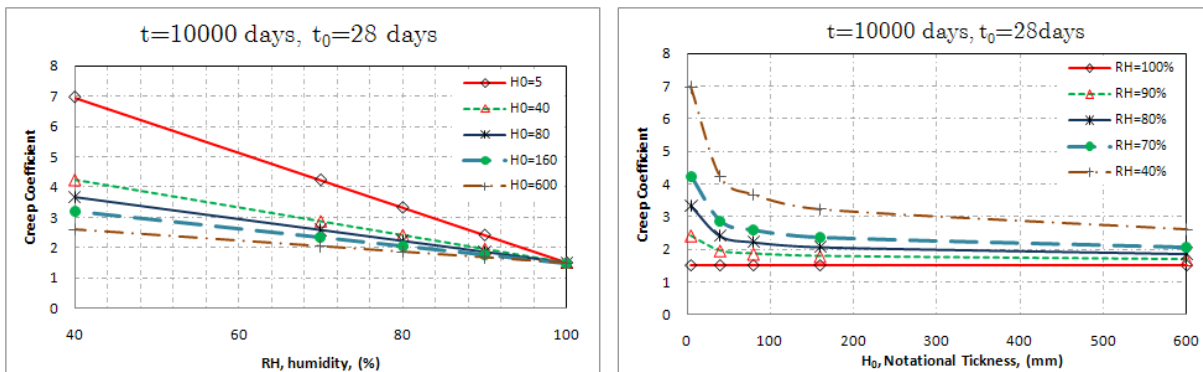
Figure A.4 Creep coefficient for concrete age of $t=10,000$ days age by CEB-FIP 78



a) Effect of humidity for various notational thicknesses

b) Effect of notational thickness for various humidity percentages

Figure A.5 Creep coefficient for concrete age of $t=10,000$ days age by fib 2010



a) Effect of humidity for various notational thicknesses

b) Effect of notational thickness for various humidity percentages

A2 Shrinkage

A2.1 Shrinkage models

Model Code CEB-FIP 78

The total shrinkage may be calculated from equations A.5 and A.6:

$$\epsilon_{cs}(t, t_0) = \epsilon_{s0} \times [\beta_s(t) - \beta_s(t_0)] \tag{Equation A.5}$$

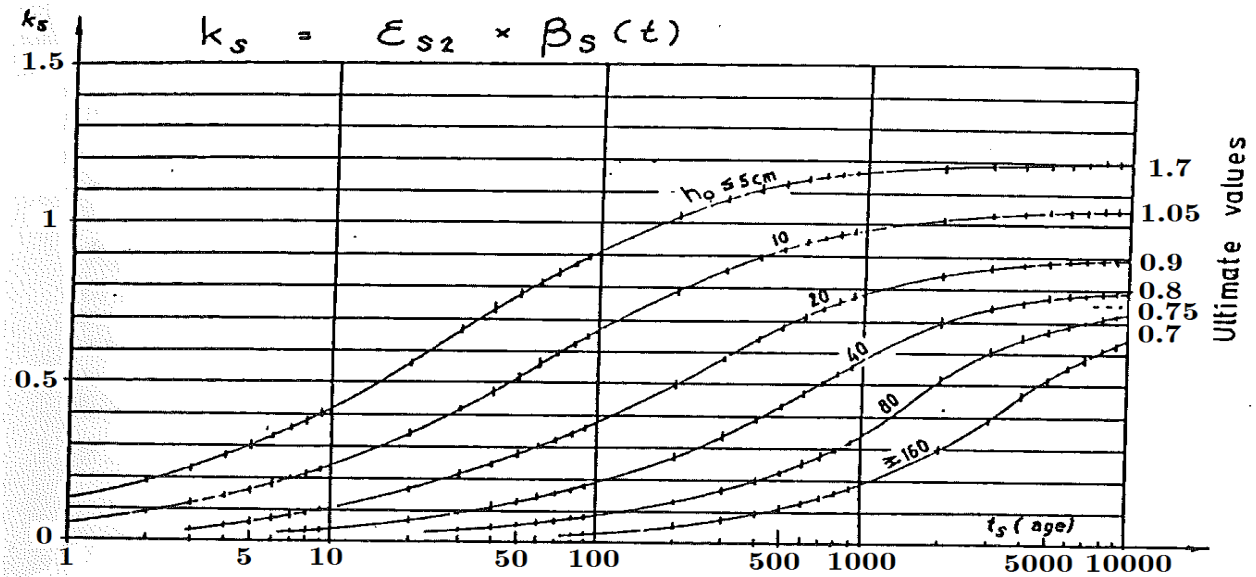
Where:

$$\begin{aligned} \epsilon_{s0} &= \epsilon_{s1} \times \epsilon_{s2} \\ k_s &= \epsilon_{s2} \times \beta_s(t) \end{aligned} \tag{Equation A.6}$$

Table A.1 Coefficient of shrinkage

Relative humidity	ϵ_{s1}
100%	+0.00010
90%	-0.00013
70%	-0.00032
40%	-0.00052

Figure A.6 Shrinkage coefficient with time



Model Code CEB-FIP 90

The total shrinkage may be calculated from equations A.7 and A.8:

$$\epsilon_{cs}(t, t_s) = \epsilon_{cs0} \times \beta_s(t - t_s) \quad \text{(Equation A.7)}$$

Where:

$$\begin{aligned} \epsilon_{cs0} &= \epsilon_s(f_{cm}) \times \beta_{RH} && \text{(Equation A.8)} \\ \epsilon_s(f_{cm}) &= [160 + 10 \times \beta_{sc} \times \gamma(f_{cm})] \times 10^{-6} \\ \beta_{RH} &= 1.55[1 - (RH/RH_0)^3] \\ \gamma(f_{cm}) &= 9 - f_{cm}/f_{cm0} \\ f_{cm0} &= 10 \text{ MPa} \\ \beta_s(t - t_s) &= \left[\frac{(t - t_s)/t_1}{350(h/h_0)^2 + (t - t_s)/t_1} \right]^{\alpha(f_{cm})} \\ \alpha(f_{cm}) &= 0.5 \\ h_0 &= 100 \text{ mm} \\ \beta_{sc} &= 5 \quad (\text{for normal portland - type cement}) \end{aligned}$$

$\alpha(f_{cm})$ = correction coefficient for the time development function, aimed at modifying the rate of shrinkage strain development with time

t_s = concrete age of curing

t_1 = 1 (day)

β_{sc} = coefficient that describes the type of cement and is equal to 5.0 for normal Portland-type cement or rapid hardening cement.

Model Code fib 2010

The total shrinkage may be calculated from equations A.9 and A.10:

$$\varepsilon_{cs}(t, t_s) = \varepsilon_{cas}(t) + \varepsilon_{cds}(t, t_s) \quad \text{(Equation A.9)}$$

Where:

$$\begin{aligned} \varepsilon_{cas}(t) &= \varepsilon_{cas0}(f_{cm}) \times \beta_{as}(t) \\ \varepsilon_{cds}(t, t_s) &= \varepsilon_{cds0}(f_{cm}) \times \beta_{RH}(RH) \times \beta_{ds}(t, t_s) \end{aligned} \quad \text{(Equation A.10)}$$

$\varepsilon_{cs}(t, t_s)$ = total shrinkage at time t

$\varepsilon_{cas}(t)$ = autogenous shrinkage at time t

$\varepsilon_{cds}(t, t_s)$ = drying shrinkage at time t

$\varepsilon_{cas0}(f_{cm})$ = notional autogenous shrinkage coefficient

$\varepsilon_{cds0}(f_{cm})$ = notional drying shrinkage coefficient

$\beta_{as}(t)$ = function to describe the time development of autogenous shrinkage

$\beta_{RH}(RH)$ = coefficient to take into account the effect of relative humidity on drying shrinkage

$\beta_{ds}(t, t_s)$ = function to describe the time development of drying shrinkage

t = concrete age [days]

t_s = concrete age at the onset of drying [days]

$t - t_s$ = duration of drying [days].

$$\begin{aligned} \varepsilon_{cds0}(f_{cm}) &= -\alpha_{as} \left(\frac{f_{cm}/10}{6 + f_{cm}/10} \right)^{2.5} \times 10^{-6} \\ \beta_{as} &= 1 - e^{(-0.2 \times \sqrt{t})} \end{aligned} \quad \text{(Equation A.11)}$$

f_{cm} = mean compressive strength at 28 days [N/mm²]

α_{as} = coefficient which depends on the type of cement, see table A.2

t = concrete age [days]

Table A.2 Coefficient of α_{as}

Strength class of cement	α_{as}
32.5N	800
32.5R, 42.5N	700
42.5R, 52.5N, 52.5R	600

A2.2 Parametric analyses of shrinkage

The aim of the parametric analyses was to study the effects of humidity percentage and notational thickness on shrinkage coefficient. To meet this aim, 3D graphs for t=100, 1,000, and 10,000 days were prepared as follows:

A2.2.1 3D graphs

The 3D graphs in figure A.7 show the effects of both notational thickness and humidity on the shrinkage coefficient predicted by CEB-FIP 78 and fib 2010, whereby the creep coefficient increases with the reduction in humidity and notational thickness.

Figure A.7 Drying shrinkage for concrete with t=100 days age

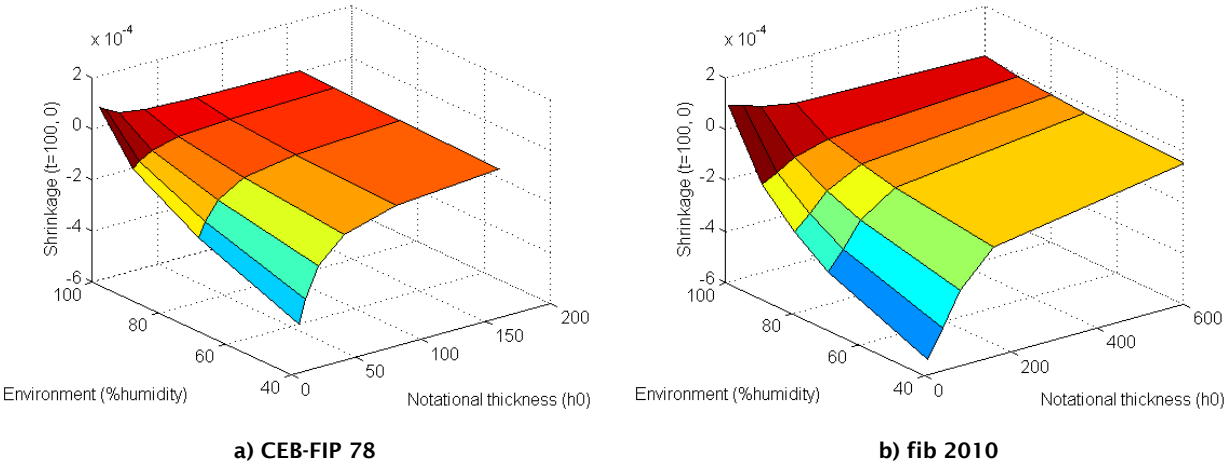


Figure A.8 Drying shrinkage for concrete with t=1,000 days age

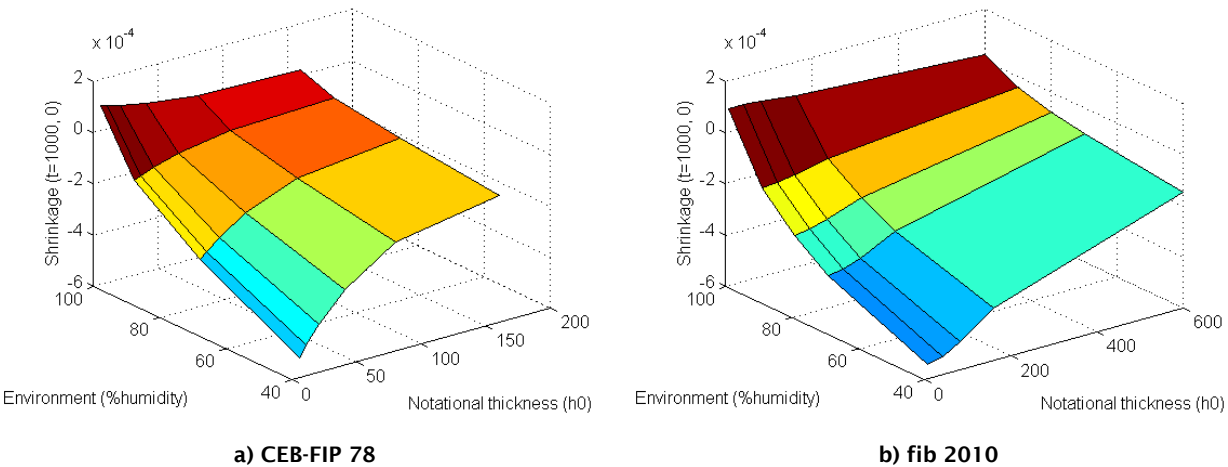
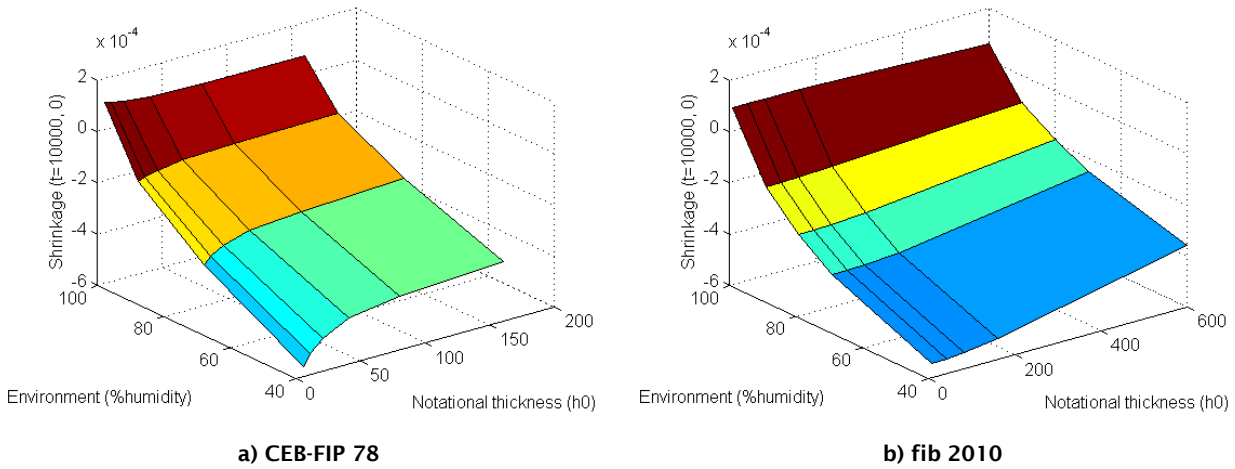


Figure A.9 Drying shrinkage for concrete with $t=10,000$ days age



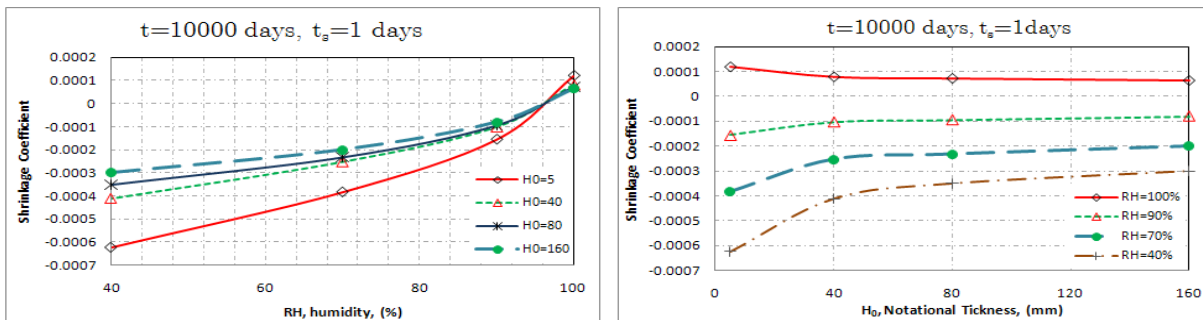
The effect of notational thickness on the shrinkage coefficient is a function of time. On the other hand in the initial stage, the shrinkage coefficient decreases significantly with the increase of notational thickness. However, the effect of notational thickness on the shrinkage coefficient can be neglected for $t \geq 10,000$ days.

A2.2.2 2D graphs

The 2D graphs in figures A.10, A.11 and A.12 show the effects of humidity and notational thickness on the shrinkage coefficient predicted by CEB-FIP 78 and fib 2010. These effects have been compared for $t = 500$ days and $t = 10,000$ days.

Model Code CEB-FIP 78

Figure A.10 Shrinkage coefficient for concrete age of $t=10,000$ days age by CEB-FIP 78



a) Effect of humidity for various notational thicknesses

b) Effect of notational thickness for various humidity percentages

fib Model Code 2010

Figure A.11 Shrinkage coefficient for concrete age of $t=10,000$ days age by fib 2010

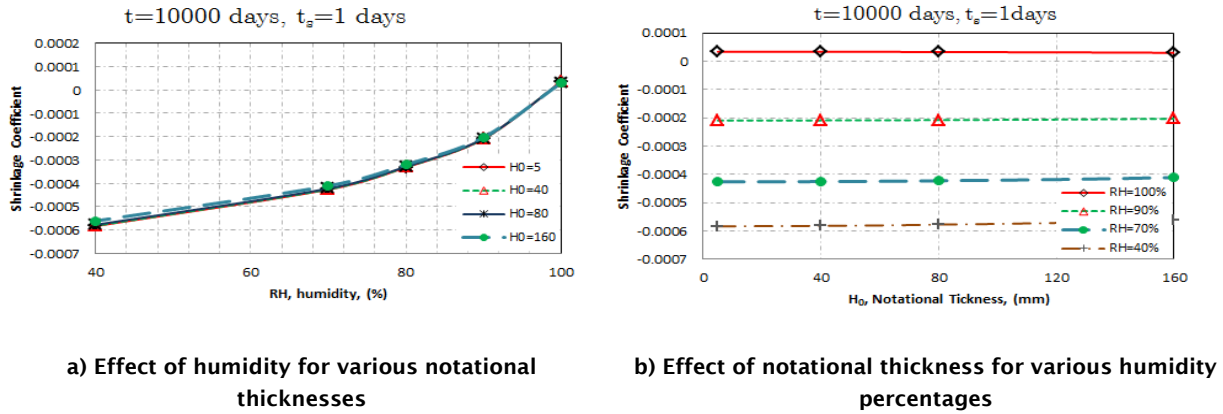
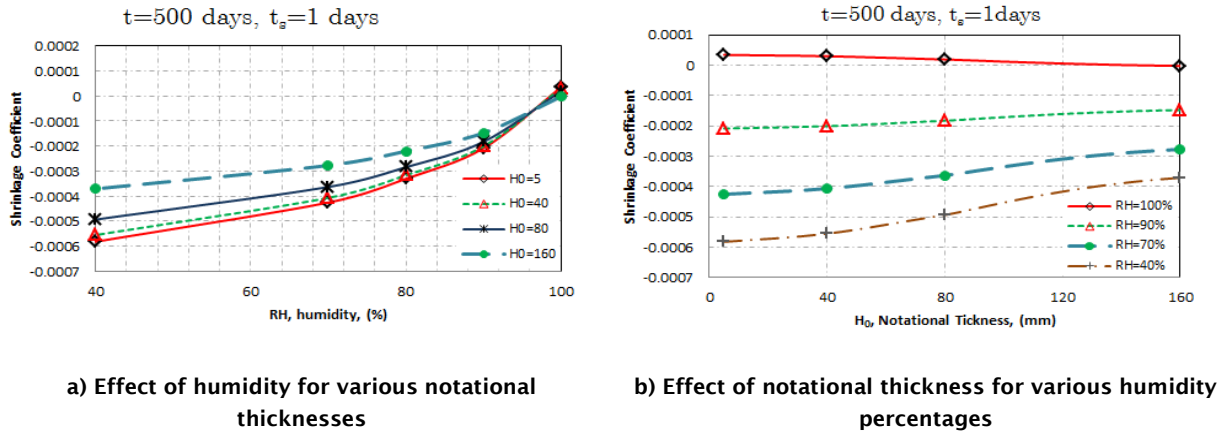


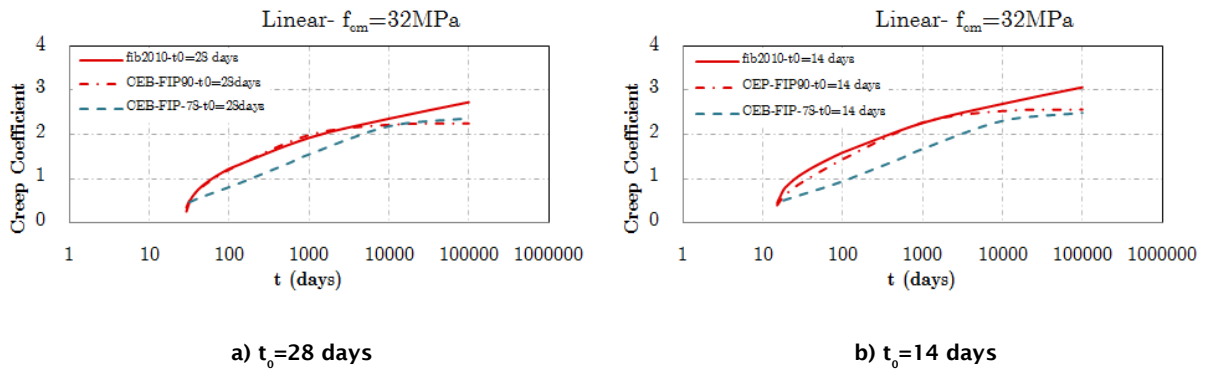
Figure A.12 Shrinkage coefficient for concrete age of $t=500$ days age by fib 2010



A3 Creep over time

Time-dependent creep coefficients have been presented for $h_0=160$ mm and 70% humidity for all selected model codes. The relationship between creep coefficients and time for all model codes is shown in figure A.13:

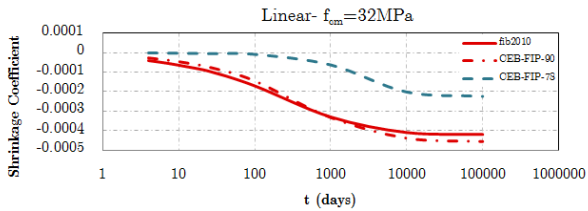
Figure A.13 Creep coefficient over time using different codes for $h_0=160$ mm and 70% humidity



A4 Shrinkage over time

Time-dependent shrinkage coefficients have been presented for $h_0=160\text{mm}$ and 70% humidity for all selected model codes. The relationship between shrinkage coefficients and time for all model codes is shown in figure A.14:

Figure A.14 Shrinkage coefficient over time using different codes for $h_0=160\text{mm}$ and 70% humidity



Appendix B: Creep and shrinkage of standard New Zealand precast concrete bridge decks

B1 Predicting creep and shrinkage of New Zealand precast concrete bridge decks

This appendix aims to predict the creep and shrinkage coefficients for typical bridge deck cross sections located in Christchurch, Wellington and Auckland, as set out in *NZ Transport Agency research report 364* (Beca and Opus 2008). To meet this goal, average relative humidities of Christchurch, Wellington and Auckland were estimated and notational thicknesses for typical cross sections presented in Beca and Opus (2008) were also calculated. Finally, shrinkage and creep coefficients for each cross section were predicted for the selected cities.

B2 Relative humidity in the selected cities

The hourly relative humidity data from the national climate database was collected for a number of stations in Christchurch, Wellington and Auckland. The average of the collected data was used as the relative humidity for each city – Christchurch 72.94%; Wellington 79.79% and Auckland 82.2%.

B3 Notational thickness and size of typical cross sections presented in Beca and Opus (2008)

Notational thickness has been mathematically presented as equation B.1 (CEB-FIP 78).

$$h_0 = \lambda \frac{2A_c}{u} \quad (\text{Equation B.1})$$

Where:

h_0 = notational thickness (mm)

A_c = concrete area (mm²)

U = perimeter in contact with atmosphere (mm)

λ = coefficient, see table B.1 :

Table B.1 Values of λ , according to CEB-FIP 78

Relative humidity	λ
100%	30
90%	5
70%	1.5
40%	1

According to table B.1 and the relative humidity estimated in section B.3, $\lambda = 1.55$, 1.66 and 1.8 for Christchurch, Wellington and Auckland respectively.

However CEB-FIP 90 and fib 2010 present notational size as in equation B.2:

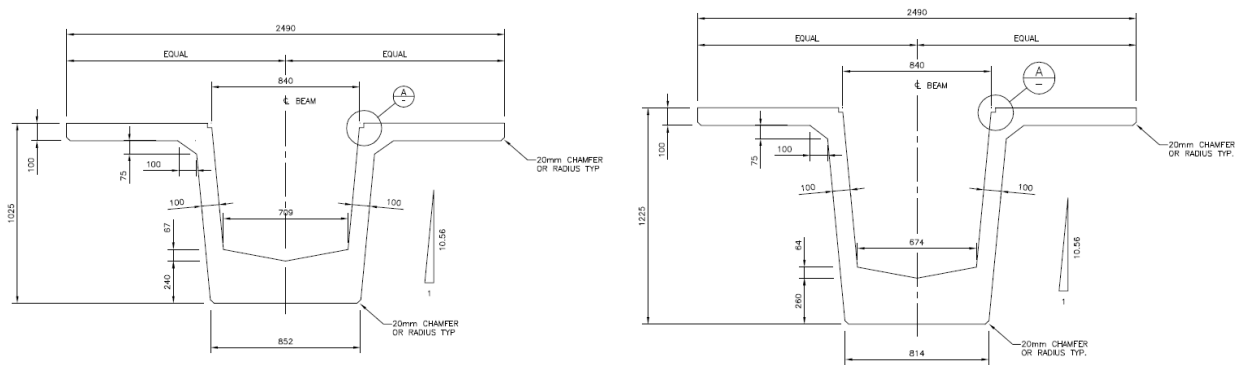
$$h = \frac{2A_c}{u} \tag{Equation B.2}$$

It is clear that the notational thickness and notational size relationship is as follows:

$$h_0 = \lambda \times h \tag{Equation B.3}$$

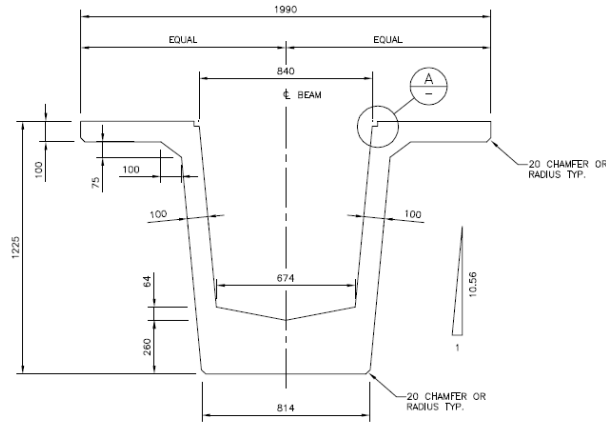
The calculated notational thickness and size and relative humidity of the selected cities are shown in table B.2. Typical cross sections in Beca and Opus (2008) are shown in figures B.1, B.2 and B.3:

Figure B.1 Typical super-tee sections



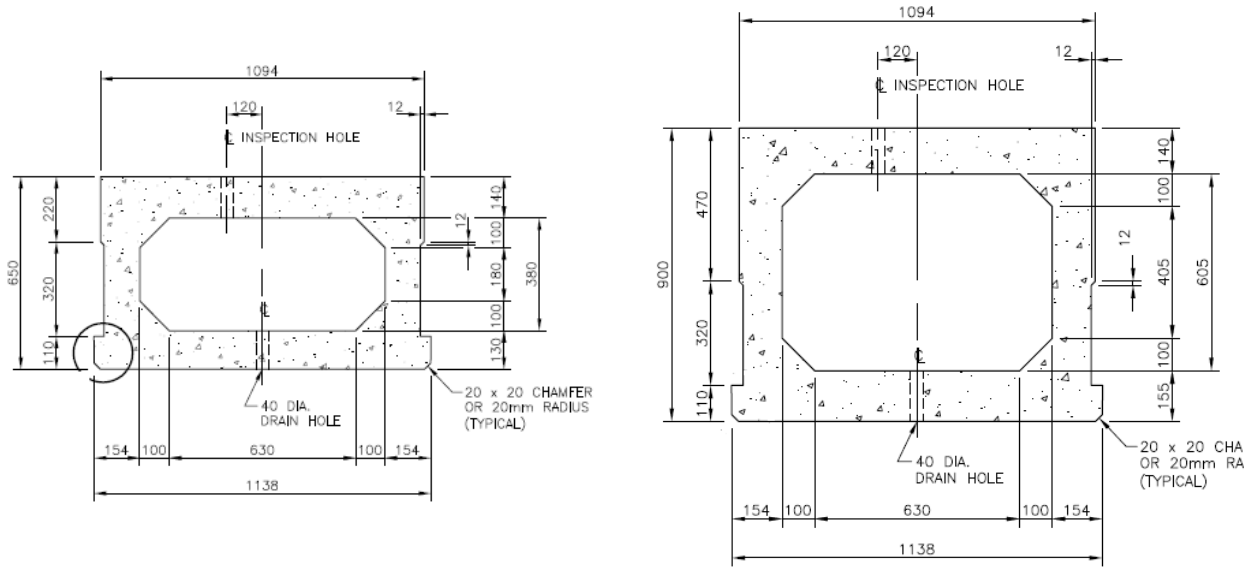
a) Typical cross section I

b) Typical cross section II



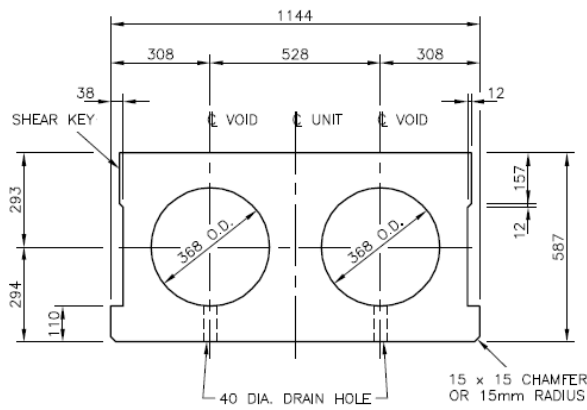
c) Typical cross section III

Figure B.2 Typical hollowcore sections



a) Typical cross section IV

b) Typical cross section V



c) Typical cross section VI

Figure B.3 Typical I-girder sections

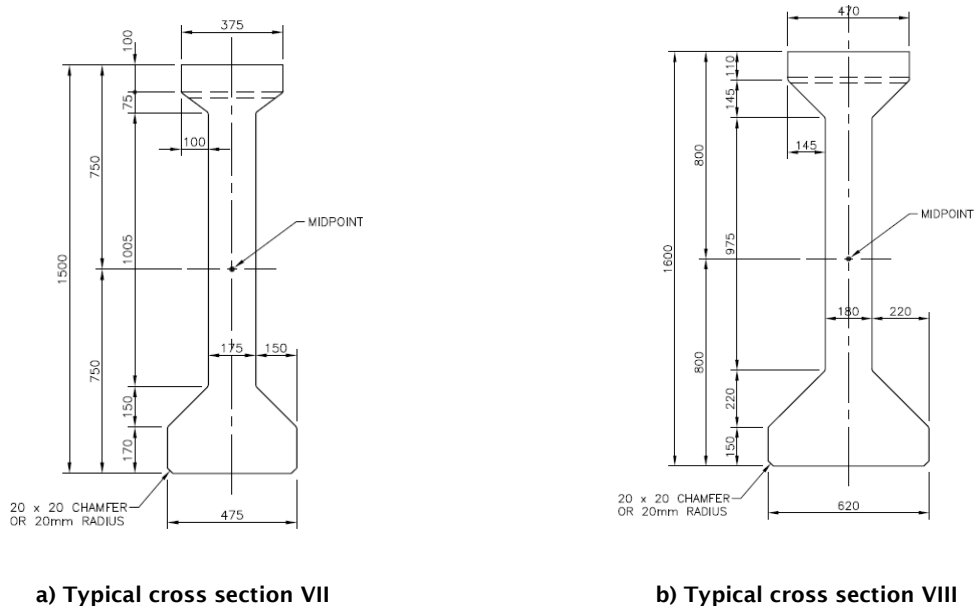


Table B.2 Notational thicknesses and sizes calculated for typical cross sections in Auckland, Christchurch and Wellington with estimated relative humidity

Cross section type	Christchurch, RH=72.94%		Wellington; RH=79.79%		Auckland; RH=82.4	
	h_0	h	h_0	h	h_0	h
I	399.56	257.78	427.91	257.78	464	257.78
II	395.25	255	423.3	255	459	255
III	406.1	262	434.92	262	471.6	262
IV	1131.5	730	1211.8	730	1314	730
V	1,368.65	883	1,465.78	883	1,589.4	883
VI	1,243.1	802	1,331.32	802	1,443.6	802
VII	304.575	196.5	326.19	196.5	353.7	196.5
VIII	342.55	221	366.86	221	397.8	221

The cross section type VII has minimum notational size indicating the greatest potential for creep and shrinkage deformations. Figures B.4 to B.9 compare time dependent creep and shrinkage coefficients for cross section VII located in Christchurch, Wellington and Auckland.

Figure B.4 Shrinkage coefficient over time calculated using fib 2010 for $h_0=196.5\text{mm}$ and humidity corresponding to ambient environment in Christchurch, Wellington and Auckland

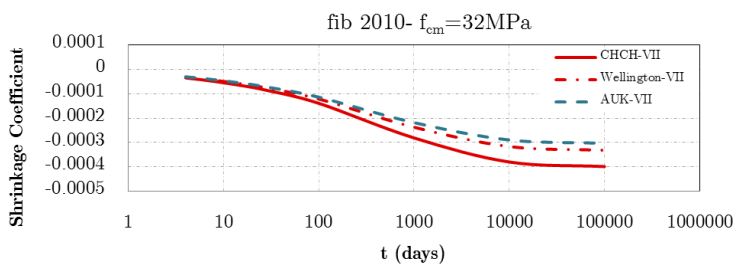


Figure B.5 Shrinkage coefficient over time calculated using CEB-FIP 90 for $h_0=196.5\text{mm}$ and humidity corresponding to ambient environment in Christchurch, Wellington and Auckland

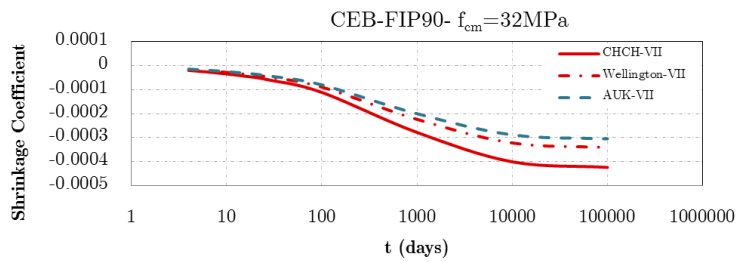


Figure B.6 Shrinkage coefficient over time calculated using CEB-FIP 78 for $h_0=196.5\text{mm}$ and humidity corresponding to ambient environment in Christchurch, Wellington and Auckland

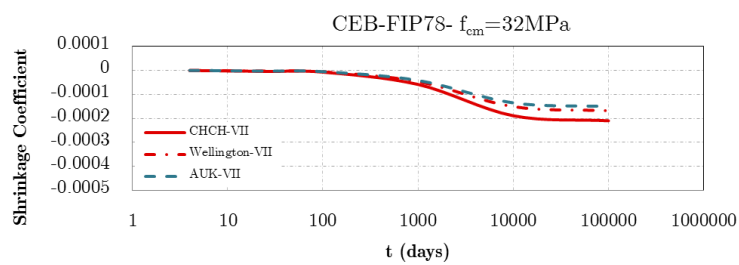


Figure B.7 Creep coefficient over time calculated using fib 2010 for $h_0=196.5\text{mm}$ and humidity corresponding to ambient environment in Christchurch, Wellington and Auckland

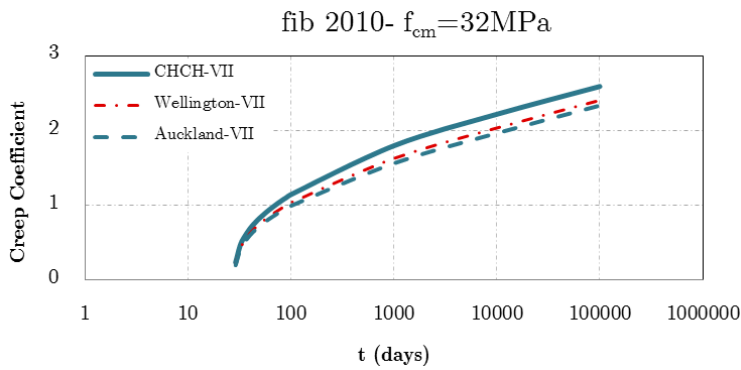


Figure B-8 Creep coefficient over time calculated using CEB-FIP 90 for $h_0=196.5\text{mm}$ and humidity corresponding to ambient environment in Christchurch, Wellington and Auckland

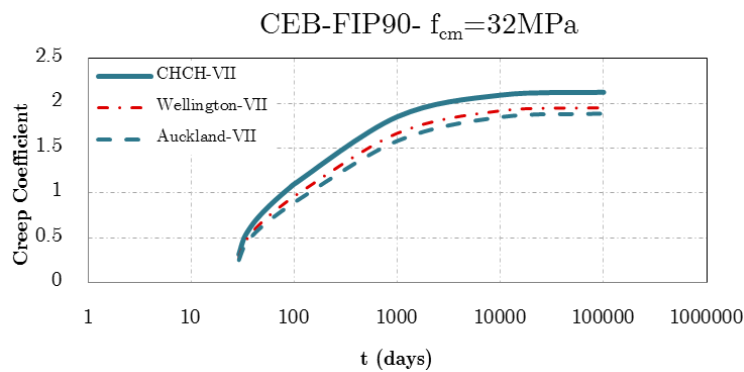
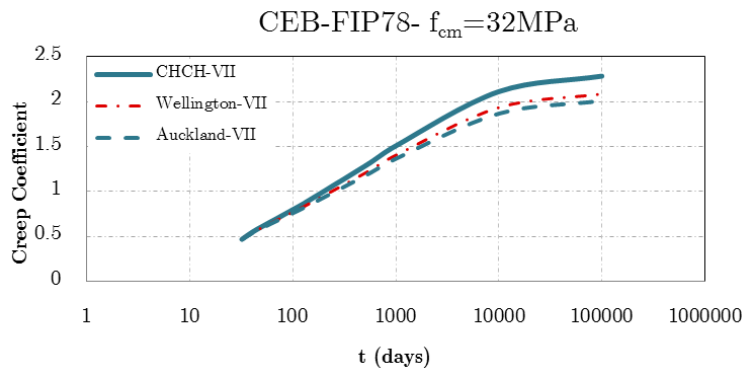


Figure B.9 Creep coefficient over time calculated using CEB-FIP 78 for $h_0=196.5\text{mm}$ and humidity corresponding to ambient environment in Christchurch, Wellington and Auckland



Appendix C: Simplified methods for creep of concrete superstructures

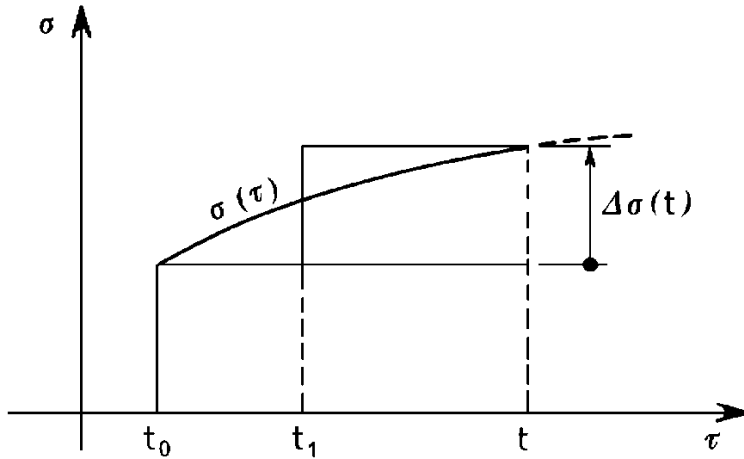
These methods simplify the complex time dependent stress-strain relationship by using one modified elastic modulus (effective modulus method) or a combination of two (age-adjusted modulus method).

A summary of the key steps are reported below. More details can be found in fib (2010) bulletins 65 and 66.

C1 Age-adjusted modulus method

Substituting the effective stress history of the creep phenomenon evaluated step-by-step ($\Delta\sigma(\tau)=\Delta\sigma(\tau)-\sigma$) with one instantaneous increase ($\Delta\sigma(t)=\Delta\sigma(t)-\sigma$) applied at an intermediate time t , algebraic expressions can be found.

Figure C.1 Age-adjusted effective modulus method



The integral is replaced as follows:

$$\int_{t_0}^t J(t, \tau) \cdot \frac{d\sigma(\tau)}{d\tau} d\tau \cong \frac{[\sigma(t) - \sigma(t_0)]}{E} \cdot [1 + \chi(t, t_0) \cdot \varphi(t, t_0)] \quad (\text{Equation C.1})$$

This solution considers the aging effect through an aging coefficient $\chi(t, t)$. It depends on the relaxation function but it is usually considered 0.8 for concrete.

Dividing the elastic contribution:

$$\varepsilon(t) - \bar{\varepsilon}(t) = \frac{\sigma(t_0)}{E} [1 + \varphi(t, t_0)] + \frac{[\sigma(t) - \sigma(t_0)]}{E} \cdot [1 + \chi(t, t_0) \cdot \varphi(t, t_0)] \quad (\text{Equation C.2})$$

This can be re-written:

$$\varepsilon(t) - \bar{\varepsilon}(t) = \frac{\sigma(t_0)}{E_{eff}} + \frac{\Delta\sigma(t)}{E_{adj}} \quad (\text{Equation C.3})$$

With:

$$E_{eff} = \frac{E_0}{1 + E_0/E_{28} \varphi_{28}(t, t_0)} \quad \text{(Equation C.4)}$$

$$E_{adj} = \frac{E_0}{1 + \chi(t, t_0) \cdot E_0/E_{28} \varphi_{28}(t, t_0)}$$

C2 Effective modulus method

Considering a single time step with $t = t_0$:

$$\varepsilon(t) - \bar{\varepsilon}(t) = \int_0^t J(t, \tau) \cdot \frac{d\sigma(\tau)}{d\tau} d\tau \cong [\sigma(t) - \sigma(t_0)] \cdot J(t, t_0) \quad \text{(Equation C.5)}$$

$$\varepsilon(t) - \bar{\varepsilon}(t) = \frac{\sigma(t)}{E_{eff}} = \frac{\sigma(t)}{E} \cdot [1 + \varphi(t, t_0)]$$

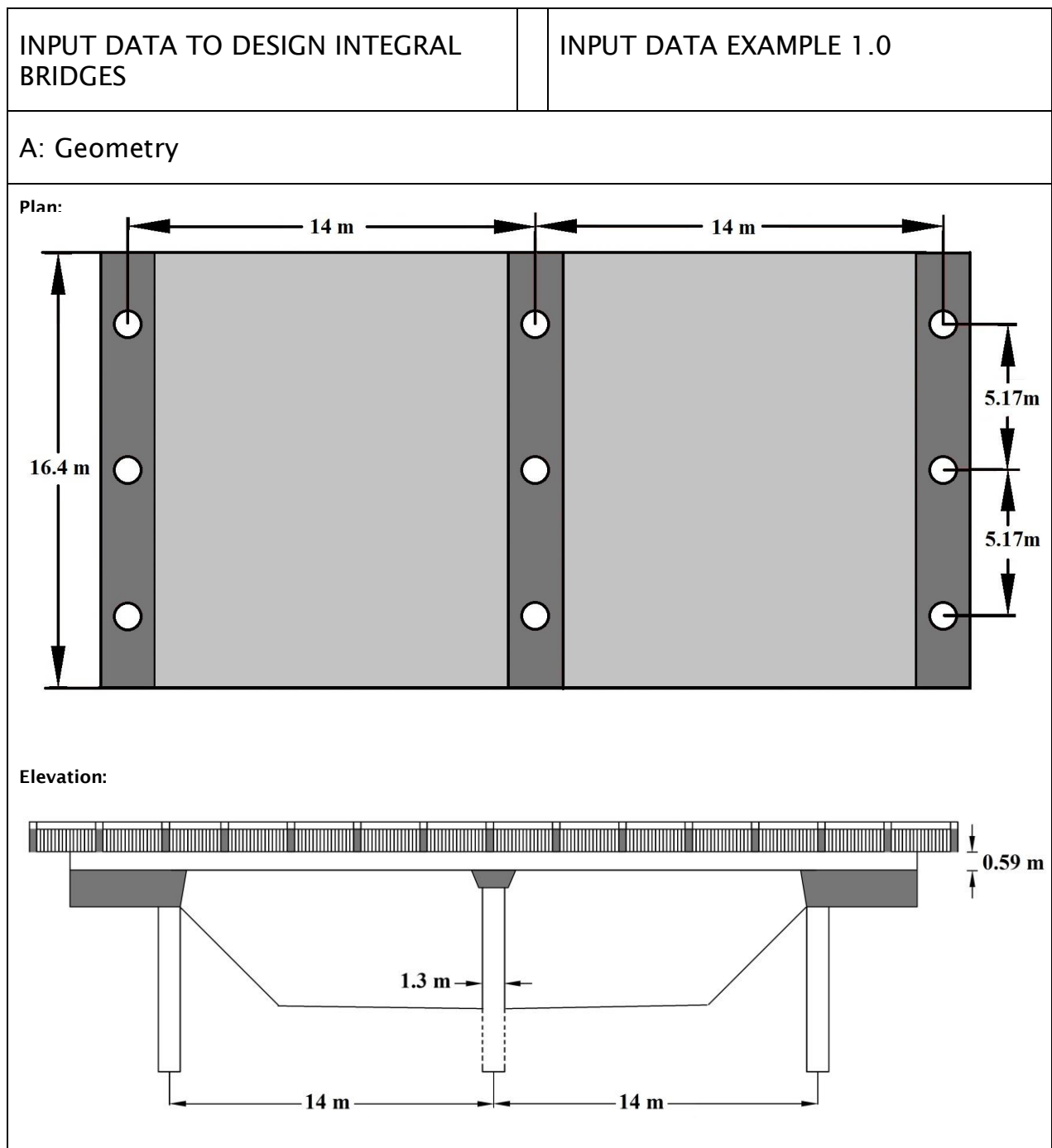
With:

$$E_{eff} = \frac{E_0}{1 + E_0/E_{28} \varphi_{28}(t, t_0)} \quad \text{(Equation C.6)}$$

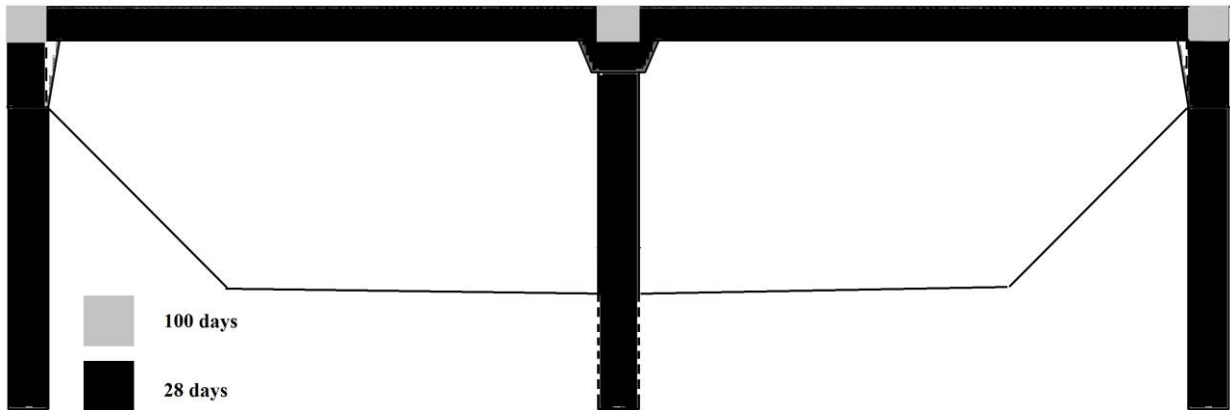
Appendix D: Design example

Fitzgerald Bridge – a case study

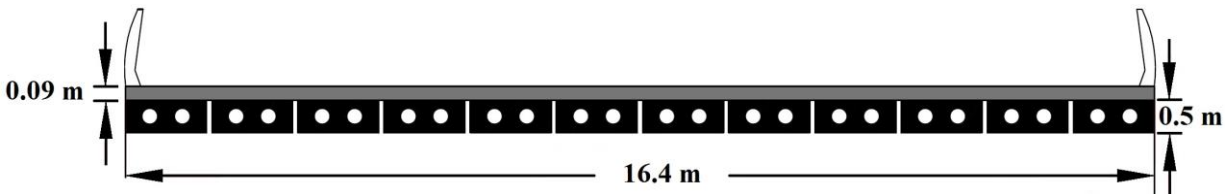
Presented below is a design example applying the principles discussed throughout the report to determine the effect of static and seismic actions on the Fitzgerald Bridge in Christchurch. Static actions, namely concrete creep, shrinkage and temperature effects, are covered in the first section, while the second section presents an example of displacement-based design principles applied to the Fitzgerald Bridge.



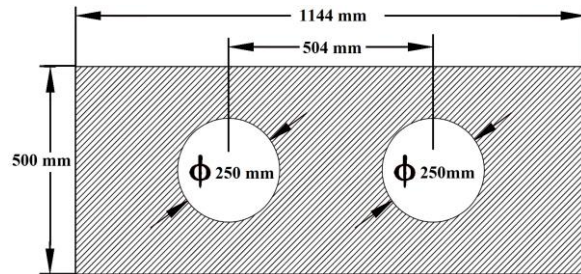
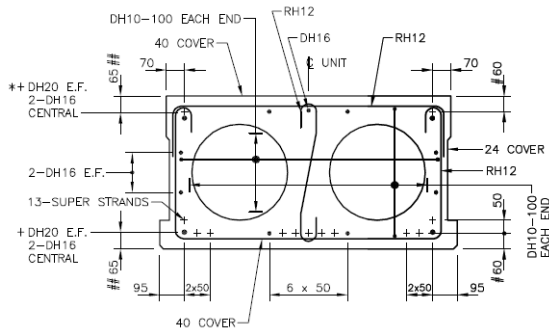
Construction stage:



Deck section:

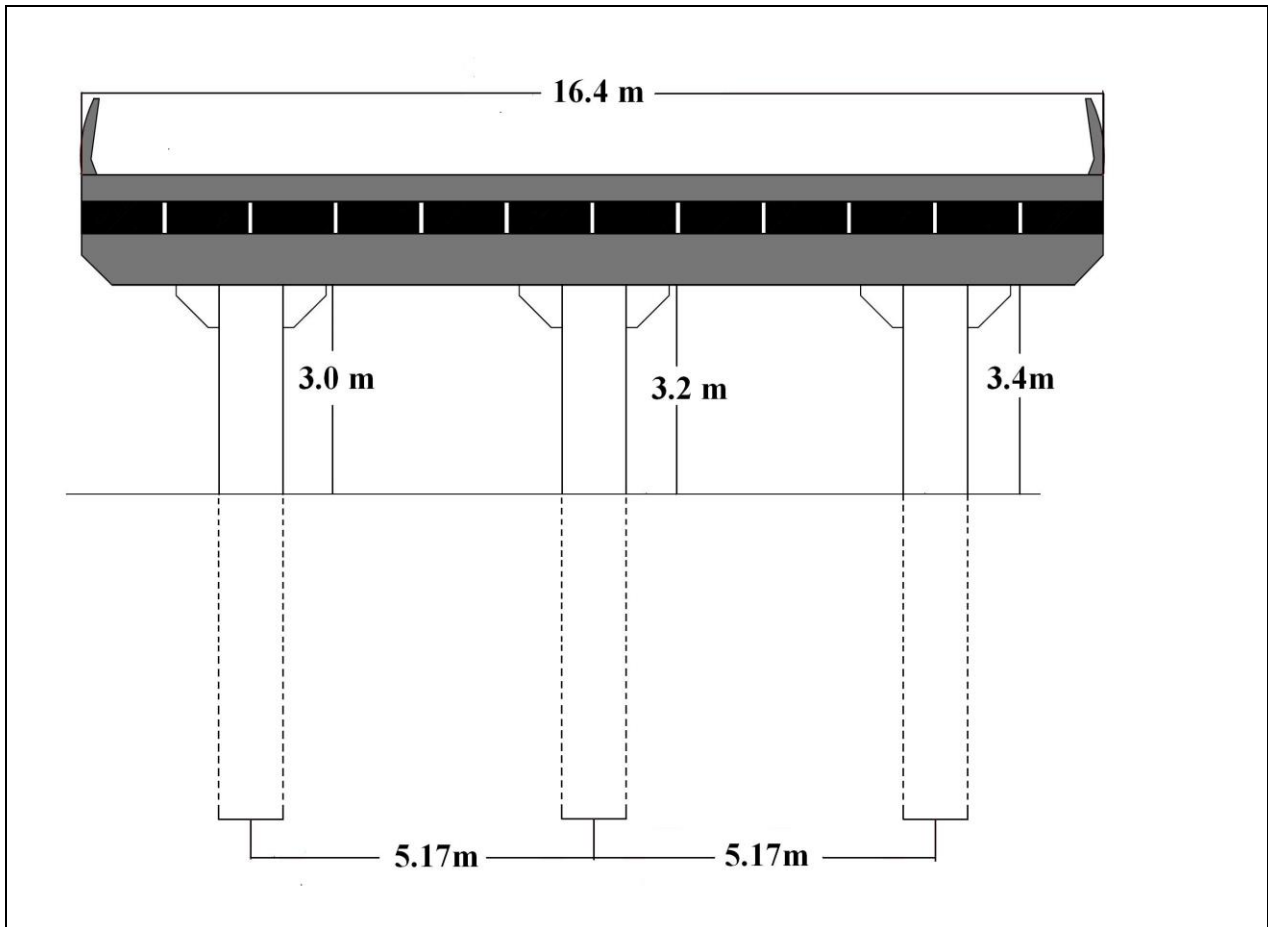


Geometry of single deck element:



Left: Typical details deck unit (Beca and Opus 2008)

Right: Details of the unit used in the Fitzgerald Bridge



B: Bridge properties

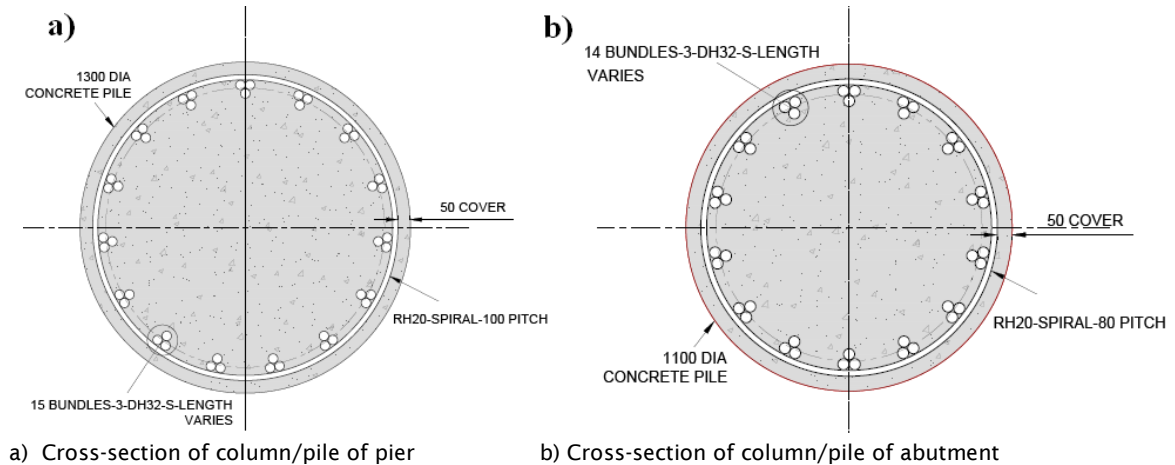
Determine properties of the bridge:

- number of supports, m
- number of girders per support, n
- angle of skew
- piers heights (clear dimensions).

B: Bridge properties, example 1.0

- Number of supports, $m = 3$
 - north abutment ($m = 1$)
 - pier ($m = 2$)
 - south abutment ($m = 3$)
- Number of girders per support, $n = 12$
- Number of columns per support = 3
- Angle of skew = 0°

Cross section of column/pile:



C: Material

Concrete

$f'_c = 50 \text{ MPa}$ Superstructure; $f'_c = 40 \text{ MPa}$ for Piers

Steel reinforcement

$f_y = 500 \text{ MPa}$; $f_{yh} = 500 \text{ MPa}$; $\epsilon_u = 0.12$

Pre-stressed steel

$f_{u1} = 1720 \text{ MPa}$; $f_{u2} = 1860 \text{ MPa}$

D: Geotechnical data

IN SITU SOIL PROPERTIES

Location	Depth range (mbgl)	Material description	Relative density	Angle of internal friction, ϕ (°)	Unit weight (kN/m ³)	Coefficient of passive earth pressure, K_p	Lateral soil modulus, K (kN/m ³)
North bank	0 - 3	SILT with sand and clay	Soft	28	16	3.1	8,140
	3 - 7	SAND with silt and gravel	Medium dense	32	19	3.7	16,300
	7 - 23	SAND	Medium dense	30	20	3.4	16,300
	23 +	GRAVEL	Very dense	40	21	5.6	34,000
South bank	0 - 3	Clayey SILT and SAND	Soft	30	18	3.4	8,140
	3 - 7.5	GRAVEL	Dense	36	21	4.5	20,000
	7.5 - 22	SAND	Medium dense	32	19	3.7	16,300
	22 - 26	SILT	Firm	28	20	3.1	30,000
	26 +	GRAVEL	Dense	38	21	5.0	34,000

The geotechnical data of the site of the bridge crossing the Avon River, Christchurch

E: Earth pressure (EP)

- Unit weight of soil (γ)
- Angle of internal friction of soil (ϕ)
- Wall friction angle ($W\phi$)
- Coefficient of at-rest earth pressure, K_0
- Coefficient of active earth pressure, K_A
- Coefficient of passive earth pressure, K_P
- Effective coefficient of at-rest earth pressure, K^* , due to thermal expansion and contraction of soil (in accordance with BA 42/96)

E:

- $\gamma = 20 \text{ kN/m}^3$
- $\phi = 30^\circ$
- $W\phi = \frac{2}{3}\phi$ FOR ACTIVE CASE
- $W\phi = \frac{1}{3}\phi$ FOR PASSIVE CASE
- $K_0 = 0.5$ FOR BACKFILL
- $K_A = 0.3$ FOR BACKFILL
- $K_P = 4.14$ FOR BACKFILL
- $K^* = 1.6$ FOR BACKFILL

F: Creep and shrinkage

The provisions of fib 2010 were used to estimate the secondary effects of creep and shrinkage, based on the following assumptions:

- 1 The in-situ concrete deck was installed at $t=28$ days (ie, no differential creep or shrinkage occurred before $t = 28$ days)
- 2 The joints were constructed at $t=100$ days (From $t = 28$ days to $t = 100$ days creep and shrinkage happened while the beams were simply supported).

Therefore the secondary effects calculations were categorised into three groups in term of time: Before $t = 28$ days; $t = 100$ days; $t = \infty = 36500$ days (representing the 100-year design life of the bridge).

F1: Time-dependent creep coefficient

Using fib (2010):

$$\varphi(t, t') = \varphi_{bc}(t, t') \times \varphi_{ac}(t, t') \quad (17)$$

$$\varphi_{bc}(t, t') = \beta_{bc}(f_{cm}) \times \beta_{bc}(t, t') \quad (18)$$

$$\beta_{bc}(f_{cm}) = \frac{1.8}{(f_{cm})^{0.7}} \quad (19)$$

$$\beta_{bc}(t, t') = \ln \left[\left(\frac{30}{t'_{adj}} + 0.035 \right)^2 \times (t - t') + 1 \right] \quad (20)$$

$$\varphi_{ac}(t, t') = \beta_{ac}(f_{cm}) \times \beta(RH) \times \beta_{ac}(t') \times \beta_{ac}(t, t') \quad (21)$$

$$\beta_{ac}(f_{cm}) = \frac{412}{(f_{cm})^{1.4}} \quad (22)$$

$$\beta(RH) = \frac{1 - RH/100}{\sqrt[3]{0.1 \times h/100}} \quad (23)$$

$$\beta_{ac}(t') = \frac{1}{0.1 + (t'_{adj})^{0.2}} \quad (24)$$

$$\beta_{ac}(t, t') = \left[\frac{(t - t')}{\beta_n + (t - t')} \right]^{\gamma(t')} \quad (25)$$

$$\gamma(t') = \frac{1}{2.3 + \frac{3.5}{\sqrt{t'_{adj}}}} \quad (26)$$

$$\beta_n = 1.5 \times h + 250 \times \alpha_{f_{cm}} \leq 1500 \times \alpha_{f_{cm}} \quad (27)$$

Where h is notational size as follows:

$$h = \frac{2A_c}{u}$$

where A_c is concrete area (mm^2), u is perimeter in contact with atmosphere (mm)

$$\alpha_{f_{cm}} = \left(\frac{35}{f_{cm}} \right)^{0.5} \quad (28)$$

$$\varphi_{\sigma}(t, t') = \varphi(t, t') e^{1.5 \times (k_{\sigma} - 0.4)} \quad (29)$$

$$0.4 < k_{\sigma} \leq 0.6 \quad k_{\sigma} = \frac{|\sigma|}{f_{cm}(t_0)} \quad (30)$$

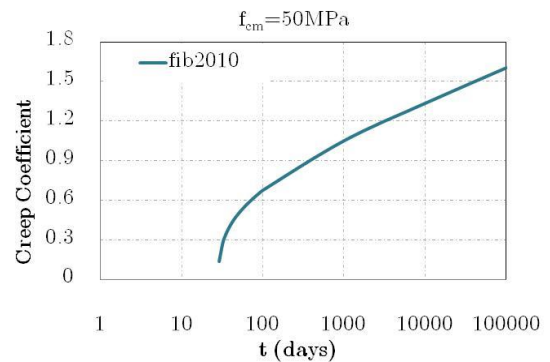
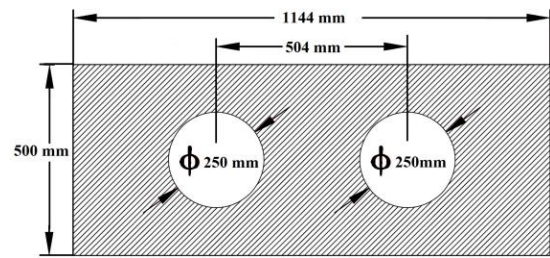
F1: Time-dependent creep coefficient - example 1.0

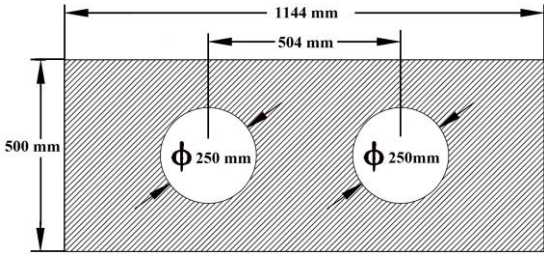
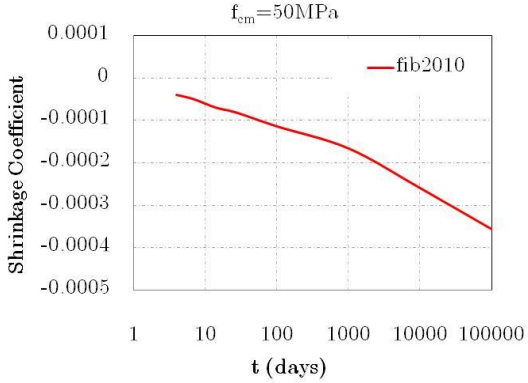
$h=828.36$ mm

$f'_c=50$ MPa

RH=72.94%

$t' = 28$ days



<p>F2: Shrinkage</p> <p>Shrinkage strain using fib 2010:</p> $\varepsilon_{cs}(t, t_s) = \varepsilon_{cas}(t) + \varepsilon_{cds}(t, t_s) \quad (44)$ <p>Where:</p> $\varepsilon_{cas}(t) = \varepsilon_{cas0}(f_{cm}) \times \beta_{as}(t) \quad (45)$ $\varepsilon_{cds}(t, t_s) = \varepsilon_{cds0}(f_{cm}) \times \beta_{RH}(RH) \times \beta_{ds}(t, t_s) \quad (46)$ <p>$\varepsilon_{cs}(t, t_s)$: Total shrinkage at time t</p> <p>$\varepsilon_{cas}(t)$: Autogenous shrinkage at time t</p> <p>$\varepsilon_{cds}(t, t_s)$: Drying shrinkage at time t</p> <p>$\varepsilon_{cas0}(f_{cm})$: Notional autogenous shrinkage coefficient</p> <p>$\varepsilon_{cds0}(f_{cm})$: Notional drying shrinkage coefficient</p> <p>$\beta_{as}(t)$: Function to describe the time development of autogenous shrinkage</p> <p>$\beta_{RH}(RH)$: Coefficient to take into account the effect of relative humidity on drying shrinkage</p> <p>$\beta_{ds}(t, t_s)$: Function to describe the time development of drying shrinkage</p> <p>t: Concrete age [days]</p> <p>t_s: Concrete age at the onset of drying [days]</p> <p>$t - t_s$: Duration of drying [days].</p> $\varepsilon_{cds0}(f_{cm}) = -\alpha_{as} \left(\frac{f_{cm}/10}{6 + f_{cm}/10} \right)^{2.5} \times 10^{-6} \quad (47)$ $\beta_{as} = 1 - e^{(-0.2 \times \sqrt{t})} \quad (48)$ <p>f_{cm}: Mean compressive strength at the age of 28 days [N/mm²]</p> <p>α_{as}: Coefficient which depends on the type of cement, see table 1</p> <p>t: Concrete age [days]</p>	<p>F2: Shrinkage - example 1.0</p> <p>$h=828.36$ mm</p> <p>$f'_c=50$MPa</p> <p>RH=72.94%</p> <p>$t_s = 5$ days</p>  <p style="text-align: center;">Table 1: Coefficient of α_{as}</p> <table border="1" style="margin-left: auto; margin-right: auto;"> <thead> <tr> <th>Strength class of cement</th> <th>α_{as}</th> </tr> </thead> <tbody> <tr> <td>32.5N</td> <td>800</td> </tr> <tr> <td>32.5R, 42.5N</td> <td>700</td> </tr> <tr> <td>42.5R, 52.5N, 52.5R</td> <td>600</td> </tr> </tbody> </table> 	Strength class of cement	α_{as}	32.5N	800	32.5R, 42.5N	700	42.5R, 52.5N, 52.5R	600
Strength class of cement	α_{as}								
32.5N	800								
32.5R, 42.5N	700								
42.5R, 52.5N, 52.5R	600								

F3: Secondary effects of creep and shrinkage

F3.1. Strain in the precast beam due to pre-stressing

$$\epsilon_{PS}^{Top} = \left(\frac{N_{P0}}{EA} - \frac{M_{P0}y_{Top}}{EI} \right)$$

$$\epsilon_{PS}^{Bot} = \left(\frac{N_{P0}}{EA} + \frac{M_{P0}y_{Bot}}{EI} \right)$$

Where ϵ_{PS}^{Top} and ϵ_{PS}^{Bot} are maximum strain in top and bottom of section of beam respectively

A , I , and E are section area, moment of inertia of the section and module of elasticity of concrete

y_{Top} and y_{Bot} are maximum distance of top and bottom of the beam section from neutral axis.

$$N_{P0} = N \times 0.6F_{Pu}$$

Where N_{P0} axial force; N = number of stands; and F_{Pu} : maximum force of each stand

$$M_{P0} = N_{P0} \times e$$

Where: M_{P0} is moment due to pre-stressing; and e is eccentricity

F3: Secondary effects of creep and shrinkage - example 1.0

F3.1. Strain in the precast beam due to pre-stressing - example 1.0

$$F_{Pu} = 160 \text{ KN}$$

$$E = 30000 \text{ MN/m}^2$$

$$I = \frac{1}{12} 0.5^3 \times 1.144 - 2 \frac{1}{4} \pi \times 0.125^4$$

$$I = 0.011533 \text{ m}^4$$

$$EI = 346 \text{ MN.m}^2$$

$$A = 0.4738 \text{ m}^2$$

$$N_{P0} = 13 \times 0.6 \times 160 = 1248 \text{ KN}$$

$$e = 0.153 \text{ m}$$

$$M_{P0} = 1248 \times 0.153 = 191 \text{ KN.m}$$

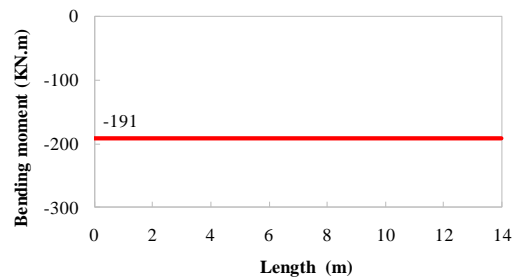
$$\epsilon_{PS}^{Top} = 8.78 \times 10^{-5} - 13.8 \times 10^{-5}$$

$$\epsilon_{PS}^{Bot} = 8.78 \times 10^{-5} + 13.8 \times 10^{-5}$$

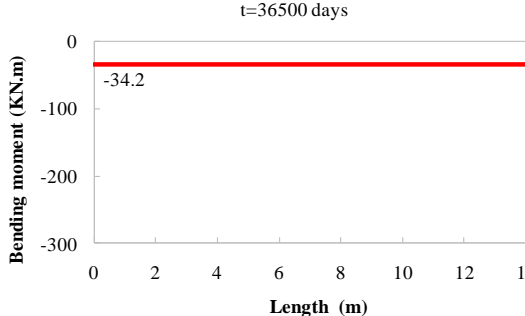
$$\epsilon_{PS}^{Top} = -5.02 \times 10^{-5}$$

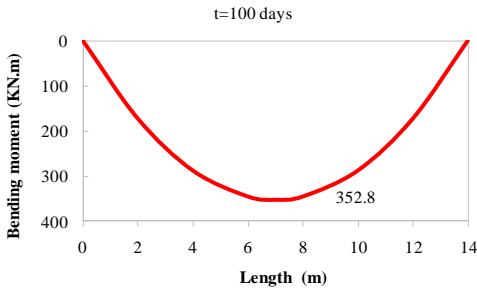
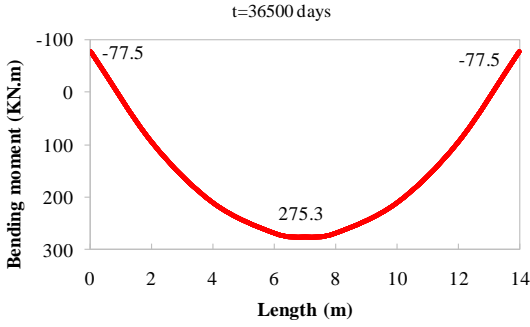
$$\epsilon_{PS}^{Bot} = +22.58 \times 10^{-5}$$

$t=100$ days



<p>F3.2: Pre-stressing induced axial force losses before casting the joints due to creep</p> <p>It was assumed that the joints were built when concrete of beam was 100 days old.</p> <p>Strain in precast beam due to permanent loads can be approximated to the centroidal strain (Nicholson 1998).</p> $\Delta\varepsilon_{PS} = \varepsilon_{PS} \times \varphi(28,100)$ $\Delta N_{PS,100} = E_{PS} \Delta\varepsilon_{PS} \times A_{PS}$ $N_{PS}(28,100) = N_{P0} - \Delta N_{PS,100}$ <p>Where ε_{PS} is the strain at the centre of the section; $N_{PS}(28,100)$ is axial force of pre-stressing stands when age of concrete of beam is 100 days; A_{PS} and E_{PS} are area and module of elasticity of pre-stressed stands respectively; ΔN_{PS} is axial force loss due to creep</p>	<p>F3.2: Pre-stressing induced axial force losses before casting the joints due to creep – example 1.0</p> <table border="1" data-bbox="807 376 1355 546"> <tr> <th colspan="4">Creep coefficient as per fib (2010)</th> </tr> <tr> <th colspan="4">$\infty = 100$ years</th> </tr> <tr> <td>$\varphi(28,100)$</td> <td>0.67</td> <td>$\varphi(28, \infty)$</td> <td>1.49</td> </tr> </table> $\varepsilon_{PS} = 8.78 \times 10^{-5}$ $\Delta\varepsilon_{PS} = 8.78 \times 10^{-5} \times 0.67 = 5.88 \times 10^{-5}$ <p>13 pre-stressed stands 12.7mm DIA.</p> $\Delta N_{PS,100} = 200 \times 10^9 \times 5.88 \times 10^{-5} \times 1.267 \times 10^{-4}$ $\Delta N_{PS,100} = 1.49 \text{ KN}$ $N_{PS}(28,100) = 1248 - 1.49 = 1246.51 \text{ KN}$	Creep coefficient as per fib (2010)				$\infty = 100$ years				$\varphi(28,100)$	0.67	$\varphi(28, \infty)$	1.49
Creep coefficient as per fib (2010)													
$\infty = 100$ years													
$\varphi(28,100)$	0.67	$\varphi(28, \infty)$	1.49										
<p>F3.3: Pre-stressing induced axial force losses after casting the joints</p> <p>The pre-stressed losses are restrained by joints</p> $\Delta\varepsilon_{PS}^{\infty} = \frac{N_{P0}}{EA} \Delta\varphi \pm \frac{M_{P0}Y}{EI} \Delta\varphi$ $\Delta\varphi(28, \infty) = \varphi(28, \infty) - \varphi(28,100)$ <p>Where $\Delta\varepsilon_{PS}^{\infty}$ is total creep strain including axial and bending creep strain.</p> $\begin{cases} \Delta\varepsilon_{PS,Axial}^{\infty} = \frac{N_{P0}}{EA} \Delta\varphi \\ \Delta\varepsilon_{PS,Bending}^{\infty} = \frac{M_{P0}Y}{EI} \Delta\varphi \end{cases}$ <p>Where $\Delta\varepsilon_{PS,Axial}^{\infty}$ and $\Delta\varepsilon_{PS,Bending}^{\infty}$ are axial and bending creep strain respectively.</p> <p>The maximum axial force loss is as follows if the deck is free at joints (this is conservative but safe).</p> $\Delta N_{PS}^{\infty} = \frac{N_{P0}}{EA} \Delta\varphi \times E \times A$	<p>F3.3: Pre-stressing induced axial force losses after casting the joints – example 1.0</p> $\Delta\varphi(28, \infty) = 1.49 - 0.67 = 0.82$ $\Delta\varepsilon_{PS}^{\infty} = 8.78 \times 10^{-5} \times 0.82 \pm 13.8 \times 10^{-5} \times 0.82$ $\Delta\varepsilon_{PS,Axial}^{\infty} = 8.78 \times 10^{-5} \times 0.82 = 7.2 \times 10^{-5}$ $\Delta\varepsilon_{PS,Bending}^{\infty} = 13.8 \times 10^{-5} \times 0.82 = 11.32 \times 10^{-5}$ $\Delta N_{PS}^{\infty} = 7.2 \times 10^{-5} \times 30000 \times 0.4738$ $\Delta N_{PS}^{\infty} = 1.0234 \text{ MN} = 1023 \text{ KN}$ <p>Note that $\Delta N_{PS}^{\infty} = 1023 \text{ KN}$ will be achieved only if beams (deck) is free at ends. This is conservative and safe. However the aforementioned loss of axial force will be restrained by stiffness property of abutments. If the abutments are fully fixed, the axial force loss will be zero. It means that joints restrain pre-stressed force losses and reduce the secondary effects.</p>												

<p>F3.4: Maximum pre-stressing induced bending moment losses</p> <p>The maximum bending moment losses can be estimated using superimposing the losses before and after casting the joints as follows:</p> $\Delta M_{PS}^{\text{Before casting}} = E_{PS} \cdot \Delta \varepsilon_{PS} \cdot A_{PS} \cdot e$ $\Delta M_{PS}^{\text{After casting}} = N_{P0} \cdot e \cdot \Delta \varphi$ $\Delta M_{PS}^{\text{Max.}} = \Delta M_{PS}^{\text{Before casting}} + \Delta M_{PS}^{\text{After casting}}$ $M_{PS}^{\infty} = M_{P0} - \Delta M_{PS}^{\text{Max.}}$ <p>The above value is conservative and safe. It should be noted that the joints reduce the maximum pre-stressing induced bending moment losses</p>	<p>F3.4: Maximum pre-stressing induced bending moment losses - Example 1.0</p> $\Delta M_{PS}^{\text{Before casting}} = 200 \times 10^9 \times 5.88 \times 10^{-5} \times 1.267 \times 10^{-4} \times 0.153 = 0.228 \text{ KN.m}$ $\Delta M_{PS}^{\text{After casting}} = 1248 \times 0.153 \times 0.82 = 156.6 \text{ KN.m}$ $\Delta M_{PS}^{\text{Max.}} = 0.228 + 156.6 = 156.8 \text{ KN}$ $M_{PS}^{\infty} = 191 - 156.8 = 34.2 \text{ KN.m}$ <p style="text-align: center;">t=36500 days</p> 		
<p>F3.5: Axial load due to shrinkage</p> <p>As the joints were built when the age of concrete was 100 days, the shrinkage of the first 100 days cannot create axial force. After casting the joints, the shrinkage axial force can be calculated as follows if abutments are fully fixed:</p> $N_{\text{axial}}^{\text{Shrinkage}} = \varepsilon_{Sh}(100, \infty) \times E \times A$ <p>This assumption is again conservative but safe. Note: The stiffness and contribution of abutments flexibility should be considered to estimate precise axial force due to shrinkage.</p>	<p>F3.5: Axial load due to shrinkage - example 1.0</p> <p>The strain due to shrinkage accordance with FIB 2010 is as follows:</p> <table border="1" data-bbox="842 1182 1430 1267"> <tr> <td>$\varepsilon_{Sh}(100, \infty)$</td> <td>$-3.23 \times 10^{-4}$</td> </tr> </table> $N_{\text{axial}}^{\text{Shrinkage}} = -3.23 \times 10^{-4} \times 30000 \times 0.4738$ $N_{\text{axial}}^{\text{Shrinkage}} = 4591 \text{ KN}$	$\varepsilon_{Sh}(100, \infty)$	-3.23×10^{-4}
$\varepsilon_{Sh}(100, \infty)$	-3.23×10^{-4}		
<p>F3.6: Bending moment and deflection in the precast beam due to dead load before casting the joints</p> <p>Initial maximum bending moment and slope at the ends in the time of installing pre-cast beams (concrete age of 28 days and beams are simply supported) is as follows:</p> $M_{\text{max}} = \frac{wl^2}{8}$ $\theta_{28} = \frac{wl^3}{24EI}$ <p>The maximum bending moment and the slope at the ends just before casting the joints (concrete age of 100 days) is as follows:</p>	<p>F3.6: Bending moment and deflection in the precast beam due to dead load before casting the joints - example 1.0</p> $w = 11.84(\text{beam}) + 2.57(\text{surface}) = 14.4 \text{ KN/m}$ <p>The maximum bending moment and slope at the ends when concrete age is 28 days are as follows:</p> $M_{\text{max};28} = \frac{14.4 \times 14^2}{8} = 353 \text{ KN.m}$ $EI = 3 \times 10^7 \times 0.011533 = 346000 \text{ KN.m}^2$ $\theta_{28} = \frac{14.4 \times 14^3}{24 \times 346000} = 0.004758$		

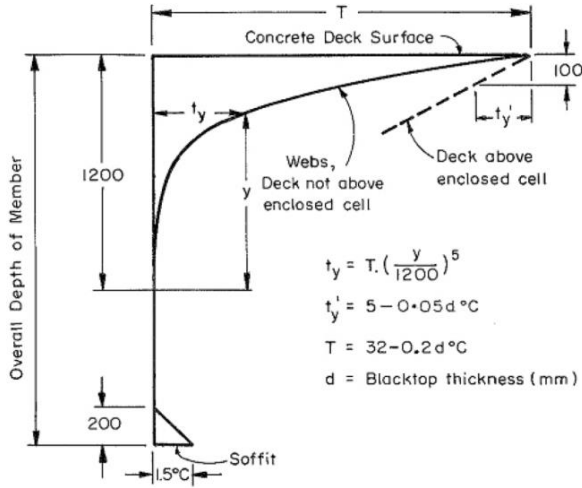
$M_{max} = \frac{wl^2}{8}$ $\theta_{100} = \frac{wl^3}{24EI} (1 + \varphi(28,100))$ <p>Before casting the joints the slope at ends increases due to moment, but bending moment doesn't change.</p>	<p>The maximum bending moment and slope at the ends when concrete age is 100 days are as follows:</p> $M_{max;100} = \frac{14.4 \times 14^2}{8} = 352.8 \text{ KN.m}$ $\theta_{100} = \frac{14.4 \times 14^3}{24 \times 346000} \times (1 + 0.67) = 0.007946$ 
<p><i>F3.7: Bending moment in the precast beam due to dead load after casting the joints</i></p> <p>Maximum bending moment after casting the joints</p> $M_{max} = \frac{wl^2}{12} \times \frac{\Delta\varphi}{1 + \varphi(28,t)}$ <p>Where $\varphi(28,t)$ is creep coefficient in time of estimation of bending moment</p>	<p><i>F3.7: Bending moment in the precast beam due to dead load after casting the joints - example 1.0</i></p> <p>Assuming $t = 36500 \text{ days} = 100 \text{ years}$</p> $M_{max} = \frac{14.4 \times 14^2}{12} \times \frac{0.82}{1 + 1.49} = 77.5 \text{ KN.m}$ 
<h3>G: Temperature</h3> <p>The effect of temperature on integral bridges can be categorised into two effects: differential temperature and seasonal temperature. Differential temperature effects are the result of a temperature profile of the superstructure varying with depth, while the change in environmental temperature throughout the year causes expansion and contraction in the superstructure.</p>	
<h4>G1: Differential temperature change</h4> <p>The objective is to estimate the stress in different depth of deck section. To this aim, a method presented by Rojas (2014) was used. This procedure has two main steps. First, the bridge is considered simply supported and self-equilibrating stresses are calculated. The self-equilibrating stresses are produced due to nonlinearity of temperature gradient. Second, the stresses caused by continuity due to restrictions at supports (restriction of rotating at the ends and displacement at the middle caused by supports) are calculated. The total stresses are some of the two aforementioned stresses.</p>	

G1: Differential temperature change

According to the *Bridge manual*, overall temperature changes for concrete bridges are as follows:

$$\pm 20^{\circ}\text{C}$$

The concept of temperature variation with depth has been illustrated as follows (*Bridge manual*):



The total 500mm depth of cross section of the bridge deck is divided to five equal layers each layer 100mm. Estimation of real strain at the bottom and the top of cross section of the beam at the mid of the bridge:

$$\begin{Bmatrix} \varepsilon_b \\ \varepsilon_t \end{Bmatrix} = \begin{bmatrix} \sum_{n=1}^n \left[\left(1 - \frac{y_n}{h}\right) A_n \right] & \sum_{n=1}^n \left[\frac{y_n}{h} A_n \right] \\ \sum_{n=1}^n \left[\left(1 - \frac{y_n}{h}\right) A_n y_n \right] & \sum_{n=1}^n \left[\frac{y_n}{h} A_n y_n \right] \end{bmatrix}^{-1}$$

$$\begin{Bmatrix} \sum_{n=1}^n A_n \varepsilon_{fn} \\ \sum_{n=1}^n A_n y_n \varepsilon_{fn} \end{Bmatrix} \quad (60)$$

$$\varepsilon_{Rn} = \left(1 - \frac{y_n}{h}\right) \varepsilon_b + \frac{y_n}{h} \varepsilon_t \quad (61)$$

$$\varepsilon_{sen} = \varepsilon_{Rn} - \varepsilon_{fn} \quad (62)$$

$$\varepsilon_{fn} = T_n \alpha_n$$

$$\sigma_{sen} = \varepsilon_{sen} E \quad (63)$$

Where:

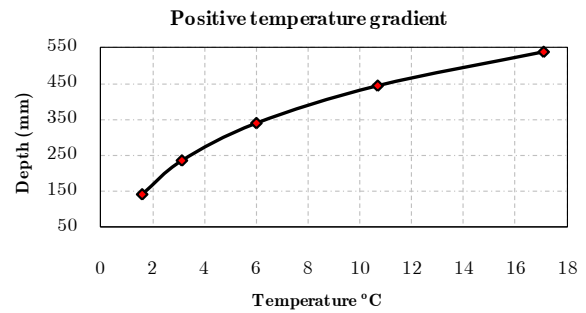
ε_b = Real strain at the bottom of the cross-section.

ε_t = Real strain at the top of the cross-section.

y_n = Distance from the bottom to the centroid of the nth layer.

G1: Differential temperature change - Example 1.0

Accordance with the *Bridge manual*, positive temperature gradient of beam can be estimated as follows:



It should be noted that in estimation of temperature gradient of the beam 90mm surface was considered on the top of beam, the beam was divided into five layers, and temperature gradient was calculated in the centre of each layer:

$$\begin{Bmatrix} \varepsilon_b \\ \varepsilon_t \end{Bmatrix} = \begin{bmatrix} 0.2369 & 0.2369 \\ 0.03697 & 0.08148 \end{bmatrix}^{-1} \times \begin{Bmatrix} 4.159 \times 10^{-5} \\ 1.509 \times 10^{-5} \end{Bmatrix}$$

$$\begin{Bmatrix} \varepsilon_b \\ \varepsilon_t \end{Bmatrix} = \begin{bmatrix} 7.727 & -22.467 \\ -3.506 & 22.467 \end{bmatrix} \times \begin{Bmatrix} 4.159 \times 10^{-5} \\ 1.509 \times 10^{-5} \end{Bmatrix}$$

$$\varepsilon_b = -1.766 \times 10^{-5}$$

$$\varepsilon_t = 19.32 \times 10^{-5}$$

The bridge has two 14m spans, so the length of deck is 28m; hence the rotation and maximum deflection of simply supported deck can be calculated as follows:

$$\Phi = \frac{\varepsilon_t - \varepsilon_b}{h} = \frac{(21.035 + 1.918) \times 10^{-5}}{0.5}$$

$$\Phi = 45.91 \times 10^{-5} \text{ rad}$$

$$\Delta = \frac{\Phi L^2}{8} = \frac{45.91 \times 10^{-5} \times 28^2}{8} = 44.98 \text{ mm}$$

A_n is area of the n^{th} layer

h is height of the cross-section

ϵ_{fn} is free strain at an n^{th} layer

T_n is temperature at the n^{th} layer

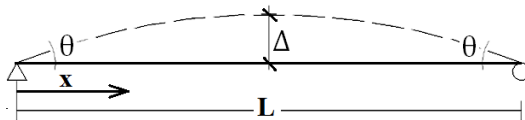
α_n is thermal expansion coefficient

ϵ_{Rn} is real strain at an n^{th} layer

ϵ_{sen} is strain due to self-equilibrating stresses at an n^{th} layer

σ_{sen} is self-equilibrating stress at an n^{th} layer

The rotation and maximum deflection at the mid-span of the simply supported bridge can be determined as follows:



$$\theta = \frac{\epsilon_t - \epsilon_b}{h} \quad (64)$$

$$\Delta = \frac{\theta L^2}{8} \quad (65)$$

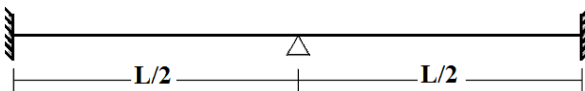
Where:

θ = Rotation

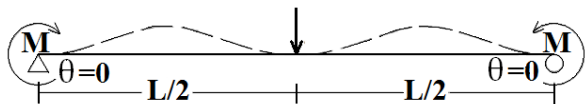
Δ = Deflection at mid-span of simply supported bridge

L = Length of the bridge

Since integral bridges are not simply supported bridges, support conditions should be applied. The support condition depends on the case study:

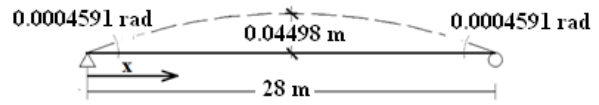


The moment and forces need to be applied to obtain the same rotation and deflection as the model of the studied integral bridge. For two-span bridges, the following relationships are applied:

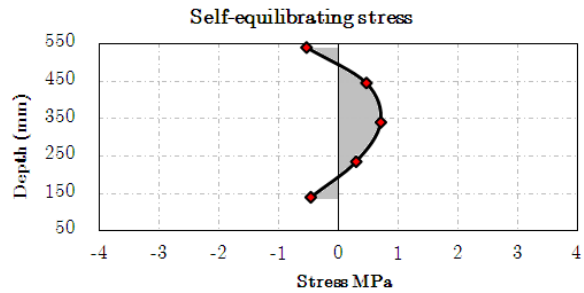


$$\frac{ML}{2EI} + \frac{PL^2}{16EI} = \theta \quad (66)$$

$$\frac{ML^2}{16EI} + \frac{PL^3}{38EI} = \Delta \quad (67)$$



The self-equilibrating stresses at the centre of each layer are as follows:



Accordance with the *Bridge manual*, cracked section properties should be used in structural analyses of members under differential temperature.

Since superstructure should remain elastic, therefore accordance with NZ3101:2006 effective moment inertia is as follows:

$$I_e = I_g$$

$$EI = 346 \text{ MN.m}^2$$

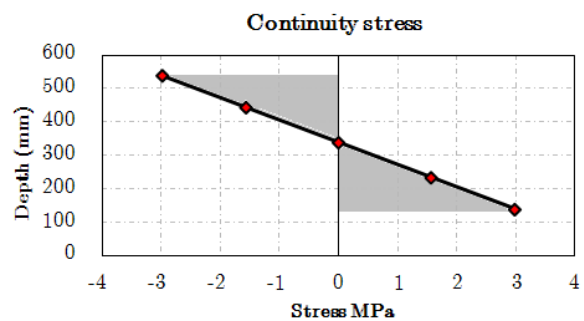
$$\frac{M \times 28}{2 \times 354} + \frac{P \times 28^2}{16 \times 354} = 45.91 \times 10^{-5}$$

$$\frac{M28^2}{16 \times 354} + \frac{P28^3}{38 \times 354} = 0.04498$$

$$P = 0.0525 \text{ MN}$$

$$M = -0.1724 \text{ MN.m}$$

The self-equilibrating stresses at the centre of each layer are as follows:



Total stress = Continuity stress + Self-equilibrium stress:

The total stresses can be calculated by combining continuity stresses and self-equilibrating stresses as follows:

$$\sigma_{cn} = \frac{M(y_c - y_n)}{I_e} \quad (68)$$

Where I_e is effective moment of inertia of the beam section

$$\sigma_{Tn} = \sigma_{sen} + \sigma_{cn} \quad (69)$$

Where:

M = Internal moment at examined cross section.

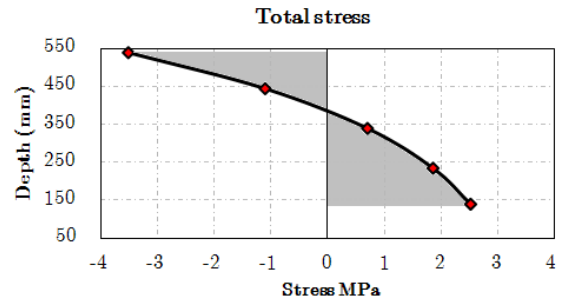
σ_{cn} = Continuity stress at the n^{th} layer of the examined cross section.

y_n = Distance from the bottom to the centroid of the cross section.

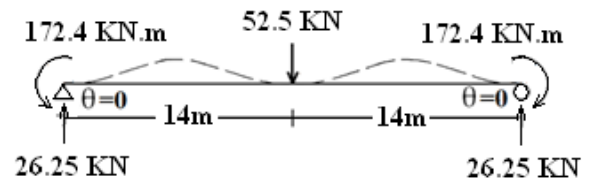
I = Moment of inertia of the cross section.

y_c = Distance from the bottom to the centroid of the n^{th} layer.

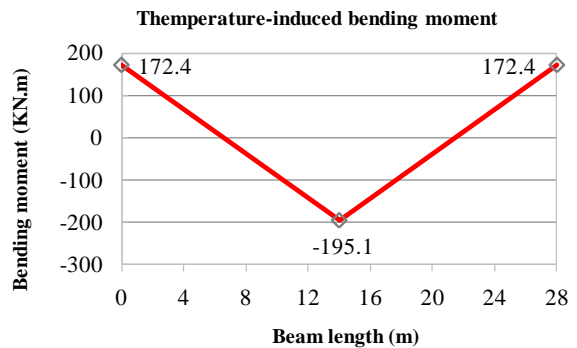
σ_{Tn} = Total stress at the n^{th} layer of the examined cross section.



Reactions at integral bridge's support, calculated based on the integral bridge's boundary conditions, are as follows:



Therefore differential temperature induced bending is as follows:



G2: Temperature-induced expansion and contraction

It has been shown that expansion and contraction cycles due to daily temperature changes cause settlement of abutment foundation and sheet pile abutment wall (England et al 2000). England et al (2000) defined the stresses at soil-abutment interface using a complex soil-structure interaction in terms of cyclic thermal movement (expansion and contraction) of the bridge deck. A numerical procedure was defined to estimate settlement of abutment foundation (England et al 2000). It should be noted that this phenomena has not been considered in this example.

The maximum horizontal displacement at the beam-abutment junction is as follows (England et al 2000):

$$d = L \times \alpha \times \frac{\Delta T}{2}$$

where d is the maximum thermal horizontal displacement; L is total length of the bridge; α is the

$$L = 28 \text{ m}$$

$$\alpha = 12 \times 10^{-6} / ^\circ\text{C} \text{ for concrete deck}$$

$$\Delta T = 40 \text{ } ^\circ\text{C} \text{ (Bridge manual 2014)}$$

<p>coefficient of thermal expansion of the bridge deck; ΔT is deck temperature change</p> <p>Absolute thermal expansion, equal to absolute thermal contraction, is equal to d.</p>	<p style="text-align: center;">$d = 0.0067 \text{ m}$</p> <p style="text-align: center;">Total thermal expansion = 0.0067 m</p> <p style="text-align: center;">Total thermal contraction = 0.0067 m</p> <p>The above values of total thermal expansion and contraction have been calculating assuming free movement at ends. This assumption is conservative and safe.</p>
--	---

H: Maximum abutment movement and rotation due to creep, shrinkage and thermal effects

The procedure utilised in this section to calculate the maximum movement and rotation due to creep, shrinkage and thermal effects was presented and defined by Nicholson (1998).

<p>The maximum movement and rotation at the end of each span can be conservatively estimated based on the very important following assumption:</p> <p>It was assumed that the bridge would have a free movement and rotation at the ends of each span.</p> <p>The calculations based on the aforementioned assumption are conservative and safe.</p>	<p>It should be noted the joints and continuity in integral bridges reduce the rotation and movement of ends.</p>
--	---

H1: Thermal-induced movement

Thermally induced movements (expansion and contraction) at the end of each span can be taken as $d/2$.

H1: Thermal-induced movement – example 1.0

Thermal expansion at each end = 0.0034 m.
Thermal contraction at each end = 0.0034 m.

H2: Rotation of each end due to differential temperature change

The section properties and layers used in the G1 section were used in this section. Therefore the section was divided into five layers (each 100mm depth). Since it has been assumed that the bridge has free movement and rotation at ends, the thermal stress at the centre of each layer based on free strain can be calculated as follows:

$$\sigma_i^{\text{Thermal}} = E \cdot \alpha \cdot T_i$$

Where T_i is temperature at the center of each layer

The moment, $M_{\text{Free strain}}^{\text{Thermal}}$ to be released is:

$$M_{\text{Free strain}}^{\text{Thermal}} = \sum_{i=1}^5 A_i y_i \sigma_i^{\text{Thermal}}$$

Deck curvature, $\kappa_{\text{Free strain}}^{\text{Thermal}}$, is:

$$\kappa_{\text{Free strain}}^{\text{Thermal}} = M_{\text{Free strain}}^{\text{Thermal}} / EI$$

Rotation, $\theta_{\text{Free strain}}^{\text{Thermal}}$ at end of each span is:

H2: Rotation of each end due to differential temperature change – example 1.0

$$EI = 346 \text{ MN/m}^2$$

$$\alpha = 12 \times 10^{-6} / ^\circ\text{C}$$

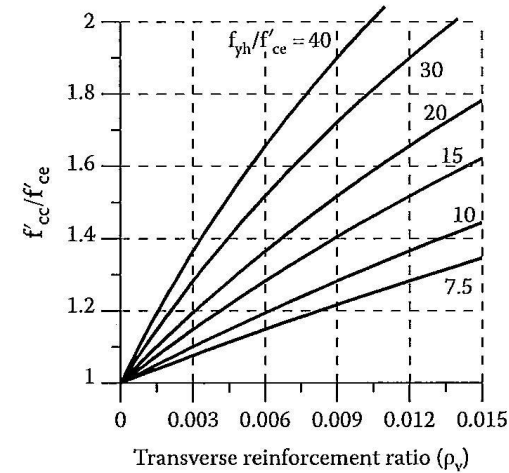
$A_i (\text{m}^2)$	$y_i (\text{m})$	$\sigma_i^{\text{Thermal}}$ MN.m ²	$A_i y_i \sigma_i^{\text{Thermal}}$
0.1144	0.2	8.77	0.2007
0.0896	0.1	3.848	0.03449
0.0657	0	2.164	0
0.0896	-0.1	1.129	-0.0101
0.1144	-0.2	0.576	-0.0103
$M_{\text{Free strain}}^{\text{Thermal}} = \sum_{i=1}^5 A_i y_i \sigma_i^{\text{Thermal}} =$			0.2119

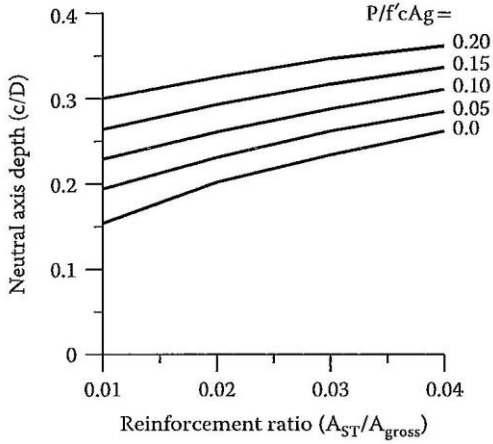
$$M_{\text{Free strain}}^{\text{Thermal}} = 0.2119 \text{ MN.m}$$

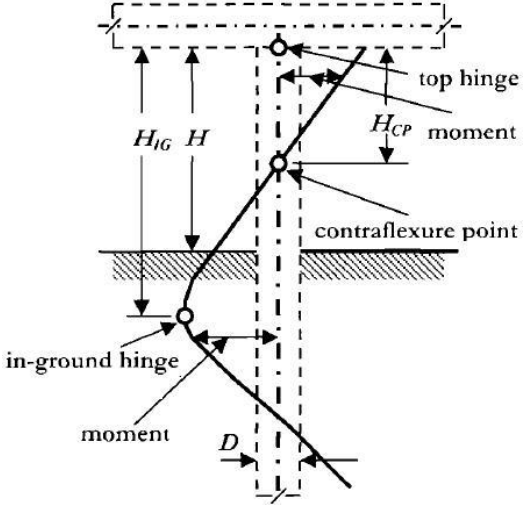
$\theta_{\text{Free strain}}^{\text{Thermal}} = L/2 \times \kappa_{\text{Free strain}}^{\text{Thermal}}$ <p>Where L is the length of span</p>	$\kappa_{\text{Free strain}}^{\text{Thermal}} = \frac{0.2119}{346} = 6.124 \times 10^{-4}$ $\theta_{\text{Free strain}}^{\text{Thermal}} = 7 \times 6.124 \times 10^{-4} = 0.004287 \text{ rad}$
<p>H3: Total shortening due to creep and shrinkage</p> <p>Creep strain neglecting pre-stressing axial force losses can be estimated as follows:</p> $\epsilon_{\text{creep}} = \sigma/E \times \varphi(28, \infty)$ <p>Recalling the approximation in section F3.2: Strain in precast beam due to permanent loads can be approximated to the centroidal strain (Nicholson 1998). It means:</p> $\sigma = \frac{N_{P0}}{A}$ <p>Recalling the shrinkage strain from F3.5, The total strain, $\epsilon_{\text{Shortening}}$, is:</p> $\epsilon_{\text{Shortening}} = \epsilon_{\text{creep}} + \epsilon_{\text{Sh}}(100, \infty)$ <p>The shortening due to creep and shrinkage neglecting pre-stressing losses axial force is as follows:</p> $\Delta_{\text{shortening}} = \epsilon_{\text{Shortening}} \times L$	<p>H3: Total shortening due to creep and shrinkage – example 1.0</p> $\epsilon_{\text{creep}} = 8.78 \times 10^{-5} \times 1.49 = 1.308 \times 10^{-4}$ $\epsilon_{\text{Sh}}(100, \infty) = 3.23 \times 10^{-4}$ $\epsilon_{\text{Shortening}} = 1.308 \times 10^{-4} + 3.23 \times 10^{-4}$ $\epsilon_{\text{Shortening}} = 16.31 \times 10^{-4}$ $L = 14 \text{ m}$ $\Delta_{\text{shortening}} = 16.31 \times 10^{-4} \times 14 = \mathbf{0.0228 \text{ m}}$
<p>I: Displacement-based earthquake design</p> <p>Accordance with the <i>Bridge manual</i>, section 5, v3.2 displacement-based earthquake design procedure will include the following steps:</p> <ol style="list-style-type: none"> 1 Determine the site seismicity in terms of the elastic design displacement spectrum. 2 Determine the yield displacements of all piers. 3 Check whether yield displacements exceed the elastic corner-period displacement. If so, standard detailing of the load resisting members in accordance with the appropriate materials standard will be adequate subject to the requirements of strength and stability under response to the CALS event being confirmed. 4 If the check in step (3) fails, determine the fundamental period of bridge in the direction considered. 5 Determine elastic displacement response at the fundamental period. 6 Check whether yield displacements exceed elastic displacements for the fundamental period. If so, standard detailing of the load resisting members in accordance with the appropriate materials standard will be adequate, subject to the requirements of strength and stability under response to the CALS event being confirmed. 7 If ductile earthquake design is indicated by the above steps, carry out displacement-based earthquake design, in accordance with the following provisions, to determine required lateral strength of piers and abutments. <p>More complete information on the procedure is available in Priestley et al (2007; 2014). The displacement based earthquake design has three parts:</p> <ol style="list-style-type: none"> 1 Single degree of freedom bridge pier to calculate design displacement of pier based on DBD methodology developed by Priestley et al (2007; 2014). 	

- 2 Multi-degree of freedom bridge longitudinal direction to calculate longitudinal lateral force. For design in longitudinal direction, the aforementioned procedure according to the *Bridge manual* section 5 V3.2 was employed.
- 3 Multi-degree of freedom bridge transverse direction to design for transverse response. For design in transverse direction the iterative procedure presented by Priestley et al (2007; 2014) was used. The results of the iteration procedure of the example have been shown in table 2. The superstructure of the example is very stiff, (the transverse moment inertia of the superstructure= 183.7893 m⁴). Therefore the example was designed assuming the transverse moment inertia of the superstructure= 0.2662 m⁴. The results have been shown in table 3.

I.1: Single-degree-of-freedom bridge pier: Design displacement for a multi-column/pile pier

<p>Step 1: Determine volumetric ratio of transverse reinforcement.</p> $\rho_v = \frac{4 \times A_b}{D' \times s}$ <p>Where, ρ_v is the volumetric ratio of transverse reinforcement, A_b is bar area, s is the spacing of the transverse reinforcement, and D' is the core diameter measured to the centre of the hoops.</p>	<p>Step 1:</p> $D' = 1300 - 100 - 20 = 1180 \text{ mm}$ $\rho_v = \frac{4 \times 314}{1180 \times 100} = 0.0106$
<p>Step 2: Determine the confined compression strength of the core concrete.</p> <p>The confined compression strength of the core concrete, f'_{cc}, can be found using the following figure (Priestley et al 2014):</p>  <p style="text-align: center;">$f'_{cc} = 1.32 \times f'_c$</p> <p>Where f_{yh} is yield strength of transverse reinforcement</p>	<p>Step 2:</p> $f'_c = 40 \text{ MPa}$ $f'_{ce} = 52 \text{ MPa}$ $f_{yh} = 500 \text{ MPa}$ $\frac{f_{yh}}{f'_{ce}} = \frac{500}{52} = 9.615$ <p>Using the figure on the left (Priestley et al 2014):</p> $\frac{f'_{cc}}{f'_{ce}} = 1.32$ $f'_{cc} = 1.32 \times 52 = 68.64 \text{ MPa}$
<p>Step 3: Determine the damage-control compression strain.</p> $\epsilon_{dc,c} = 0.004 + 1.4 \frac{\rho_v f_{yh} \epsilon_{su}}{f'_{cc}}$ <p>Where ϵ_{su} is ultimate strain</p>	<p>Step 3:</p> $\epsilon_{dc,c} = 0.004 + 1.4 \frac{0.0106 \times 500 \times 0.12}{68.64} = 0.01697$

<p>Step 4: Determine the column axial force ratio.</p> $P/f'_{ce} \times A_g$	<p>Step 4:</p> $P/(f'_{ce} \times A_g) = \frac{1.7}{52 \times 1.327} = 0.0246$
<p>Step 5: Estimate neutral axis depth.</p> <p>The neutral axis depth can be estimated given the column axial force ratio, and longitudinal reinforcement to column area ratio using the following figure:</p> 	<p>Step 5:</p> $\frac{A_{ST}}{A_{gross}} = \frac{0.036191}{1.3273229} = 0.027266$ <p>Using the represented figure (Priestley et al 2014):</p> $\frac{c}{D} = 0.24$ $D = 1.3 \text{ m}$ $c = 0.312 \text{ m}$
<p>Step 6: Determine the critical limit-state curvature.</p> $\phi_{ls,c} = \frac{\epsilon_{c,ls}}{c}$ $\phi_{ls,s} = \frac{\epsilon_{s,ls}}{d - c}$ <p>The smallest value between the two will be selected</p>	<p>Step 6:</p> $\phi_{ls,c} = \frac{0.01697}{0.312} = 0.0554/m \text{ Govern}$ $\phi_{ls,s} = \frac{0.06}{1.21 - 0.312} = 0.0668/m$
<p>Step 7: Plastic hinge length</p> $L_p = K \times L_C + L_{SP} \geq 2L_{SP}$ $K = 0.2(f_u/f_{ye} - 1)$ $f_{ye} = 1.1f_y$ $L_C = H_{CP} = 0.52 H_{IG}$ $L_{SP} = 0.022f_{ye}d_{bl}$ <p>Where d_{bl} is diameter of longitudinal reinforcement For sand, $\phi = 30^\circ$:</p> $H_{IG}/D = 4.39 + 0.82 \times \left(\frac{H}{D}\right)$	<p>Step 7:</p> <p>The pier has three column, and the critical column, shortest, has been selected to calculate design displacement</p> <p>H = 3m critical height of column</p> $H_{IG}/D = 4.39 + 0.82 \times \left(\frac{3}{1.3}\right) = 6.44$ $H_{IG} = 8.372 \text{ m}$ $L_C = H_{CP} = 0.52 H_{IG} = 4.26 \text{ m}$

 <p style="text-align: center;"> $L_{SP} = 0.022 \times f_{ye} \times d_{bl}$ $k = 0.2(f_u/f_{ye} - 1) \leq 0.08$ </p> <p>Where d_{bl} is diameter of longitudinal reinforcement, and f_u is ultimate stress, and $f_{ye} = 1.1f_y$.</p>	<p style="text-align: center;"> $f_{ye} = 1.1 \times 500 = 550 \text{ MPa}$ $K = 0.07$ $L_{SP} = 0.022 \times 550 \times 32 = 387.2 \text{ mm}$ $L_P = 0.07 \times 4.26 + 0.387 = 687\text{mm} < 2 \times 387$ </p> <p>Therefore:</p> <p style="text-align: center;"> $L_P = 2L_{SP} = 0.774 \text{ m}$ </p>
<p>Step 8: Estimate design displacement</p> $\Delta_D = \Delta_y + C_3(\phi_{IS} - \phi_y) \times L_P \times H_{IG}$ <p>For sand: $C_3 = 1.68$ (Priestley et al 2007) Where Δ_D is design displacement, and $\Delta_{y,F}$ is yield displacement, ϕ_{IS} is govern limit state curvature, ϕ_y is yield curvature.</p> $\Delta_y = C_1 \times \phi_y \times (H_{IG} + L_{SP})^2$ $C_1 = 0.31 - 0.0301 \times \ln(H/D)$ $\phi_y = 2.25 \times \frac{\epsilon_y}{D}$ $\epsilon_y = f_{ye}/E$	<p>Step 8</p> $C_1 = 0.31 - 0.0301 \times \ln(3/1.3) = 0.285$ $\epsilon_y = 550/200000 = 0.00275$ $\phi_y = 2.25 \times \frac{0.00476}{1.3} = 0.00476/m$ $\Delta_y = 0.285 \times 0.00476 \times (8.372 + 0.387)^2$ $\Delta_y = 0.104\text{m}$ $\Delta_D = 0.104 + 1.68(0.0544 - 0.00476) \times 0.774 \times 8.372$ $\Delta_D = 0.644 \text{ m}$
<p>Step 9: Estimate displacement ductility:</p> $\mu_D = \frac{\Delta_D}{\Delta_y}$ <p>Where μ_D is displacement ductility The estimated displacement ductility must be less than maximum allowable value presented in table 5.4 of the <i>Bridge manual</i>, section 5-v3.2. The maximum allowable ductility for multi column-pile</p>	<p>Step 9:</p> $\mu_D = \frac{0.644}{0.104} = 6.19 > 2.5$

<p>pier is 2.5:</p> $\mu_D = \Delta_D / \Delta_y < 2.5$	<p>Therefore:</p> $\mu_D = 2.5$
<p>Step 10: Estimate damping of column(s): For sand and fixed head columns:</p> $\xi = 0.075 + 0.03(\mu_m - 1) \leq 0.0135$	<p>Step 10:</p> $\xi = 0.075 + 0.03(2.5 - 1) = 0.12$
<p>I.2 Multi-degree-of-freedom bridge: longitudinal direction (Priestley et al 2007)</p>	
<p>Step 1: Elastic displacement design spectra (Elastic corner period displacement):</p> $\Delta(T) = R_u \cdot Z \cdot N(T, D) \cdot \Delta_h(T)$ <p>Assume: $D > 20 \text{ km}$ Assume soil category D: Deep soil</p> $\Delta_d(T) = M_\xi \times \Delta(T)$ $M_\xi = \left(\frac{0.07}{0.02 + \xi_e} \right)^\alpha$	<p>Step 1:</p> $R_u = 1/3$ for APE: $\frac{1}{1000}$ NZS 1170.5: 2004 $Z = 0.22$ for Christchurch NZS 1170.5: 2004 $T = 3 \text{ sec}$ $N(T, D) = 1$ $\Delta_h(3) = 1585 \text{ mm}$ $\Delta(T) = 453 \text{ mm}$ $\xi_e = \xi_{\text{pier}} = 0.12$ $\alpha = 0.5$ $M_\xi = \sqrt{2}/2$
<p>Step 2: Determine the yield displacement at piers:</p> $\Delta_{y \text{ pier}} = \text{critical yield displacement}$	<p>Step 2:</p> $\Delta_{y \text{ pier}} = 0.104 \text{ m}$
<p>Step 3: Check whether yield displacement of all piers exceed the elastic corner-period displacement. If step 3 failed go to step 4.</p>	<p>Step 3:</p> $\Delta_{y \text{ pier}} = 0.104 \text{ m} > \Delta_d(3) = 0.32 \text{ m} \rightarrow \text{Not accepted.}$

<p>Step 4: Determine the fundamental period of the bridge in the direction considered (longitudinal):</p> $T_f = 2\pi \sqrt{\frac{m}{k_e}}$ $k_e = k_{\text{pier}} + 2k_{\text{Abutment}}$ <p>Where m is mass of superstructure, and cap beam, and 1/3 columns, and k_e is effective stiffness of the bridge can be estimated from section analysis of columns.</p>	<p>Step 4:</p> $k_e = 234 \frac{MN}{m}$ $m_{\text{Pier}} = 5000 \text{ KN}$ $m_{\text{Abutment}} = 3000 \text{ KN}$ $m_{\text{Bridge}} = m_{\text{Pier}} + 2 \times m_{\text{Abutment}}$ $m_{\text{Bridge}} = 5000 + 2 \times 3000 = 11000 \text{ KN}$ $m = \frac{11000}{9.81} = 1121 \text{ Ton}$ $T_f = 0.43 \text{ sec}$
<p>Step 5: Determine elastic displacement response at fundamental period:</p> $\Delta(T_f) = \Delta_d(T) \times \frac{T_f}{T}$	<p>Step 5:</p> $\Delta(T_f) = 0.0463$
<p>Step 6: Check whether yield displacement exceed elastic displacement for fundamental period:</p> $\Delta_{y \text{ pier}} > \Delta(T_f)$	<p>Step 6:</p> $\Delta_{y \text{ pier}} = 0.104 \text{ m} > \Delta(T_f) = 0.043 \text{ m} \quad \text{O.K.}$ <p>It means the bridge will respond elastically and no specific seismic design is needed.</p>
<p>Step 7: Determine design base shear:</p> $V_{\text{Base}} = k_e \Delta_D = \frac{4\pi^2 m_e}{T_c^2} \times \frac{\Delta_{c,5}^2}{\Delta_D} \times \left(\frac{0.07}{0.02 + \xi} \right)^{2\alpha}$ $K_e = \frac{4\pi \times m_e}{T_e^2}$ $T_e = T_c \times \frac{\Delta_d}{\Delta_{c,5}} \times \left(\frac{0.02 + \xi}{0.07} \right)^{0.25}$ <p>Note: the schematic bending moment of the column/pile has been shown in the figure presented in step 7, section I.1. More details can be found in Priestley et al (2007).</p>	<p>Step 7:</p> $T_e = 2.43 \text{ sec}$ $K_e = 7.474 \text{ MN.m}$ $V_{\text{Base}} = 1.943 \text{ MN}$ <p>Note: the above base shear is column's base shear, and the base shear of pier (3 columns) is $3V_{\text{Base}}$</p> <p>Therefore:</p> $V_{\text{Base}}^{\text{Pier}} = 3 \times 1943 = 5829 \text{ KN}$
<p>Step 8: Check $P - \Delta$:</p> <p>For concrete structures, the stability index, θ_Δ, must be less than 0.1. The stability index is represented as follows:</p> $\theta_\Delta = \frac{P \Delta_{\text{max}}}{M_D}$ $M_D = FH + P \Delta_{\text{max}}$	<p>Step 8:</p> $P = 1700 \text{ KN for a column}$ $\Delta_{\text{max}} = \Delta_d = 0.26 \text{ m}$ $\theta_\Delta = \frac{1700 \times 0.26}{1943 \times 4.26 + 1700 \times 0.26} = 0.0507$ $< 0.1 \text{ accepted}$

<p>If the check failed the lateral force should be increase as follows:</p> $F = V_{Base} + C \times \frac{P\Delta_{max}}{H}$ <p>$C = 0.5$ for concrete structures</p>	$H = H_{CP} = 4.26 \text{ m} \quad \text{for column pile}$ $M_D = 1943 \times 4.26 + 1700 \times 0.26 = 8729 \text{ MN.m}$
<p>Step 9: Check moment capacity: Required moment capacity, M_{bp}, should be less than existing capacity, M_{bc}:</p> $M_{bp} < M_{bc}$ $M_{bp} = \frac{M_{P-\Delta}}{2} + M_b$ <p>Where M_b is required design base moment capacity:</p> $M_b = V_{Base} \times \frac{H_{CP}}{3}$ $M_{P-\Delta} = P\Delta_{max}$	<p>Step 9:</p> $M_b = 1943 \times \frac{4.26}{3} = 2759 \text{ KN.m}$ $M_{P-\Delta} = 1700 \times 0.26 = 442 \text{ KN.m}$ $M_{bp} = \frac{1700 \times 0.26}{2} + 2759 = 2980 \text{ KN.m}$ $M_{bc} = 9500 \text{ KN.m} \quad \text{obtained from section analyses}$ $M_{bp} < M_{bc} \quad \text{O.K.}$
<p>I.3 Multi-degree-of-freedom bridge: transverse direction (Priestley et al 2007)</p> <p>Since the displacement profile and the fraction of load carried by superstructure bending back to the abutments are initially assumed, an iteration procedure is needed in the transverse direction of loading as follows:</p>	
<p>Step 1: Estimate fraction of lateral force carried out by superstructure bending:</p> <p>In the absence of guidance, assume $x = 0.5$ for restraint at abutment (integral bridges).</p>	<p>Step 1:</p> $x = 0.5$
<p>Step 2: Estimate initial displacement profile:</p> <p>The initial displacement profile is assumed to be Parabolic with following condition:</p> $\Delta_{Pier} = \Delta_D; \quad \Delta_{Abutment} < \Delta_y^{Abutment}$ <p>Note that for multi-pier bridges (more than 2 span) design displacement of critical pier should be defined and the displacement of other piers should be estimated based on this and the displacement profile.</p>	<p>Step 2:</p> $\Delta_{Abutment} = 0.03 \text{ m}$ $\Delta_{Pier} = 0.26 \text{ m}$
<p>Step 3: Determine the SDOF system displacement:</p> $\Delta_d = \frac{\sum_{i=1}^n (m_i \Delta_i^2)}{\sum_{i=1}^n (m_i \Delta_i)}$ <p>Where $i = 1$ and $i = n$ refer to abutments and number between refer to pier(s), and m_i are inertia weight carried by i^{th} pier or abutment, and Δ_i is its displacement obtained from step 2.</p>	<p>Step 3:</p> $n = 3$ $m_1 = m_3 = 3000 \text{ KN}$ $m_2 = 5000 \text{ KN}$

	$\Delta_d = \frac{2 \times 3000 \times 0.03^2 + 5000 \times 0.26^2}{2 \times 3000 \times 0.03 + 5000 \times 0.26} = 0.232 \text{ m}$
<p>Step 4: Determine effective mass:</p> $m_e \times g = \frac{\sum_{i=1}^n (m_i \Delta_i)}{\Delta_d}$	<p>Step 4:</p> $m_e = \frac{2 \times 3000 \times 0.03 + 5000 \times 0.26}{0.232 \times 9.81} = 650 \text{ Ton}$
<p>Step 5: Determine pier displacement ductility and equivalent viscous damping:</p> $\mu_\Delta = \frac{\Delta_{Pier}}{\Delta_y}$ <p>Pile/column fixed to superstructure; sand (<i>Bridge manual</i>, section 5, v3.2):</p> $\xi_{Pier} = 0.075 + 0.03(\mu_\Delta - 1) \leq 0.135$	<p>Step 5:</p> $\Delta_y^{Pier} = 0.104 \text{ m}$ obtained from section I.1 $\Delta_{Pier} = 0.26$ from step 2 $\mu_\Delta = 2.5$ $\xi_{Pier} = 0.12$
<p>Step 6: Determine the ratio of shear forces carried by the pier and abutments:</p> $V_{Pier} = (1 - x) \cdot \sum_{i=1}^n F_i \times \left[\frac{\frac{1}{H_i}}{\sum_{i=2}^{n-1} \frac{1}{H_i}} \right]$ $V_{Abutment}^1 + V_{Abutment}^2 = x \cdot \sum_{i=1}^n F_i$ <p>Where H_i is height of i^{th} pier</p>	<p>Step 6:</p> $V_{Pier} = 0.5 \times \sum_{i=1}^3 F_i$ $V_{Abutment}^1 + V_{Abutment}^2 = 0.5 \times \sum_{i=1}^3 F_i$
<p>Step 7: Determine effective damping</p> $\xi_e = \frac{x(\Delta_d - \Delta_a)\xi_{SS} + x\Delta_a\xi_a + (1-x) \frac{(\sum_{i=2}^{n-1} \frac{1}{H_i} \Delta_i \xi_i)}{\sum_{i=2}^{n-2} \frac{1}{H_i}}}{x(\Delta_d - \Delta_a) + x\Delta_a + (1-x) \frac{(\sum_{i=2}^{n-1} \frac{1}{H_i} \Delta_i)}{\sum_{i=2}^{n-2} \frac{1}{H_i}}}$ <p>Assuming $\xi_{SS} = \xi_a$ the above equation will be simplified as follows for the example bridge:</p> $\xi_e = \frac{x\Delta_d\xi_{SS} + (1-x)\Delta_{Pier}\xi_{Pier}}{x\Delta_d + (1-x)\Delta_{Pier}}$ <p>Where ξ_{SS} and ξ_a are viscous damping of superstructure and abutment respectively, and Δ_a is abutment displacement from step 2.</p>	<p>Step 7:</p> $\xi_{SS} = \xi_a = 0.05$ $\xi_e = \frac{0.5 \times 0.232 \times 0.05 + 0.5 \times 0.26 \times 0.12}{0.5 \times 0.232 + 0.5 \times 0.26}$ $\xi_e = 0.087$

<p>Step 8: Determine effective period, stiffness and design base shear:</p> $T_e = T_c \times \frac{\Delta_d}{\Delta_{c,5}} \times \left(\frac{0.02 + \xi_e}{0.07} \right)^{0.5}$ $K_e = \frac{4\pi \times m_e}{T_e^2}$ $V_{Base} = K_e \cdot \Delta_d$	<p>Step 8:</p> $T_e = 3 \times \frac{0.232}{0.453} \times \left(\frac{0.02 + 0.087}{0.07} \right)^{0.5} = 1.9 \text{ sec}$ $K_e = \frac{4\pi \times 650}{1.9^2} = 7111 \frac{\text{KN}}{\text{m}}$ $V_{Base} = 7111 \times 0.232 = 1650 \text{ KN}$
<p>Step 9: Distribute base shear force to inertia mass locations:</p> $F_i = \frac{V_{Base} \times (m_i \Delta_i)}{\sum_{i=1}^n (m_i \Delta_i)}$	<p>Step 9:</p> $F_{Abutment} = \frac{1650 \times (3000 \times 0.03)}{2 \times 3000 \times 0.03 + 5000 \times 0.26}$ $F_{Abutment} = 100 \text{ KN}$ $F_{Pier} = \frac{1650 \times (5000 \times 0.26)}{2 \times 3000 \times 0.03 + 5000 \times 0.26}$ $F_{Pier} = 1450$
<p>Step 10: Estimate abutment and pier effective stiffness:</p> $V_{Pier} = 0.5 \times \sum_{i=1}^3 F_i$ $V_{Abutment}^1 + V_{Abutment}^2 = 0.5 \times \sum_{i=1}^3 F_i$ $K_{Pier}^e = \frac{V_{Pier}}{\Delta_{Pier}}$ $K_{Abutment}^e = \frac{V_{Abutment}}{\Delta_{Abutment}}$	<p>Step 10:</p> $\sum_{i=1}^3 F_i = V_{Base} = 1650 \text{ KN}$ $V_{Abutment}^1 + V_{Abutment}^2 = 825 \text{ KN}$ $V_{Pier} = 825 \text{ KN}$ $V_{Abutment} = 412.5 \text{ KN}$ $K_{Pier}^e = 3173 \text{ KN}$ $K_{Abutment}^e = 13750 \text{ KN}$
<p>Step 11: Analysis the structure under lateral forces obtained in step 9, and using the effective stiffness obtained in step 10.</p> <p>2D frame elements can be used to define superstructure and springs to define the effective stiffness of abutments and piers.</p>	<p>Step 11:</p> $\Delta_{Pier} = 0.0548 \text{ m}$ $\Delta_{Abutment} = 0.0537 \text{ m}$
<p>Step 12: Compare the displacement of critical pier or abutment obtained from step 11 with the limit state displacement from step 2. If the displacement of the critical pier or abutment exceeds the design limits, then assume a new value for x (x_{new}). For further details in this regard refer to (Priestley et al 2014, section 6.3.2.2).</p> <p>After estimation of x_{new}, the ratio of shear forces carried</p>	<p>Step 12:</p> $x_{new} = 0.65$ $\Delta_{Pier} = 0.0446 \text{ m}$ $\Delta_{Abutment} = 0.0434 \text{ m}$

<p>by the pier and abutments should be calculated and effective stiffness of pier(s) and abutments should be recalculated based on the new shear forces. The structure should be re-analysed using the stiffness obtained in step 12 and same lateral forces obtained in step 9.</p>	$\alpha = \frac{\Delta_{Pier}}{\Delta_{Abutment}} = \frac{0.0446}{0.0434} = 1.02765$
<p>Step 13: Revise displacement profile by scaling the profile obtained from step 12 to the target critical displacement of pier or abutment. Repeat steps 1 to 12 until convergence is reached for displacement profile and x. Use x_{new} in step 1 of next iteration, and use displacement profile and values (obtained in step 13) in step 2 of next iteration.</p> <p>The summary of iteration procedure has been shown in table 2.</p> <p>Accordance to the literature, if the superstructure is very stiff (like this example) the displacement of the critical pier will be less than design displacement even with $x = 1$ (Priestley et al 2014). Therefore, the same bridge example with a rather flexible superstructure was analysed and the results of the iteration procedure are summarised in table 3.</p>	<p>Step 13: it can be observed the displacement of pier is less than the limit design displacement (0.26m), but the displacement of abutment exceed the design limit state (0.03 m). Therefore, the abutment displacement should be kept at 0.03m. The displacement profile is as follows:</p> $\Delta_{Pier} = \alpha \times \Delta_{Abutment}$ $\Delta_{Abutment} = 0.03 \text{ m}; \Delta_{Pier} = 0.0308 \text{ m}$

Table 2: Results of iterative design procedure. Transverse moment inertia of superstructure = 183.7893 m ⁴					
Steps	Parameters	1 st iteration	2 nd iteration	3 rd iteration	4 th iteration
Step 1	x	0.5	0.65	1	1
Step 2	Δ_{Pier}	0.26	0.0308	0.0437	0.0426
	Δ_{Abut}	0.03	0.03	0.03	0.03
Step 3	Δ_d	0.232	0.03036	0.0375	0.0367
Step 4	m_e	650	1121	1083	1088
Step 5	μ	2.5	$\mu < 1$	$\mu < 1$	$\mu < 1$
	ξ_{Pier}	0.12	0.05	0.05	0.05
Step 6	V_{Pier}	$0.5 \sum F_i$	$0.35 \sum F_i$	0	0
	V_{Abut}	$0.5 \sum F_i$	$0.65 \sum F_i$	$1 \sum F_i$	$1 \sum F_i$
Step 7	ξ_e	0.087	0.05	0.05	0.05
Step 8	T_e	1.9	0.2	0.248	0.2437
	K_e	7111	1106884	693234	723180
	V_{Base}	1650	33605	25996	26613
Step 9	F_{Pier}	1450	15494	14254	14423
	F_{Abut}	100	9055	5871	6094
Step 10	V_{Pier}	825	11762	0	0
	K_{Pier}	3173	38187	0	0
	V_{Abut}	412	10922	12998	13307
	K_{Abut}	13750	364066	433267	433550
Step 11	Δ_{Pier}	0.0548	0.0321	0.0426	0.0428
	Δ_{Abut}	0.0536	0.0293	0.03	0.03
Step 12	x_{news}	0.65	1	1	1

Appendix D: Design example

	V_{Pier}	578	0	0	0
	K_{Pier}	2223	0	0	0
	V_{Abut}	536	16803	12998	13307
	K_{Abut}	17875	560000	433267	443550
	Δ_{Pier}	0.0446	0.0437	0.0426	0.0428
	Δ_{Abut}	0.0434	0.03	0.03	0.03
Step 13	Δ_{Pier}	0.0308	0.0437	0.0426	0.0428
	Δ_{Abut}	0.03	0.03	0.03	0.03

Table 3: Results of iterative design procedure. Transverse moment inertia of superstructure = 0.2662 m⁴

Steps	Parameters	1 st iteration	2 nd iteration	3 rd iteration	4 th iteration	5 th iteration	6 th iteration
Step 1	x	1	0.9	0.85	0.84	0.83	0.827
Step 2	Δ_{Pier}	0.26	0.26	0.26	0.26	0.26	0.26
	Δ_{Abut}	0.04	0.04	0.039	0.04	0.04	0.04
Step 3	Δ_d	0.225	0.225	0.225	0.225	0.225	0.225
Step 4	m_e	195	195	195	195	195	195
Step 5	μ	2.5	2.5	2.5	2.5	2.5	2.5
	ξ_{Pier}	0.12	0.12	0.12	0.12	0.12	0.12
Step 6	V_{Pier}	0	$0.1 \sum F_i$	$0.15 \sum F_i$	$0.16 \sum F_i$	$0.17 \sum F_i$	$0.173 \sum F_i$
	V_{Abut}	$1 \sum F_i$	$0.9 \sum F_i$	$0.85 \sum F_i$	$0.84 \sum F_i$	$0.83 \sum F_i$	$0.827 \sum F_i$
Step 7	ξ_e	0.05	0.058	0.062	0.063	0.0634	0.0636
Step 8	T_e	1.5	1.57	1.612	1.622	1.626	1.6287
	K_e	3474	3119	2966	2930	2917	2908
	V_{Base}	782	702	667	659	656	654
Step 9	F_{Pier}	659	592	562	555	553	551
	F_{Abut}	61	55	53	52	52	51
Step 10	V_{Pier}	0	71	100	105	112	113
	K_{Pier}	0	273	385	405	272	435
	V_{Abut}	391	319	283	277	430	270
	K_{Abut}	9775	7976	7087	6925	6806	6761
Step 11	Δ_{Pier}	0.3715	0.296	0.27	0.265	0.2616	0.26
	Δ_{Abut}	0.0399	0.0389	0.0397	0.0398	0.04	0.04
Step 12	x_{news}	0.9	0.85	0.84	0.83	0.827	0.0827
	V_{Pier}	78	106	107	112	113	113
	K_{Pier}	301	408	410	431	436	436
	V_{Abut}	352	301	280	273	271	270
	K_{Abut}	8798	7533	7004	6837	6781	6761
	Δ_{Pier}	0.3217	0.2795	0.2674	0.2623	0.261	0.26
	Δ_{Abut}	0.0389	0.039	0.0398	0.0399	0.0401	0.04
Step 13	Δ_{Pier}	0.26	0.26	0.26	0.26	0.26	0.26
	Δ_{Abut}	0.04	0.039	0.04	0.04	0.04	0.04

References

- Beca, Carter, Hollings & Ferner Ltd (Beca) and Opus International Consultants Ltd (Opus) (2008) Standard precast concrete bridge beams. *NZ Transport Agency research report 364*. 57pp.
- fédération internationale du béton (fib) (2010) fib model code for concrete structures 2010 (fib 2010) – final draft. Lausanne, federation internationale du beton bulletin nos. 65/66.
- England, GL, NCM Tsang and DI Bush (2000) *Integral bridges a fundamental approach to the time-temperature loading problem*. London: Thomas Telford Publishing.
- Highways Agency (1996) *BA 42 – The design of integral bridges: design manual for roads and bridges*. Vol 1.2.12. London: The Stationery Office.
- NZ Transport Agency (2014) (SP/M/022) *Bridge manual*. 3rd edition, amendment 1. Wellington: NZ Transport Agency.
- Nicholson BA (1998) *Integral abutment for prestressed beam bridges*. Prestressed Concrete Association.
- Priestley, M, GM Calvi and MJ Kowalsky (2007) Direct displacement-based seismic design of structures. *Paper 18, Proceedings of NZSEE Conference*, Palmerston North. 30 March – 1 April 2007.
- Priestley, M, MJ Kowalsky and GM Calvi (2014) Displacement-based seismic design of bridges. Pp 201–236 in *Bridge engineering handbook, second edition: seismic design*. W-F Chen and L Duan (Eds) Boca Raton, Florida: Taylor and Francis Group.
- Rojas, E (2014) *Uniform temperature predictions and temperature gradient effects on I-girder and box girder concrete bridges*. MSC thesis. Utah, USA: Utah State University.
- Standards New Zealand Technical Committee (2004) *NZS 1170.5: 2004 Structural design actions*. Wellington, New Zealand.
- Standards New Zealand (2006) *NZS 3101: 2006 Concrete structural standard*. New Zealand.